Erbium-Doped Fiber Amplifier Applications in WDM Transport Systems and Networks

by

Farideh Khaleghi, B.A.Sc., M.Sc.

A thesis
submitted to the School of Graduate Studies and Research
in partial fulfillment of the requirements for the
Degree of Doctor of Philosophy
in Electrical Engineering

Ottawa-Carleton Institute for Electrical Engineering
Department of Electrical Engineering
Faculty of Engineering
Ottawa, Ontario
Canada

May 1996

ISBN 0-612-19975-4

Canada

UNIVERSITÉ D'OTTAWA
UNIVERSITY OF OTTAWA

Abstract

New expressions are derived for wavelength-dependent gain variations of the EDFA due to changes in the pump power, total input power, and the power distribution among different wavelength channels in a wavelength-division multiplexing (WDM) system. A simple method is proposed to compensate for the changes in the amplifier gain spectrum. This method is based on adjusting the pump power. Two different novel gain equalization techniques are presented. A tunable coherent optical transversal filter is designed as a gain equalizer. The filter operation is based on coherently combining the tapped signals. It is shown that, although the N tapped signals after being weighted according to the filter parameters are recombined by a tree of 2×2 couplers, the coupling loss experienced at the output is much less than the noncoherent coupling loss $[10log(N)]$. For a multi-wavelength input, the spectrum of the amplifier output power is evaluated before and after the equalizer, using the numerical full spectrum model of the amplifier. The impact of the laser phase noise on the performance of this equalizer is studied. Another gain equalization technique is presented where high- and moderate-inversion EDFAs are used alternatively in order to equalize both signal power and signal-to-noise ratio (SNR) of multiple wavelength channels in WDM transmission systems. This technique is based on the fact that the gain slope is a function of the inversion level in amplifiers. This is confirmed experimentally. The performance of the equalized WDM system is examined by a numerical analysis based on the full spectrum model of the amplifier.

The interferometric conversion of the phase-to-intensity noise is studied. The probability density function (pdf) of the intensity noise at the output of a multi-tap filter is derived. The degradation of the filter response is evaluated. The power penalty due to this noise is derived for amplitude modulated signals modulated using different bit rates. The power penalty due to interferometric noise caused by multiple reflections is also derived.

A novel bidirectional EDFA configuration is proposed where the power penalty associated with the amplifier due to both the signal-spontaneous noise and the interferometric noise is substantially reduced. The experimental results are presented where a gain of 36 dB is achieved, and a 2.5 Gb/s bidirectional transmission over 300 km is realized. The power penalty is as low as 0.5 dB.

Application of EDFA in an optical network is presented. The multi-access scheme in this local network is code-division multiple access (CDMA). A new correlator receiver architecture for noncoherent optical CDMA networks is proposed based on a modified version of unipolar-bipolar correlation functions for known bipolar codes. These functions are studied. Average bit error rate (BER) performance is evaluated for this architecture. The results indicate that bipolar capacity can be achieved by this architecture.

Acknowledgements

I am very grateful to my supervisor, Dr. Mohsen Kavehrad who has been very supportive of this work. His interest, guidance, and encouragement are greatly appreciated. I would also like to thank the members of my Ph.D. examining committee, Drs. William Steenaart, Reza Soleimani, David Gibbons, Mohammad El-Tanani, and Langis Roy for their helpful recommendations. I am very grateful to Dr. Randy Giles of AT&T Bell Labs, New Jersey for taking the time to read the thesis and for his many valuable suggestions that helped greatly to improve the thesis.

I am grateful to Dr. Jinghui Li, for his continued encouragement, many valuable discussions and assistance, specially with the theoretical work of chapter 5 and experimental work of chapter 7, while he was a member of Broadband Communications Research Laboratory (BCRL). I am thankful to Dr. Chris Barnard for his interest, and assistance in the numerical modeling of chapter 3.

Also, special thanks go to Mr. H. Kim of Nortel for providing me with generous access to BNR facilities and the valuable guidance he offered during the experimental phase of the research.

This work was supported partly by the Telecommunication Research Institute of Ontario (TRIO), Optical Network Systems project and partly by the National Science and Engineering Research Council of Canada (NSERC). I am grateful to both of these organizations.

Also, many thanks to my colleagues at BCRL of University of Ottawa: Dr. Q. Jiang, for hours of valuable discussions, and Dr. E. Simova, for her valuable advice and words of encouragement in very right moments; and graduate students: Lucie Adam, Chris Barnard, Denis Zaccarin, Sudakar Ganti, Gang Yun, Mark Hawryluck, Reza Pakravan, and Y.D. Jin for their interest and encouragements. An overdue thanks goes to Niloufar Tayebi, a former colleage and a dear friend for caring and for her help.

Most importantly, thanks are given to my parents, my sister, freshteh, and my brother, Ali, for their constant encouragements and support and, above all, glory to God, for holding my hand in a rather difficult time of my life.

Table of Contents

List of Figures

List of Tables

List of Abbreviations and Symbols

α_k	Absorption Constant
$\alpha(\lambda)$	Absorption (dB/m)
A_{eff}	Effective Dopant Area m^2
APD	Avalanche Photodiode
ASE	Amplified Spontaneous Emission
ASK	Amplitude Shift Keying
ATM	Asynchronous Transfer Mode
AWGN	Additive White Gaussian Noise
a	Fiber Core Area
b	Effective Erbium Radius
BEDFA	Bidirectional Erbium-Doped Fiber Amplifier
BER	Bit Error Rate
BISDN	Broadband Integrated Services Distribution Network
BPF	Band-Pass Filter
BPSK	Binary Phase Shift Keying
CDMA	Code Division Multiple Access
CDMA/FDMA	Code Division Multiple Access/Frequency Division Multiple Access
CTB	Composite Triple Beat
dB	decibel
CW	Continuous Wave
DFB	Distributed Feed-Back
DPSK	Differential Phase Shift Keying
DQDB	Distributed Queue Dual Bus
DS	Direct Sequence
DS/SSMA	Direct Sequence/Spread Spectrum Multiple Access
E/O	Electro-Optic
EDF	Erbium-Doped Fiber
EDFA	Erbium-Doped Fiber Amplifier
ESA	Excited State Absorption
FDDI	Fiber Distributed Data Interface
FDMA	Frequency Division Multiple Access

FP	Fabry Perot
FSK	Frequency Shift Keying
FTRA	Frequency-Tunable Reflection Attenuator
FWHM	Full-width at half maximum
Γ_k	Overlap Integral for the k-th Signal
G_k	Gain at k-th Wavelength
$g^*(\lambda)$	Gain (dB/m)
GaAsP	Gallium Arsenide Phosphide
GQR	Gauss Quadrature Rule
h	Plank's Constant (J/s)
$I_k(r, \phi, z)$	Light intensity distribution of the k-th beam at position (r, ϕ, z)
IC	Integrated Circuit
IMD	Intermodulation Distortion
IMP	Intermodulation Product
L	EDF Length
λ_k	Wavelength of the k-th signal
LAN	Local Area Network
LED	Light Emitting Diode
LO	Local Oscillator
MZ	Mach-Zehnder
ν_k	Frequency of the k-th beam
N_t	Total density of dopant ions
N_1	Ground level population
N_2	Metastable level population
N_{eq}	Equivalent input noise
n_{sp}	Spontaneous emission factor
NF	Noise Figure
NNR	Non-Reciprocal Rotator
O/E	Opto-Electronic
OOK	On-Off-Keying
P_{ASE}	Spontaneous emission power
$P_k(z)$	Power of k-th beam at position z
P_k^{IS}	Intrinsic Saturation Power
P_k^{in}	Input Power at k-th Wavelength
P_{in}	Total Input Power

P_k^{out}	Output Power at k-th Wavelength
P_{out}	Total Output Power
pdf	Probability density function
PGF	Probability Generation Function
PIN diode	Positive-Intrinsic-Negative diode
PN	Pseudonoise
PBS	Polarization Beam Splitter
PSO	Peak Second-Order Distortion
RIN	Relative Intensity Noise
RR	Reciprocal Rotator
σ_{ek}	Emission Cross Section
σ_{ak}	Absorption Cross Section
SAW	Surface Acoustic Wave
SAW-MF	SAW-Matched Filter
SCM	Subcarrier Multiplexing
SF	Single Frequency
SIK	Shift Inversion Keying
SNR	Signal-to-Noise Ratio
SONET	Synchronous Optical Network
T	Temperature (K)
T	Bit duration
u_k	Unit vector in z direction of k-th wavelength
TDM	Time-Division Multiplexing
TDMA	Time-Division Multiple Access
WAN	Wide Area Network
WDM	Wavelength-Division Multiplexing
WDMA	Wavelength Division Multiple Access

Chapter I

Introduction

I.1 Motives

Erbium-doped fiber amplifiers (EDFAs) and wavelength-division-multiplexing (WDM) technology offer a unique capability to expand the capacity in transmission systems. EDFAs consisting of a short length of erbium-doped fiber (EDF) and a semi-conductor laser that excites erbium ions to provide gain in the 1.55 μm wavelength region, can boost the power of optical signals without the need for opto-electronic and electro-optic conversion as in conventional lightwave repeaters. The amplification is independent of the operating data rate and can simultaneously accommodate many WDM channels. Traditionally, capacity upgrade by increasing the data rate has proven to be more economical than using multichannel WDM. However, developing photonics and electronics operating at speeds beyond 10 Gb/s can be very costly.

Optical fiber amplifiers will change the traditional view by allowing WDM technology and architecture to be utilized in a very cost-effective manner. First, the repeater span can be increased considerably. This can present significant savings in the initial cost of construction and maintenance cost of existing routes. Second, each amplifier can support many WDM channels. This can be done

by simply increasing the pump power to accommodate more channels. Third, capacity upgrade is easily implemented at the nodes, by adding the channels that use available equipment such as that developed for SONET (synchronous optical network) or SHD (synchronous digital hierarchy) operation at 2.488 Gb/s data rate. Fourth, the flexibility of WDM technique in upgrading capacity provides cost-effective means to provide route redundancy for network restoration.

Although various technologies for building an amplified WDM transmission system are available for experimental demonstrations, there are many issues requiring attention and further research. The choice of pumping wavelength is no longer an issue. Pumping at 980 nm gives better noise performance and lower dissipation, compared to pumping at 1480 nm. One of the major difficulties facing the implementation of amplified WDM lightwave systems appears to be that of gain equalization. Because of the wavelength-dependent gain profile and saturation characteristics of erbium-doped fiber amplifiers, each signal in a WDM system experiences a different gain. Therefore, the signal-to-noise ratio (SNR) in each channel may be very different. It is desirable to equalize the SNRs at the receiver in order to assure a certain bit error rate (BER) for all channels. In a transmission system where multiwavelength signals must pass through a cascade of EDFAs, the amplifiers' nonflat gain spectra impose size and capacity limits. These limits can be extended by flattening the amplifiers' gain profile with an equalization technique.

The EDFA can serve as a transmitter power booster and, with proper design, as a high-performance repeater amplifier to compensate for both fiber and component losses. The optical amplification, however, is obtained at the expense of noise being added to the output signal. In a chain of repeater amplifiers, amplified

spontaneous emission (ASE) generated in each amplifier will accumulate and be further amplified by the succeeding amplifiers. The accumulated ASE noise is proportional to the gain of each amplifier and the number of amplifiers.

In amplified bidirectional WDM systems, the interferometric conversion of phase-to-intensity noise due to multiple reflections is intensified by the gain of the amplifier. This relative intensity noise can cause severe system performance degradations.

Regarding the EDFA applications in WDM systems, these are some of the issues that are addressed in this thesis. However, there are many other issues that require more work such as those of WDM multiplexer, tunable lasers, fiber nonlinearities, etc. Some of these research topics are mentioned in chapter 10, as suggestions for future work.

Large bandwidth and low propagation loss of fiber along with the introduction of optical fiber amplifiers that offer the capability to exploit this tremendous available bandwidth makes single-mode fiber the medium of choice for long-haul transmissions. However, the existence of optical local area networks (LANs) relies upon the availability of an efficient multiple-access technique capable of using the vast available bandwidth of fiber to accommodate a large number of users. The code-division multiple-access (CDMA) technique has the capability to utilize the optical channel bandwidth in order to provide simultaneous access to multiple users.

With regard to the amplified optical networks, EDFAs can be used to compensate for both the splitting and attenuation losses. At the receiver, the detected noise due to ASE noise consists of two components: spontaneous-spontaneous

and signal-spontaneous noise. The second component which arises from the beats between the signal and the ASE dominates in practical systems. The effect of this noise is to be studied on the system performance in an optical network. In this thesis, the performance of an amplified CDM LAN is studied where a new noncoherent code-division multiplexing (CDM) receiver architecture is proposed.

Many issues remain for both amplified WDM transmission systems and amplified networks. In this thesis, we address and present solutions to some of these problems.

I.2 Contributions and Outline of the Thesis

In chapter 2, after a brief description of erbium-doped fiber amplifiers and their operation, we present an analytical model for these amplifiers. Using the calculation convenience and intuition provided by this model compared to the numerical models, we investigate the behaviour of the EDFA in WDM systems. It is confirmed that the gain variations of the EDFA are wavelength-dependent, and that they not only depend on the total input signal power, but also, on the distribution of the power among wavelength channels. It is shown that if the gain at one wavelength is fixed by adjusting the pump power, the entire gain spectrum maintains its original profile. This point is further examined by studying the gain spectrum using a more accurate numerical model that is described in chapter 3. Since the EDFA gain dynamics are very slow; in the order of 1 ms, an electronic compensation circuit is suggested. Part of these findings are published in [43]. Our contribution includes the development of new expressions for the gain variations of the EDFA at different wavelengths, due to the changes in the

total input power and its distribution among different wavelengths, and also pump power. Furthermore, we present a method for maintaining the EDFA gain profile, and describe a compensation circuit. Although tunable, it is extremely difficult to make an adaptive optical equalizer; therefore, the gain profile based on which the tunable equalizer is tuned has to be preserved to make the equalization effective.

In chapter 3, a classification of the existing amplifier models is followed by the description of a numerical model of the amplifier. This model is refined to include the effect of ASE where the full ASE spectrum is resolved. Throughout chapter 3 to the end of this thesis, this model is used to predict the EDFA behaviour. A transversal coherent filter is suggested as a gain equalizer. Although this method is not very cost-effective at this point in time, this study outlines how coherent optical transversal filters can be designed for different purposes. This filter operates based on coherently combining the tapped signals. For the first time, it is shown in this thesis that although the tapped signals after being weighted according to the filter coefficients are recombined by a tree of 2×2 couplers, the noncoherent coupling losses can be avoided. The practical issues are also discussed. This work is published in [43]. Absorption and emission cross section spectra of the erbium-doped fiber govern the ASE spectrum. At the end of chapter 3, the experimental measurements of the fiber gain and loss spectra are described. The absorption and emission cross section spectra are extracted from the measured spectra. The cross section values are used in the following chapters to predict the EDFA behaviour using the full spectrum model. We often use these results to compare to the experimental results, and investigate the system performance under different conditions where experimentation is not possible.

In chapter 4, we describe the ASE generation in the EDFA. ASE spectrum

closely emulates the gain spectrum. Using this model, we define the spontaneous noise factor n_{sp} of the EDFAs. n_{sp} is a measure of the degree of inversion achieved in the amplifier. The noise performance of the EDFA basically is determined by n_{sp}, and is best when $n_{sp} = 1$, i.e., full inversion of the amplifier. Using this factor, the optical signal-to-noise ratio at the amplifier input and output, and amplifier noise figure (NF) are defined. The electrical signal-to-noise ratio and BER evaluations for an amplitude modulated signal are also presented. At the end of chapter 4, we present our experimental results on the ASE spectrum under different conditions corresponding to different inversion levels. These results indicate that the gain slope of the EDFA at 1550 nm window can change based on the changes in the inversion level. This observation is the basis of the equalization method described in chapter 5.

In chapter 5, a new simple gain equalization method is presented, where high- and moderate-inversion EDFAs are used alternatively in order to achieve less interchannel power variation and SNR differential. EDFAs in high-inversion regimes present a flatter gain, however, the SNR in this case degrades very fast after a few cascaded amplifiers. This is due to a strong ASE peak around 1530 nm of the EDFAs operating in a high-inversion regime. The 1530 nm ASE peak is automatically removed by alternative use of high- and medium-inversion amplifiers, without inserting additional optical filters. The achieved SNRs and SNR differential in the compensated system were compared with those of a system containing a chain of either high- or medium-inversion EDFAs. The results show that the proposed system outperforms both other systems. We partly presented this work in [53] and [54].

In chapter 6, we study the effect of the interferometric phase-to-intensity

noise conversion. The probability density function (pdf) of the intensity noise is evaluated at the output of a two- and a multi-tap coherent optical filter. We state under which conditions the pdf can be assumed Gaussian. The exact pdf for a two-tap filter is evaluated. These derivations, developed for the first time, are applied to the designed transversal filter gain equalizer in chapter 3 to examine the filter response degradation due to phase noise. Also, the power penalty due this noise is evaluated for the on-off-keying (OOK) modulated signals at different bit rates. The phase noise can be converted to the intensity noise due to multiple reflections, as well. This effect is magnified when the reflected signals are amplified by a gain medium. The power penalty associated with an amplifier due to this effect is also evaluated. The results are used in chapter 7.

In chapter 7, bidirectional amplification is studied. A main source of impairments in these systems is the interferometric conversion of the laser phase noise to intensity noise due to multiple reflections. A novel bidirectional EDFA is presented where the power penalty associated with the amplifier due to both the interferometric noise and the signal-spontaneous beat noise, which as mentioned is the dominant noise component in the amplified systems, is substantially reduced. The experimental results confirm these findings. We were able to achieve a gain of 36 dB, and increase the bidirectional repeater span to 300 km for a 2.5 Gb/s signal. The description of this configuration can be found in our US patent application 71493-65 [47]. Using the measured cross sections spectra of the EDF used in this experiment, the EDFA is modeled and numerical analyses are used to investigate different ways of improving the EDFA performance. Alternative configurations are also presented at the end of the chapter. We published part of this work in [42] and [46].

Chapter 8 provides an overview on all-optical networks. In chapter 9, the application of EDFA in an optical CDMA local area network (LAN) is studied. A star topology is used to provide the multi-user connectivity, where EDFAs will extend the limitation on the number of users in a power limited system. A new correlator receiver architecture based on a modified version of unipolar-bipolar correlation is proposed for noncoherent optical fiber CDMA networks. For this architecture, the receiver average bit error rate (BER) performance is numerically evaluated. The BER performance is also evaluated by a closed-form formula that is developed in this thesis. Comparison of the results from the latter with numerical results show that the formula provides a good approximation to the system performance. Furthermore, the closed form solution suggests that the system can achieve the bipolar capacity. In the literature, various schemes are presented on the use of bipolar codes in optical CDMA networks. In chapter 9, we introduce a technique by which bipolar capacity is achieved while employing conventional bipolar codes. The technique removes the effect of unbalanced codes by applying a simple modification to the unipolar-bipolar correlation receiver. We show that the multi-user interference term that is obtained using a modified unipolar-bipolar correlation is a scaled version of that obtained in a bipolar DS-CDMA scheme. That is, not only is the offset in the autocorrelation term removed, the offset (DC component) in the interference term is also forced to zero. This technique is especially suitable for a combined WDM/CDM system, where an optical filter can separate different wavelength channels. This work is published in [44] and [45]. Finally, in chapter 10, we give a summary of results and suggestions for future work.

Chapter II

Gain Properties of Erbium-Doped Fiber Amplifiers for Multi-Wavelength Signals

II.1 Introduction

In an erbium-doped fiber amplifier (EDFA), light from a pump laser is coupled with light from longer wavelength signals into the doped fiber. The pump excites the rare-earth ions within the fiber core to create a population inversion, from which amplification at the signal wavelength occurs by stimulated emission.

In EDFAs, the active erbium-doped fiber (EDF) (Fig. 2.1) supports only one mode. The single mode maintains high pump and signal intensities over long interaction lengths resulting in the favourable combination of low loss and high gain from low-input pump power.

The combined EDFA characteristics of gain, saturation power and noise are often referred to as the EDFA performance. Within the 1550 nm telecommunications window, the notable results achieved with erbium-doped-fiber amplifiers are 51-dB optical gain, 100-mW saturated output power and 3-dB noise figure [26]. Furthermore, EDFAs are able to amplify a multiple number of channels because of their large bandwidth and negligible interwavelength crosstalk.

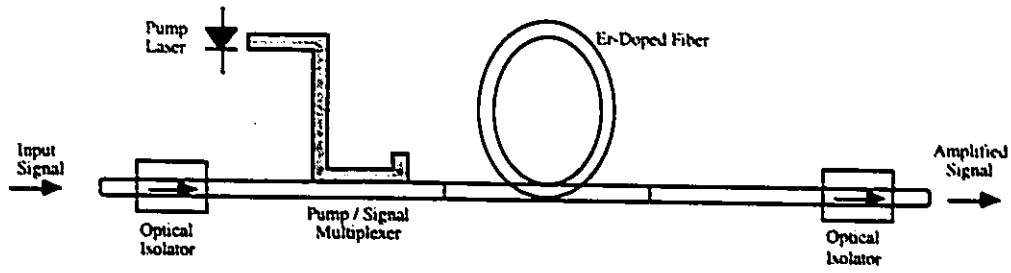

Fig. 2.1. Schematic diagram of an erbium-doped fiber amplifier

In wavelength-division multiplexing (WDM) systems, the usable optical bandwidth is divided into multiple channels, where each wavelength channel has enough capacity to accommodate the peak rate of electronics. The large bandwidth and other properties of EDFAs allows the WDM systems to be extended over a large geographical span. These amplifiers can replace regenerators thereby avoiding opto-electronic and electro-optic conversion. However, because of the wavelength-dependent gain profile and saturation characteristics of the fiber amplifiers, each signal experiences a slightly different gain. In a WDM system where multi-wavelength signals pass through a cascade of EDFAs, the amplifiers' nonflat gain spectra impose a capacity limit on the system. This limit can be exceeded by flattening the amplifier's gain profile.

In this chapter, we use the EDFA analytical model, developed by Saleh [77], to examine the multi-wavelength gain properties of EDFAs. The amplified spontaneous emission (ASE) noise is neglected in this model. The model is valid for amplifiers with a gain less than 20 dB, or an input signal power of more than -20 dBm so that the input signal power is significantly above the equivalent input ASE noise. Although, this model does not possess the accuracy that many numerical models do, it provides the calculation convenience and intuition to understand the amplifier behaviour.

This chapter is organized as follows. Section 2 states the spectroscopic properties of the Er^{+3} ion dopant. Section 3 provides the fiber amplifier theory for an ion modeled by a two-level system, beginning with the rate equations. The analytical solution to the rate equations is also given. In section 4, we use this analytical solution for the case of wavelength-division-multiplexed (WDM) systems to demonstrate that the gain profile of the EDFA is not only a function of the total average input signal power, but also of the WDM input signal spectrum. In section 5, we show that if the gain is fixed in one wavelength by adjusting the pump power, the gain profile maintains its original shape. In section 6, the conclusions are presented.

II.2 Spectral properties of Er

Fig. 2.2 shows a simplified model of the energy level for a three-level ion and its decay times. Erbium is modeled with a three-level model. It has a signal wavelength between 1520 and 1570 nm. It can be pumped at 510, 532, 665, 810, 980, and 1480 nm with the latter two wavelengths being advantageous [26]. In Fig. 2.1, a $I^4_{11/2}$-$I^4_{15/2}$ (pump level-metastable level) transition corresponds to the 980 nm pump band and the $I^4_{13/2}$-$I^4_{15/2}$ (metastable level-ground level) transition corresponds to 1520-1570 nm signal band and the resonant pumping in the 1460-1480 nm band. The decay time from pump level τ_{32} is much shorter than that from metastable level τ_{21}. Other pump bands and potential for excited-state absorption (ESA) are associated with other energy levels of Er^{3+}, but are not included in the figure.

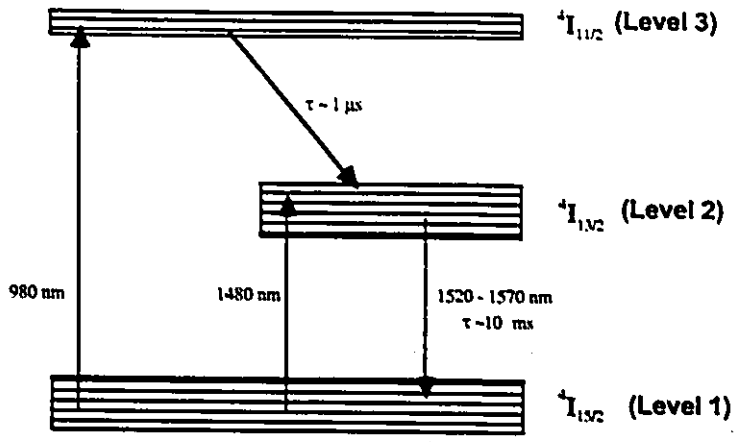

Fig. 2.2. Energy level diagram for a three-level system

A two-level model of the amplifier gain medium can be used for 980 nm pumped EDFAs. For pumping into the 980 nm absorption band, this implies that the population in the level three manifold is negligible. This assumption is nominally satisfied when the nonradiative decay rate from the pump level $1/\tau_{32}$ is much higher than the pumping rate $W_{pump} = P_p\sigma_{ap}/(h\nu_p A)$ where P_p is the pump power, ν_p is the pump frequency, σ_{ap} is the absorption crosssection at the pump wavelength, and A is the mode area. For typical fiber amplifier parameters, treating the 980 nm pumped amplifier with a two-level model is valid for average pump powers less than 1W. Finally, direct pumping into the metastable level in 1480 nm pumped amplifiers also behaves as a two-level system.

II.3 Theory of Fiber Amplifiers

II.3.1 Rate Equations

The rate equations are based on the energy-level diagram for a two-level system. Rate equations describe the effects of absorption, stimulated emission, and

spontaneous emission on the populations of the ground and metastable states. The fiber is doped with $N_t(r, \Phi, z, t)$ active ions per unit volume with $N_i(r, \Phi, z, t)$ ions per unit volume in the ith level at position (r, Φ, z) and time (t). Rate equations are written for K signals, where in a two-level theory, it is not necessary to differentiate between pump and signal beams, since they interact with the same energy level. Integrating the light intensity distribution of the kth beam $I_k(r, \phi, z)$ over the transverse plane gives the beam's total power $P_k(z)$ at position z in the fiber amplifier.

$$P_k(z) = \int I_k(r, \phi, z) dA$$

where $dA = r dr d\phi$.

For this two-level system with the K optical beams [26]:

$$N_t = N_1 + N_2 \tag{1}$$

$$\frac{\delta N_2}{\delta t} = \sum_k \frac{I_k}{h\nu_k}(\sigma_{ak} N_1 - \sigma_{ek} N_2) - \frac{N_2}{\tau} \tag{2}$$

Eq. (1) is the particle conservation for the two-level system, where N_t is the erbium ion density. In eq. (2), σ_{ak}, σ_{ek} denotes the absorption (emission) cross-section of the signal and the pump at the wavelength of the kth beam. I_k denotes the intensity of the kth signal beam and τ denotes the decay time from the metastable level. The remaining equations describe the propagation of the beams through the fiber, i.e.,

$$\begin{aligned} \frac{\delta P_k}{\delta z} &= u_k \int (N_2 \sigma_{ek} - N_1 \sigma_{ak}) I_k dA \\ &\quad + u_k \int N_2 \sigma_{ek} \frac{I_k}{P_k} mh\ \nu_k\ \Delta\nu_k dA \end{aligned} \tag{3}$$

where each beam is traveling either in the forward ($u_k = 1$) or backward ($u_k = -1$) direction. Here, $mh\nu_k\ \Delta\nu_k$ is the contribution of spontaneous emission, and its

growth through the amplifier, where $h\nu$ is the photon energy and m is the number of modes in the erbium-doped fiber which is normally 2. Features in the ASE spectrum are well resolved with $\Delta\nu_k = 125$ GHz (1 nm). In the numerical analysis of the EDFA behaviour, the same step size of 1 nm is used in this thesis.

As seen, the rate equations are given in terms of difficult to measure constants such as absorption and emission cross sections, dopant concentration, and dopant and fiber geometries. It is very desirable to combine the fiber and atomic constants into directly measurable values like loss and gain coefficients and saturation power levels, and to be able to fully characterize EDFAs by these parameters.

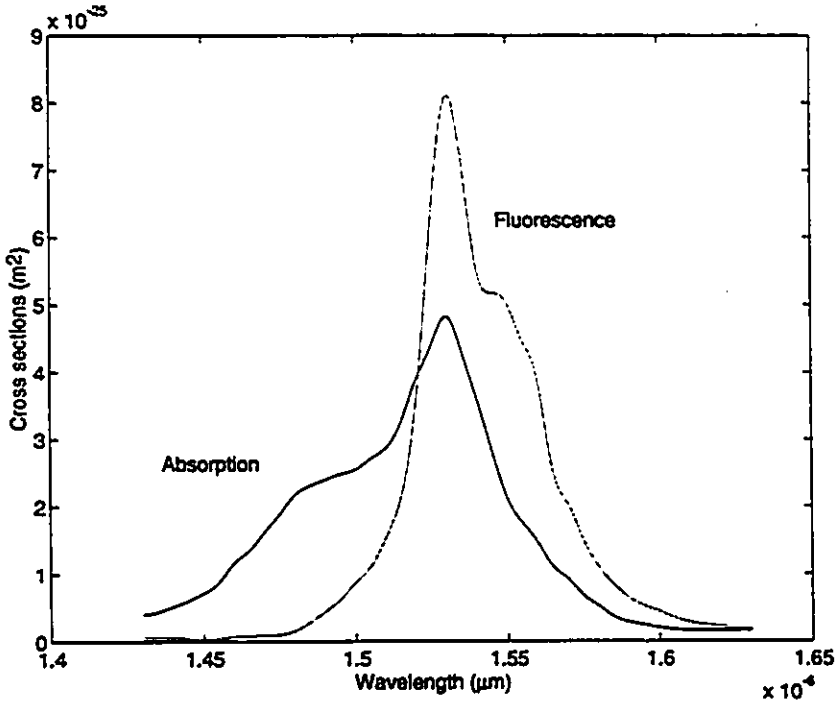

Fig. 2.3. Fluorescence (emission) and absorption cross sections around $\lambda = 1.53\mu m$.

An example of the room-temperature absorption and emission spectra obtained from an erbium-doped fiber glass is shown in Fig. 2.3. Several numerical models and analytical solutions exist that are based on different simplifying assumptions. Many of these approaches require knowledge of fiber parameters that are difficult to measure such as optical mode distributions, dopant-ion concentration and distribution within the fiber, emission and absorption cross sections and decay times. Preferred models are those that give an analytical solution expressed in terms of easily measurable parameters. Saleh's analytical model predicts EDFA gain from four measurable parameters [77]. These are the fiber attenuation coefficients α_p and α_s and saturation powers P_p^{IS} and P_s^{IS} at the pump and signal wavelengths, respectively. These parameters can be easily found by fitting theoretical curves to nonlinear transmission measurements.

If the amplifier is not saturated by ASE, as Saleh et al. [77] have shown, the two-level amplifier model reduces to one implicit equation that can be solved by the Newton-Raphson technique. Although the numerical models can prevail against most of the problems of fiber amplifiers, the penalty of such generality is the loss of calculation convenience and some intuition about the amplifier behavior. For example, by Saleh's model it can be simply shown that a fixed gain-equalizer, under the conditions where the input powers at different wavelengths vary as a function of time, does not perform properly. This is because of the dependence of the gain profile of the amplifier on the input power distribution.

II.3.2 Saleh's Model

Ignoring the contribution of the spontaneous emission in eq. (3), the equations

governing the EDFA operation are summarized as follows:

$$N_t = N_1 + N_2 \tag{4}$$

$$\frac{\partial N_2}{\partial t} = \sum_k \frac{I_k}{h\nu_k}(\sigma_{ak}N_1 - \sigma_{ek}N_2) - \frac{N_2}{\tau} \tag{5}$$

$$\frac{\partial P_k}{\partial z} = u_k \int (N_2\sigma_{ek} - N_1\sigma_{ak})I_k \, dA \tag{6}$$

Integrating the light intensity distribution of the kth beam $I_k(r, \phi, z)$ over the transverse plane gives the beam's total power $P_k(z)$ at position z in the fiber amplifier.

$$P_k(z) = \int \frac{I_k(r, \phi, z)}{h\nu_k} dA$$

where $dA = rdrd\phi$, and optical power is expressed in the unit of photons per unit time, i.e., the actual power is normalized by the photon energy.

We consider the case of an amplifier average ion density N_t within an active volume of cross-sectional area A_{eff}. Substituting the integrated form of eq. (6) into eq. (5) gives:

$$\frac{\partial \bar{N}_2}{\partial t} = -\frac{\bar{N}_2}{\tau} - \frac{1}{N_t A_{eff}} \sum_k u_k \frac{\partial P_k}{\partial z} \tag{7}$$

where $\bar{N}_2$ is the fractional population (N_2/N_t). In the remaining of this chapter, all optical powers are expressed in units of photons per unit time.

By integrating eq. (6) over the transverse plane, the change of power in the kth beam is described by

$$\frac{\partial P_k}{\partial z} = u_k N_t \Gamma_k [(\sigma_{ek} + \sigma_{ak})\bar{N}_2 - \sigma_{ak}]P_k \tag{8}$$

where the fractional population of the lower state $\tilde{N}_1 = (N_1/N_t)$ is substituted from $\tilde{N}_1 + \tilde{N}_2 = 1$, and the transverse dependence is contained in average ion density N_t, and overlap integrals Γ_k. Γ_k is the overlap integral between the optical mode and the erbium ions [26].

In eq. (8), $\tilde{N}_2$ is substituted by the value obtained from eq. (7) under steady-state conditions ($\frac{\partial \tilde{N}_2}{\partial t} = 0$) to give the final differential equations for both pump and signal beams:

$$(\frac{u_k}{P_k(z)})\frac{dP_k}{dz} = -\left[\alpha_k + \frac{1}{P_k^{IS}}\sum_{k=1}^{K} u_k \frac{dP_k(z)}{dz}\right] \tag{9}$$

where α_k and P_k^{IS} are, respectively, the absorption constant and intrinsic saturation power of the kth beam. Intrinsic power is defined by:

$$P_k^{IS} = \frac{A_{eff}}{\Gamma_s \tau}\frac{1}{\sigma_{ek} + \sigma_{ak}}$$

Solving eq. (9) for the output powers, P_k^{out} by integrating from $z = 0$ to $z = L$, yields;

$$P_k^{out} = P_k^{in} e^{-\alpha_k L} e^{\frac{(P_{in} - P_{out})}{P_k^{IS}}} \tag{10}$$

The wavelength-dependent constant P_k^{IS} in eq. (10) is the intrinsic saturation power for the kth signal as defined in [77].

II.4 Gain and Saturation Properties of Multi-Wavelength Amplification

II.4.1 Gain Profile Variations Due to Different Input Signal Power Patterns

In this section, we use Saleh's model to find how the pump input power and

the input signal power pattern affect the amplifier's gain profile. As seen, for an EDFA of length L with a total input power P_{in} and pump input power P_p^{in}, the input and output powers of the kth beam are related by eq. (10):

$$P_k^{out} = P_k^{in} e^{-\alpha_k L} e^{\frac{(P_{in} - P_{out})}{P_k^{IS}}}$$

where

$$P_{in} \equiv \sum_{j=1}^{N} P_j^{in} = P_s^{in} + P_p^{in} \tag{11}$$

$$P_{out} \equiv \sum_{j=1}^{N} P_j^{out} = P_s^{out} + P_p^{out} \tag{12}$$

are the total input and output powers, respectively. Note that, in these equations, powers are also in units of photons per second [77]. By taking the derivative of the gain, $G_k = \frac{P_k^{out}}{P_k^{in}}$ with respect to the total signal input power, P_s^{in}, from eq. (10) we will get:

$$\begin{aligned} \frac{\delta G_k}{\delta P_s^{in}} &= \frac{1}{P_k^{IS}} e^{-\alpha_k L} e^{\frac{(P_{in} - P_{out})}{P_k^{IS}}} \left(1 - \frac{\delta P_{out}}{\delta P_s^{in}}\right) \\ &= \frac{G_k}{P_k^{IS}} \left(1 - \frac{\delta P_{out}}{\delta P_s^{in}}\right) \end{aligned} \tag{13}$$

or

$$\Delta G_k = \frac{G_k}{P_k^{IS}} (\Delta P_s^{in} - \Delta P_{out}) \tag{14}$$

This means the gain variation ΔG_k due to the changes in the total signal input power ΔP_s^{in} is proportional to $(\Delta P_s^{in} - \Delta P_{out})$ and the gain itself and is inversely proportional to the wavelength-dependent constant P_k^{IS}. Since P_k^{IS} is a wavelength-dependent parameter, the gain variations for different signals will be different and wavelength-dependent. Note that, ΔP_{out} in eq. (14) represents the

output signal power changes caused by the input signal power variations. ΔP_{out} is not just a function of the total input signal power but also the way that this power is distributed among wavelengths. Therefore, both total input signal power and its distribution among different wavelengths determine the kind of gain profile the amplifier exhibits. In the saturation mode, $(\Delta P_s^{in} - \Delta P_{out})$ is not necessarily zero. This point is demonstrated in Appendix II.A where $(\Delta P_s^{in} - \Delta P_{out})$ is calculated for the case of multiple wavelength operation when the amplifier operates in its saturation mode. We also derive an analytical expression that demonstrates the complexity by which the changes in the multi-wavelength input signal power pattern affects the output signal power.

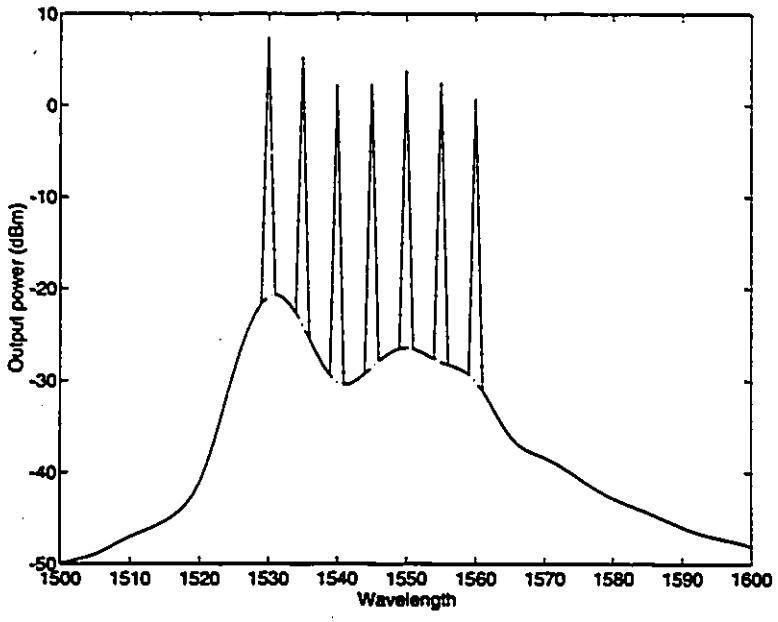

Fig. 2.4. EDFA output signal and ASE output power: pump power = 60 mW at 980 nm; input signal power at each wavelength=-13 dBm (50 μm).

Fig. 2.4 shows the output power of an amplifier fed with the multi-wavelength

input signal consisting of 7 different wavelength channels (1530, 1535, 1540, 1545, 1550, 1555, 1560 nm). The input power at each wavelength is adjusted to 50 μW. The amplifier is forward pumped with 60 mW of light at 980 nm. The length of the erbium doped fiber is set to 10 m.

We computed the gain profile of the amplifier for the input signal power patterns tabulated in Table 2.1. As expected, the computed results show that the gain profile is a function of the input signal power as well as the input signal power distribution among different wavelengths. For each input signal power pattern in table 2.1, we compared the gain at each wavelength with the original gain profile plotted in Fig. 2.4. The computed gain differences at different wavelengths are plotted in Fig. 2.5. The changes in the gain profile are wavelength-dependent. The gain at shorter wavelengths experiences larger changes.

Input power	λ_1 1530	λ_2 1535	λ_3 1540	λ_4 1545	λ_5 1550	λ_6 1555	λ_7 1560
Pattern 1	50μW	50μW	50μW	50μW	50μW	50μW	50μW
Pattern 2	*0μW	50μW	50μW	50μW	50μW	50μW	50μW
Pattern 3	50μW	50μW	50μW	*0μW	50μW	50μW	50μW
Pattern 4	100μW	50μW	50μW	50μW	50μW	50μW	50μW
Pattern 5	50μW	50μW	50μW	50μW	*0μW	*0μW	50μW

Table 2.1. Five different input signal patterns

* No input signal power present at these wavelengths

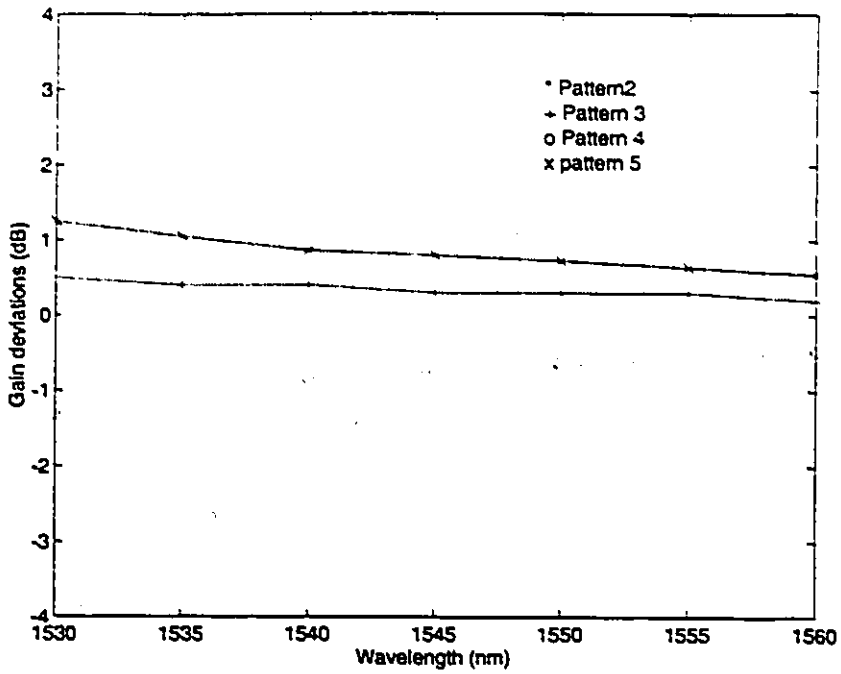

Fig. 2.5. Changes of the gain profile for the cases 2, 3, 4, and 5 in reference to case 1, in Table 2.1.

II.5 Compensation of the Wavelength-Dependent Changes in the EDFA Gain Profile

In the following, we show that if the gain of the amplifier at one wavelength is fixed by a proper adjustment in the input pump power, the entire gain profile maintains its original shape. Thus, by the adjustment of the pump power, the wavelength-dependent changes in the EDFA gain profile caused by input signal power variations can be compensated for. By rearranging eq. (10) and assuming one pump wavelength, we would have:

$$P_k^{out} = P_k^{in} e^{-\alpha_k L} e^{\frac{(P_p^{in} + P_s^{in} + P_p^{out} - P_s^{out})}{P_k^{IS}}} \tag{15}$$

where P_p^{in} and P_s^{in} are pump and signal powers, respectively. By taking the

derivative of the gain $G_k = \frac{P_k^{out}}{P_k^{in}}$ with respect to the input pump power, P_p^{in}, we will have,

$$\Delta G'_k = \frac{G_k}{P_k^{IS}}(\Delta P_p^{in} - \Delta P_s^{out} - \Delta P_p^{out}) = \frac{G_k}{P_k^{IS}}(\Delta P_p^{in} - \Delta \overline{P}_{out}) \qquad (16)$$

$\Delta \overline{P}_{out}$ in eq. (16) represents the changes in the output power caused by the changes in the pump input power. By comparing eqs. (14) and (16), it can be seen that, if the gain variation caused by the input pump power adjustments $\Delta G'_k$ is negatively equal to the change caused by the input signal power variations ΔG_k, the amplifier would maintain its gain. By setting $\Delta G_k + \Delta G'_k$ to zero, we get:

$$\Delta P_s^{in} - \Delta P_{out} + \Delta P_p^{in} - \Delta \overline{P}_{out} = 0 \qquad (17)$$

P_{in}-Pattern	P_p^{in} (mW)
Pattern 2	46.0
Pattern 3	55.5
Pattern 4	74.0
Pattern 5	49.1

Table 2.2. The required pump power for maintaining the same gain profile for the cases indicated in Table 2.1.

We notice that, if eq. (17) is satisfied, $\Delta G_k + \Delta G'_k$ for any arbitrary wavelength k would be zero. In other words, if the gain in one wavelength is fixed, the gain at all wavelengths would be maintained. Table 2.2 presents the required input pump

power for cases number 2,3,4,and 5 for maintaining the same gain profile. In practice, an unused wavelength channel can be employed for monitoring purposes. An unmodulated light at the monitoring wavelength is multiplexed to the input signal channels. The output power at the monitoring wavelength is sampled and used for adjusting the pump power by modulating the pump laser bias current.

The results of a study on the temporal response of the erbium-doped amplifiers show that in contrast with semiconductor optical amplifiers, the gain dynamic of the fiber amplifier is modified by relatively long time constants in the order of 1 msec. The response of the gain to intensity fluctuations is damped by the carrier life time. These time constants are much longer than those in semiconductor optical amplifiers and such a slow gain response of the fiber amplifiers prevents any high-frequency gain modulation. Therefore, the changes of the gain profile of the amplifiers because of their low-frequency nature can easily be taken care of by an electronic compensation circuit. This circuit samples the output power of the amplifier at the monitoring wavelength, then compares it with a reference value and changes the pump power bias current, accordingly. Otherwise, the wavelength-dependent change in the gain profile will limit the applications of an EDFA. For example, in the network environment, if one wavelength signal is withdrawn for a relatively long time, the gain profile is changed, completely. This makes any attempt in gain equalization ineffective.

II.6 Conclusions

We have taken advantage of the simple analytical solution of the Saleh's model to demonstrate that in the amplified WDM systems, if the signal power at each

wavelength varies, the gain spectrum of the amplifier changes as a result. This fact implies that if the changes in the gain profile of the amplifier are not considered, any static gain equalization will be inefrective. This leaves us with two solutions: 1) fixing the gain spectrum, 2) using tunable gain equalizers.

Using the closed-form formulae provided by this method, we were able to come up with a simple solution to fix the gain spectrum. Although the solution was inspired by the analytical method, the numerical model was used to examine the technique. The numerical model is described in the next chapter. This model accurately predicts the amplifier behaviour. Thus, it can be concluded that the gain profile can be maintained by the adjustment of the pump power.

Appendix II.A

Amplifier Output Power Variations due to the Pump and Input Signal Power Variations while Operating Under Saturation

In multiple wavelength operation when the amplifier operates in its saturation mode, the gain for each wavelength is less than the small-signal gain at the wavelength. However, in this case, the signal gain for different wavelengths drops by different factors from its small-signal gain. Therefore, the saturation output power, P_{out}^{sat} for which the signal gain at wavelength j drops by a factor of e^{a_j} from its small-signal gain can be shown as follows.

$$\begin{aligned} P_{out}^{sat} &= \sum_{j=1}^{N} (e^{-a_j}) P_j^{in} e^{-\alpha_j L} e^{(P_p^{in} - P_{p,0}^{out})/P_j^{IS}} \\ &= \sum_{j=1}^{N} P_j^{in} e^{-\alpha_j L} e^{(P_p^{in} + P_{in} - P_p^{out} - P_{out}^{sat})/P_j^{IS}} \end{aligned} \tag{1}$$

where $P_{p,0}^{out} = P_p^{in} e^{-\alpha_p L} e^{\frac{(P_p^{in} - P_{p,0}^{out})}{P_p^{IS}}}$ is the pump output power with no signal input and P_j^{in} is the jth input signal power. Parameter N represents the total number of input signals. From eq. (9);

$$P_p^{out} = P_{p,0}^{out} e^{(P_s^{in} - P_p^{out} - P_{out}^{sat} + P_{p,0}^{out})/P_p^{IS}} \tag{2}$$

Since in eq. (1), the equality for all the elements of the summation holds one-by-one, we will have

$$-a_j P_j^{IS} - P_{p,0}^{out} = P_s^{in} - P_p^{out} - P_{out}^{sat} \tag{3}$$

or by summing over j,

$$-\sum_{j=1}^{N} a_j P_j^{IS} - N P_{p,0}^{out} = N P_s^{in} - N P_p^{out} - N P_{out}^{sat} \tag{4}$$

Substituting eq. (4) in eq. (2), it is shown that

$$P_S^{in} - P_{out}^{sat} + \overline{P}_s^{IS} + P_{p,0}^{out} = P_{p,0}^{out} e^{-\overline{P}_s^{IS}/P_p^{IS}} \tag{5}$$

or simply,

$$P_{out}^{sat} = P_s^{in} + \overline{P}_s^{IS} + P_{p,0}^{out}\left(1 - e^{-\overline{P}_s^{IS}/P_p^{IS}}\right) \tag{6}$$

where $\overline{P}_s^{IS} = \sum_{j=1}^{N} \frac{a_j P_j^{IS}}{N}$. Since the signal input power variations change the gain compression coefficient at each wavelength $a_j s$, eq. (6) verifies that $\Delta P_{out}^{sat} \neq \Delta P_s^{in}$. In fact;

$$\Delta P_{out}^{sat} - \Delta P_s^{in} = \sum_{j=1}^{N} \Delta a_j P_j^{IS}/N \tag{7}$$

Chapter III

Gain Equalization I

III.1 Introduction

Despite the large gain bandwidth product of an EDFA, as it is evident from the model presented in the previous chapter, the amplifier gain spectrum is not flat and a small gain imbalance is unavoidable. This leads to a large gain imbalance in multistage amplifiers. Depending on the amplifier conditions, such as the pumping power and the gain saturation condition, the gain imbalance of each amplifier is different. Therefore, to compensate for the gain imbalance, if possible, tunable equalization is desired. Various proposals have been made for gain equalization. Tachibana, et al. [94] reported gain equalization using a fiber grating filter. Although a large 3 dB bandwidth is obtained for the amplifier, it seems difficult for this technique to adaptively compensate the accumulated gain imbalance. Giles, et al. [26] utilized two kinds of fiber amplifiers. Although dynamic equalization was achieved, applicable wavelengths were limited in their method. Inoue et al. [38] have realized a gain equalizer using a waveguide type Mach-Zehnder optical filter. Although tunable gain equalization was achieved, the filter bandwidth was limited to 7 nm. In this chapter, we describe a tunable gain equalization using a waveguide type transversal optical filter [83]. Theoretically, this filter can have a bandwidth of 30 nm or more.

To design the equalizer, the amplifier gain for multi-wavelength signals is

required. In the previous chapter, amplified spontaneous emission (ASE) was neglected in the amplifier model. As mentioned above, this is valid for EDFAs if the gain is less than 20 dB or the signal input is greater than -20 dBm. However, EDFAs in many applications such as preamplification typically have greater than 20 dB gain and less than -20 dBm input signal power. In this chapter, the amplifier model is refined to include the effects of ASE.

This chapter is organized as follows. The amplifier full spectrum model using a two-level approximation is described in section 2. In section 3, gain of the amplifier for WDM signals is evaluated using the amplifier numerical model. Based on the amplifier gain profile, the equalizer design is described. In section 4, the realization feasibility of such a filter is discussed and finally conclusions are presented in section 5.

III.2 Amplifier Models Including ASE

III.2.1 Full Spectrum Model

As mentioned, models of two-level systems are useful for EDFAs pumped in the 1480 and 980 nm absorption bands. The rate equations for a two-level system with K optical beams are given by [26]:

$$N_t = N_1 + N_2 \tag{1}$$

$$\frac{\delta N_2}{\delta t} = \sum_k \frac{I_k}{h\nu_k}(\sigma_{ak}N_1 - \sigma_{ek}N_2) - \frac{N_2}{\tau} \tag{2}$$

Eq. (1) is the particle conservation for the two-level system, where N_t is the erbium ion density. In eq. (2), σ_{ak}, (σ_{ek}) denotes the absorption (emission)

cross-section of the kth beam. I_k denotes the intensity of the kth signal or pump beam and τ denotes the decay time from the metastable level. The light in the amplifier is thought to be propagating as a number of optical beams of frequency bandwidth $\Delta\nu_k$ centered at the optical wavelength $\lambda_k = c/\nu_k$. This notation describes both narrow linewidth beams such as pump and signal sources when $\Delta\nu_k = 0$, and broadband amplified spontaneous noise (ASE) where $\Delta\nu_k$ equals the frequency steps to resolve the ASE spectrum. Therefore, the integration over optical frequency is approximated by a summation over k. Integrating the light intensity distribution of the kth beam $I_k(r, \Phi, z)$ over the radial and azimuthal coordinates gives the beam's total power $P_k(z)$ at position z in the fiber amplifier

$$P_k(z) = \int_0^{2\pi} \int I_k(r, \Phi, z) r dr d\Phi.$$

The remaining equations describe the propagation of the beams through the fiber, i.e.,

$$\begin{aligned} \frac{\delta P_k}{\delta z} &= u_k \int (N_2\sigma_{ek} - N_1\sigma_{ak}) I_k dA \\ &\quad + u_k(mh\ \nu_k\ \Delta\nu_k) \int (1/P_k)(N_2\sigma_{ek} I_k) dA \end{aligned} \tag{3}$$

where each beam is traveling either in the forward ($u_k = 1$) or backward ($u_k = -1$) direction. Here $mh\nu_k\ \Delta\nu_k$ is the contribution of spontaneous emission, and its growth through the amplifier. The number of modes m is normally 2, as in the case of the optical fiber supporting only two polarization states of the lowest order optical mode.

Ignoring the noise term and using the effective overlap integral Γ_k, the integration of eq. (3) over the transverse plane gives:

$$\frac{dP_k}{dz} = \Gamma_k(N_2\sigma_{ek} - N_1\sigma_{ak})P_k(z) \tag{4}$$

Solving this first order differential equation, the amplifier gain G_k (in dB) is given by integrating eq. (4) over the amplifier length L.

$$G_k = 0.43\Gamma_k L(N_2\sigma_{ek} - N_1\sigma_{ak}) \tag{5}$$

In the full spectrum model that we use in our numerical analysis, both forward and backward components of ASE are included. In eq.(3) however, the propagation of the signal and noise is described in only positive direction. Fig. 3.1 shows a tree diagram of several (not all) possible amplifier models. For CW beams, or those modulated at frequencies greater than 10 kHz [23], [50], the time derivative in eq. (2) can be set to zero, reducing the problem to the steady-state case. For steady-state models, the diagram branches between models that include the radial optical and erbium distributions, and those that utilize an effective overlap integral. Branching also occurs between models that include ASE and those that ignore it. ASE terms are required for calculating amplifier noise and gain saturation caused by ASE. ASE can be modeled as optical power in effective noise bandwidth $\Delta\nu_{eff}$. Otherwise, the full ASE spectrum could be resolved [26].

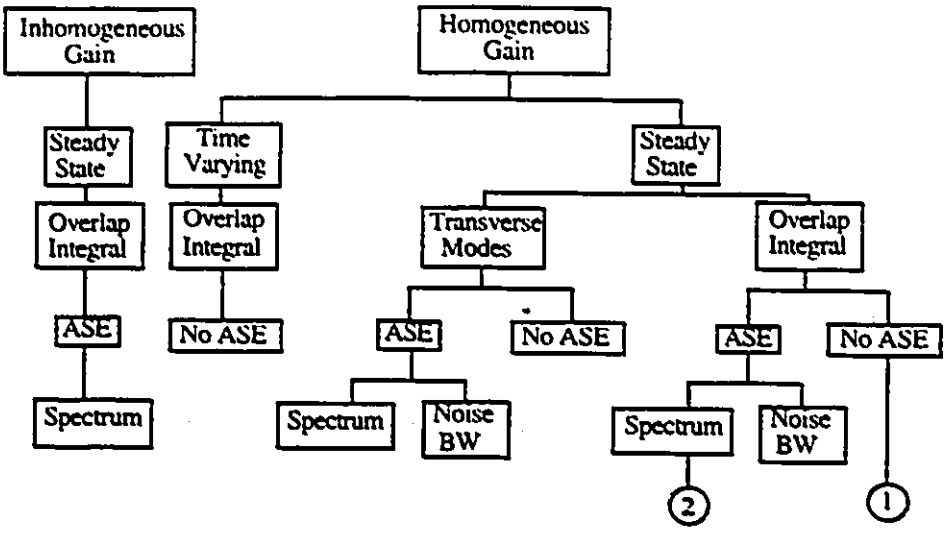

Fig. 3.1. Tree diagram of existing amplifier models. Number 1 indicates the analytical model and number 2 indicates the full-spectrum model.

In our simulation studies, we have resolved the full ASE spectrum. We have also used the effective overlap integral $\Gamma(\lambda)$. Using Γ greatly reduces the computational complexity. The models labeled as (1) and (2) in Fig. 3.1 correspond to the analytical model described in the previous chapter and the numerical full spectrum model described in this chapter, respectively.

In our numerical analysis, we used the absorption and emission cross section spectra of the erbium-doped fiber (EDF) of Fig. 2.3. The absorption and emission cross section values are related to the loss spectrum $\alpha(\lambda)$ and gain spectrum $g^*(\lambda)$ by

$$\alpha(\lambda) = \sigma_a(\lambda)\Gamma(\lambda)N_t$$

$$g^*(\lambda) = \sigma_e(\lambda)\Gamma(\lambda)N_t \qquad (6)$$

where $\Gamma(\lambda)$ is the overlap integral between the optical mode and the erbium ions and N_t is the density of erbium ions. The absorption and emission cross sections are $\sigma_a(\lambda)$ and $\sigma_e(\lambda)$, respectively.

One of the difficulties in characterizing erbium-doped fibers is to accurately measure $\sigma_a(\lambda)$ and $\sigma_e(\lambda)$. In Appendix III.A, the measurement techniques are described for loss and gain spectra. Different methods are discussed for extracting cross section values from the measured loss and gain spectra.

Written in terms of these new parameters, the amplifier propagating equation (3) becomes

$$\frac{dP_k}{dz} = (\alpha_k + g_k^*)P_k(z) + g_k^* m h\nu_k \Delta\nu_k - (\alpha_k + l_k)P_k(z) \tag{7}$$

The additional loss term l_k has been added to the propagation equation to account for excess fiber loss. The set of equations is completed with the steady-state approximation to the metastable population, which from (2) is

$$\frac{N_2}{N_t} = \frac{\Sigma_k \frac{P_k(z)\alpha_k}{h\nu_k \zeta}}{1 + \Sigma_k \frac{P_k(z)(\alpha_k + g_k^*)}{h\nu_k \zeta}} \tag{8}$$

The new fiber parameter, $\zeta = A_{eff} N_t / \tau$ is the ratio of ions to the metastable lifetime. The values of $A_{eff} = \pi b^2$ and τ are usually provided by the fiber provider, where b is the effective erbium radius. In the effective overlap approximation, a fiber is completely characterized knowing the gain and absorption coefficients and also ζ.

The EDFA is numerically modeled with equations (7) and (8) which are the rate equations for the population levels and pump, signal, and noise powers using

a two-level approximation. Numerically integrating the equations over the ASE bandwidth and the fiber length gives the signal gain and ASE output power.

III.3 Amplifier Gain for WDM Signals and Gain Equalization

III.3.1 Equalizer Configuration and Operation Principles

We notice that, the arbitrary characteristics:

$$H(\omega) = \Sigma_{k=0}^{N-1} c_k exp(-jk\omega\tau) \tag{9}$$

can be generally constructed by a tapped delay line. Fig. 3.2 shows a 7-tap coherent optical transversal filter configuration that can have a frequency response expressed by (9), where N is equal to 7.

The filter operates based on coherently combining the tapped signals. An N-tap filter can be designed so that it produces the exact desired frequency responses at N arbitrary frequencies. We use this feature to equalize the gain of the amplifier at N signal wavelengths and design the gain equalizer parameters for a system consisting of 7 WDM signals.

Depending on the unit delay-line length, the unit delay-time, τ is determined. The frequency characteristic has a periodic shape every $1/\tau$ Hz. By selecting the filter response at N arbitrary frequencies; from (9), a set of N equations is formed. The solution set determines the complex tap coefficients c_k's. The number of taps N is also the maximum number of the frequencies at which the filter response can exactly be selected. The spacing between these N frequencies can assume any value. If the wavelength channels are located at N designated wavelengths and the

modulation bandwidth of these signals is typically very much smaller than their carrier frequencies, we only need to compensate for the gain imbalance at these frequencies. Complex tap coefficients c_k's can be set so that the gain imbalance for these frequencies is compensated for.

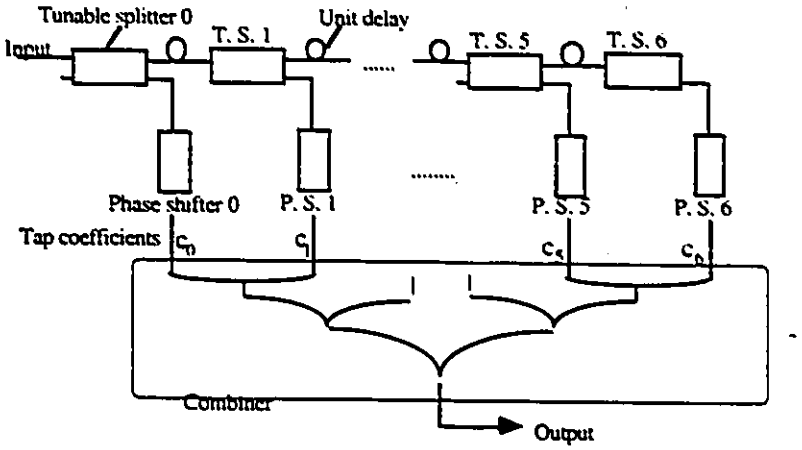

Fig. 3.2. A seven-tap coherent optical transversal filter configuration.

In multi-stage amplifiers where the spontaneous noise must pass through a cascade of EDFAs, the noise finally dominates the amplifier saturation and decreases the signal gain. Another advantage of transversal filter equalization is that its frequency response at the middle wavelengths between the signal channels can also be controlled. The frequency response can be designed so that the spontaneous noise at the middle wavelengths is attenuated. However, the number of the required taps is doubled. In the next section, we present the calculated tap coefficients and also the response of the gain equalizer.

III.3.2 Design Example

Fig. 3.3 shows the output power of an amplifier fed with the multi-wavelength input signal consisting of 7 different wavelength channels (1530, 1535, 1540, 1545, 1550, 1555, 1560 nm). The input power at each wavelength is adjusted to 50 μW. The amplifier is forward pumped with 60 mW of light at 980 nm. The length of the erbium-doped fiber is set to 10 m. The erbium fiber is codoped with Al and Ge, and has core radius 2.1 μm, erbium radius 1.7 μm, and NA of 0.18, and 340 ppm Er. A metastable decay time of 12 ms is assumed. Cross-sections are given in Fig. 2.3. The amplifier gain at 7 frequencies corresponding to (1530, 1535, 1540, 1545, 1550, 1555, 1560 nm) is (20.41, 18.34, 15.27, 15.39, 16.80, 15.51, 13.82 dB), respectively. With only one signal present at 1530 nm, the gain of the amplifier is 35 dB. In multi-wavelength operation mode, the amplifier is saturated by the multiple signals and exhibits a lower gain. In order to reject the spontaneous noise between the wavelength channels, we would set the frequency response of the filter at wavelengths (1527.5, 1532.5, 1537.5, 1542.5, 1547.5, 1552.5, 1557.5 nm) to -40 dB. These wavelengths are located exactly between signal wavelengths. Therefore, designing a 14-tap filter is required. The magnitude squared of the filter response is set so that the overall power gain of the amplifier and the equalizer at 7 signal wavelengths is identical and the noise at the midband frequencies is attenuated by 40 dB.

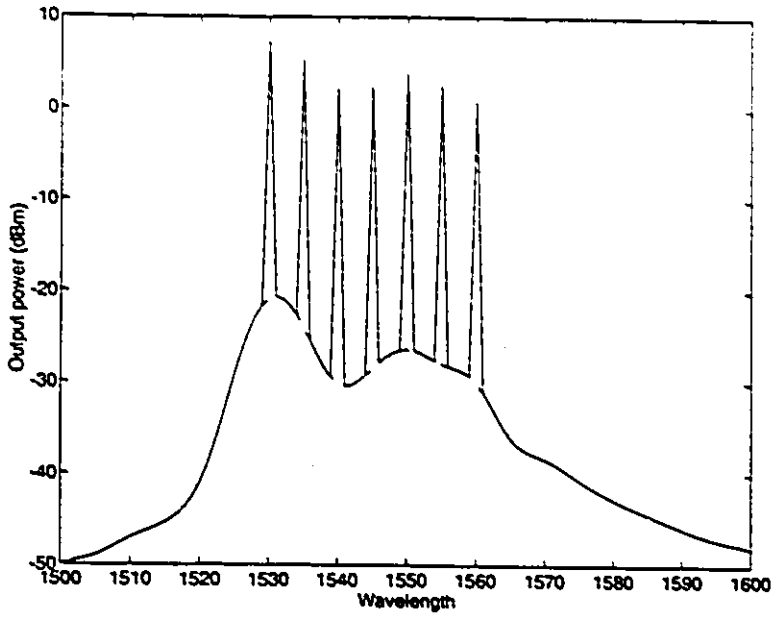

Fig. 3.3. EDFA output signal and ASE power.

Fig. 3.4 shows the calculated complex tap coefficients of the filter. By choosing the unit delay-line of length 79.43 m, the frequency response of the filter would have a period of 3.7769 THz. This corresponds to the bandwidth of 30.05 nm around 1545 nm. In the choice of unit delay-line length two parameters have been considered. First, the frequency corresponding to the wavelength 1527.5 nm is an integer multiple of the frequency period, 3.7769 THz. Second, the frequency period that is chosen as filter bandwidth is made large enough. In this case, the corresponding bandwidth around 1545 nm is 30.05 nm. The spacing between the channels except for the filter tap values do not affect the other parameters as long as the desired filter bandwidth is the same. In fact, smaller channel spacings for the same number of channels lead to a narrower-bandwidth filter (smaller $\frac{1}{\tau}$). This leads to longer unit delay-lines thereby easing manufacturability.

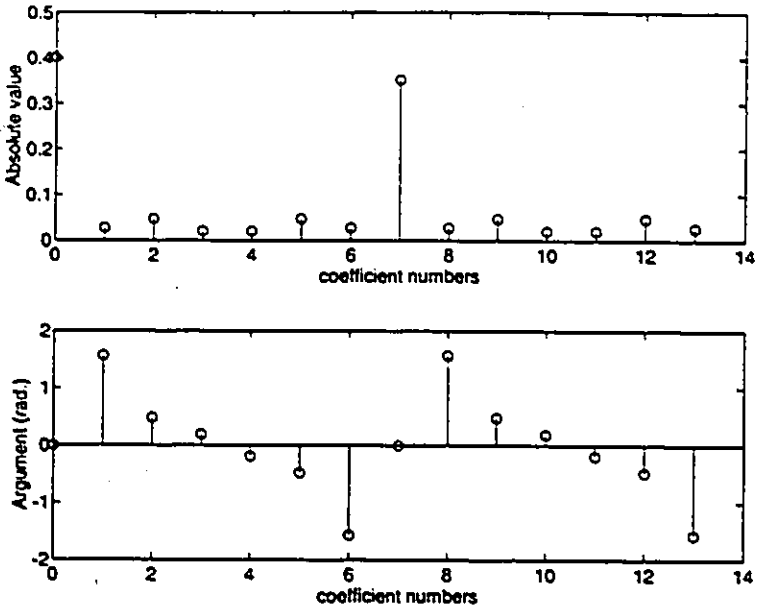

Fig. 3.4. Filter tap coefficients.

III.3.3 Results

The calculated frequency response of the gain equalizer for the interval of 1527.5 to 1560 nm is shown in Fig. 3.5(a). The phase response of this filter is shown in Fig. 3.5(b). As the figure depicts, the phase response of the equalizer at all the channel signals is linear. The output power spectrum after the gain equalization is plotted in Fig. 3.6. As is evident, since the spontaneous emission noise has almost the same spectrum as the signal, the noise components at these signal wavelengths (1530, 1535, ... (nm)) are also equalized. The figure shows that, the noise at the middle wavelengths (1532.5, 1537.5, ... (nm)) is attenuated. The overall signal gain at all signal wavelengths is equal.

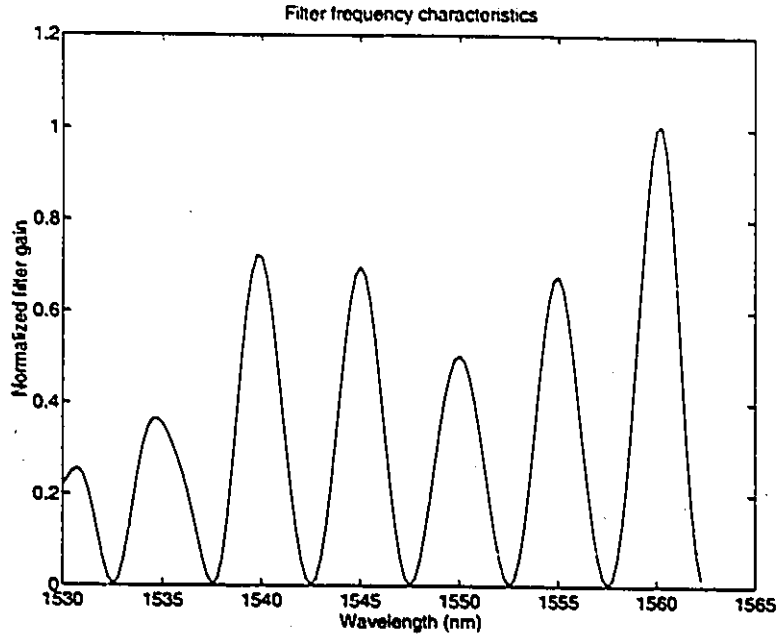

(a)

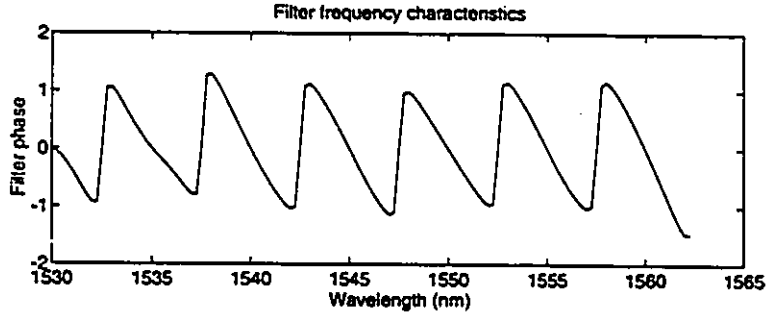

(b)

Fig. 3.5. (a) Frequency characteristics of the gain equalizer, $|H(\omega)|^2$.
(b) Phase response of the gain equalizer.

By a 7-tap filter, we can still equalize the gain of the amplifier at 7 signal frequencies. However, the amount of noise that gets through to the next stage in the latter case would be larger. By calculating the area under $|H(\omega)|^2$ for two

cases, we notice that the 14-tap equalizer will attenuate the noise by 3.1 dB more. Also note that even for the 7-tap equalizer the noise is rejected by 2.3 dB more compared to an equalizer that flattens the entire band.

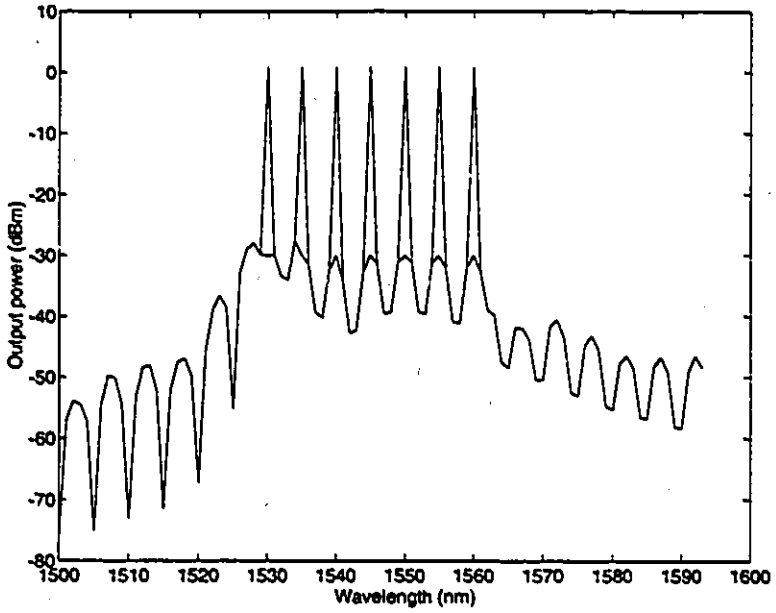

Fig. 3.6. Output signal and noise power spectra after the gain equalizer.

As we explain in the next chapter, the noise figure of an EDFA is typically dominated by signal-spontaneous beat noise and spontaneous-spontaneous beat noise. Spontaneous-spontaneous beat noise which dominates at lower input powers depends on the total noise spectrum so that it can be reduced by optical filtering. At higher input powers, signal-spontaneous beat noise dominates. This noise component depends on the noise spectral density only at the signal wavelength so that it can not be reduced by optical filtering. For the design example of 7 signals, the noise figure at 1550 nm is 3.6 dB. Since this is dominated by signal-spontaneous beat noise for the large input signal power, the difference in noise figure between the filtered and unfiltered case is less than 0.1 dB. However, when

only one signal is present, the noise figure improves from 5.3 dB for the unfiltered case to 3.5 dB for the filtered case. The most significant advantage of the noise filtering is in networks with cascaded amplifiers where the filtering reduces the input noise saturation of downstream amplifiers.

III.4 Equalizer Realization

III.4.1 Waveguide Delay-Line Filters

Optical transversal filters using coherent interference can have arbitrary tap-weight coefficients and can process signals without an inherent combining power loss. Waveguide delay-line filters in contrast with fiber delay-line filters can operate stably and the delay can be precisely determined. Optical signal processing using waveguides as a delay medium has the advantage of being able to process broadband signals because of their large available bandwidth. The results of experimental lowpass and highpass filters using silica-based single-mode optical waveguides monolithically integrated on silicon substrates were reported in [83]. Silica-based single-mode optical waveguides have a low propagation loss and an extremely low fiber coupling loss thanks to compatibility with single-mode optical fibers. Monolithic integration ensures short and precise delay-lines and many taps. To coherently combine tapped signals, the optical carrier phase of each tapped signal is adjusted by a phase shifter. By using tunable optical power splitters and phase shifters, it is possible to produce complex tap coefficients expressed by electric-field amplitude and carrier phase of the tapped signals.

III.4.2 Practical Performance Issues:

Signals introduced to the filter are delayed, tapped, weighted and then coherently combined. As seen from eq. (9), the filter characteristics depend on how the signals are delayed and weighted. The signals are delayed using optical-waveguide delay lines. The tapped delay-line structure consists of an optical waveguide with taps distributed at constant intervals along its length. Tap weighting coefficients c_k's are complex coefficients. Tapping and weighting functions are done by the optical components: tunable splitters and phase shifters. Tunable splitters distribute optical signals to taps whose electric-field amplitude distribution ratio corresponds to the ratio of the absolute value of the complex coefficients. Phase shifters shift the optical carrier phase of the tapped signals corresponding to the argument of the complex coefficients. The third essential function in the operation of this filter is the coherent combining of the weighted-tapped signals. The tapped signals are combined by a tree of 2x2 couplers. For a 3-dB coupler, the relationship between the input and output complex electric field strengths is represented by the matrix:

$$\begin{pmatrix} \frac{1}{\sqrt{2}} & \frac{-j}{\sqrt{2}} \\ \frac{-j}{\sqrt{2}} & \frac{1}{\sqrt{2}} \end{pmatrix}$$

As it can be seen, if the 90-degree shift between two inputs is taken care of, there will be no combining loss for two coherent input signals of the same amplitude and phase. If an optical signal of unity power is equally splitted into N branches, the amplitude of the signals at each branch is going to be $1/\sqrt{N}$. If these signals have the same phase and are combined, the amplitude of the resulting signal will be $N/\sqrt{N}$, of course without considering the coupling loss. Coupling adds a factor of $1/\sqrt{N}$, and therefore, the resulting signal will have the same

unity power. Therefore, no loss is anticipated for N coherent signals of the same amplitude and phase combined through a tree of couplers. If these signals are combined noncoherently, a $[10log(N)]$ dB power loss is unavoidable.

In the case of the equalizer being discussed, the amplitude and phase of the tapped signals, although known, are not the same. This will introduce some power loss which is much less than noncohernt combining loss, $[10log(N)]$ dB, but not zero. In other words, because of the difference between the amplitude and phase of the tapped signals, the amplitude of the signal at the wavelength-peak of the filter 1560nm is less than 1. The power ratio of the tapped optical signals corresponds to the ratio of the squared absolute value $|c_k|^2$ of the filter coefficients. Therefore, the complex coefficients are normalized so that the sum of the squared absolute value of these coefficients is one. The values of these coefficients determine the amplitude of the signal at the filter wavelength-peak. For the normalized coefficients, the output signal amplitude at the wavelength-peak 1560 nm (see Fig. 3.5(a)) is $(1.44/\sqrt{14})$. This corresponds to 5.09 dB power loss, whereas noncoherent combining would have produced $10log(14) = 11.46$ dB power loss.

This loss depends on the shape of the filter and is further reduced if the filter response does not differ very much from one wavelength to another. For example, the gain of the same EDFA for 7 input signals of 20 μW power at wavelengths 1538, 1541, 1544, 1547, 1551, 1554, 1557 nm is 20.61, 21.51, 21.69, 20.99, 19.92, 19.98, and 18.35 dB. A filter with the same number of taps (14) can be designed to equalize the signal powers at these wavelengths. We found that the output signal amplitude at its wavelength-peak (1557 nm in this case) is $2.92/\sqrt{14}$. This corresponds to 2.17 dB power loss.

For the waveguide in [83], a propagation loss of 0.25 dB/cm has been reported. Considering a unit delay-line length of 80 μm, this loss would be negligible. It is also reported that the splitting operation of the tunable splitters has a broad bandwidth of over 20 nm. Concerning the degradation of the filter performance due to the deviations of the power coupling ratio and the delay-line lengths, it is observed that the performance was more sensitive to deviations of delay-line lengths. However, delay-line deviations by 1% do not degrade the filter performance. Waveguides with deviations within a wavelength order do exist. Therefore, degradation caused by imprecise delay-line lengths need not be considered.

In short, we propose a new type of wideband filter based on the reported narrowband filter. The reported results suggest the realization feasibility of such a gain equalizer.

III.5 Conclusions

In this section, we proposed a tunable coherent optical transversal filter as a gain equalizer. Since depending on the amplifier conditions such as the pumping power and the gain saturation conditions, the gain imbalance of each amplifier is different, tunable equalization is desired. A fixed gain equalizer is designed for a particular system and amplifier parameters, i.e., input power, pump power, etc.. With a slight change in these parameters, the equalizer needs to be redesigned. However, tunable equalizers can be adjusted according to these changes. Although tunable, it is extremely difficult to make an adaptive optical equalizer, therefore, the gain profile based on which the tunable equalizer is tuned has to be preserved to make the equalization effective. A tunable coherent optical transversal gain

equalizer is presented that operates based on coherently combining tapped signals. We showed that, an N-tap equalizer provides a separate control over the gain at N arbitrary wavelengths. By doubling the number of the taps, we benefit from the available independent control over 2N arbitrary frequencies and attenuate the spontaneous noise at the midband wavelengths. The results show that, the noise is rejected by more than 5 dB. The design parameters and the results for gain equalization of an EDFA are presented.

Appendix III.A

Fiber Cross Section Measurements

III.A.1 Fiber Cross Section Values

The absorption and emission spectra obtained from an erbium-doped fiber glass are shown in Fig. 3.A.1. The absorption and emission cross section values are extracted from the measured loss and gain spectra. The measurement methods are described in the following.

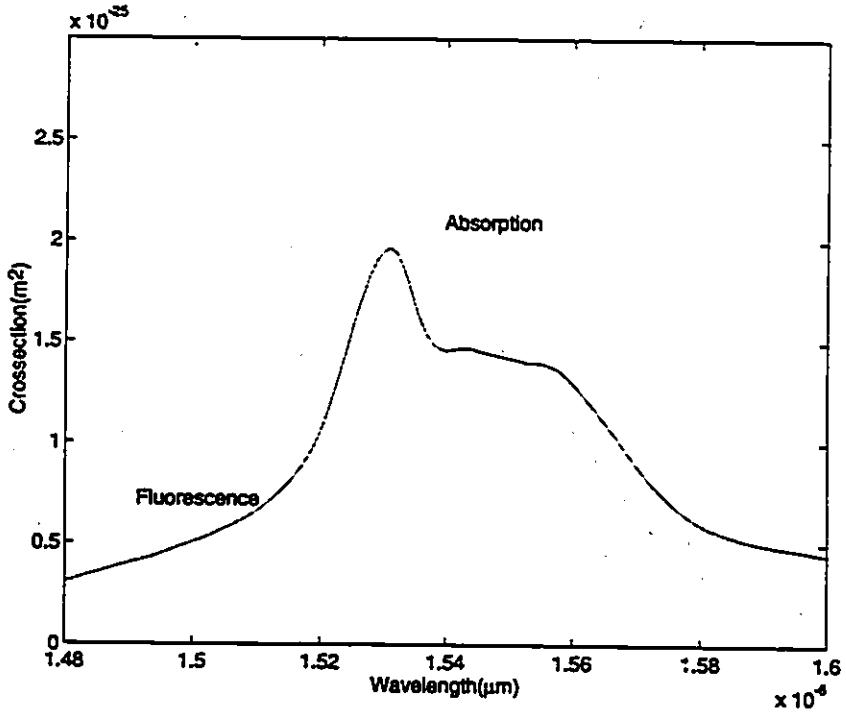

Fig. 3.A.1. Fluorescence (emission) and absorption cross sections around $\lambda = 1.53\mu m$.

Cross section values can be calculated from the loss and gain spectra by eq. (6) of this chapter. However, studies show that, the assumption of a constant Γ_k is not valid, unless b the radius of the doped region is smaller than beam radius w in a Gaussian optical mode profile $i_k = (1/\pi w^2)exp(-r^2/w^2)$. Under this condition, the optical intensity is nearly constant through the doped region. The beam radius for different wavelengths and a certain core radius can be calculated by [59]:

$$w = a[0.65 + \frac{1.619}{V^{3/2}} + \frac{2.879}{V^6}] \quad (1)$$

where $V = \sqrt{n_1^2 - n_2^2}(2\pi/\lambda)b$, and n_1 and n_2 are the refractive indicies of core and cladding, respectively. For an erbium radius of b, the value of Γ can be calculated by [26]: $\Gamma = 1 - e^{-2b^2/w^2}$.

III.A.2 Measuring absorption and emission cross-section profile of erbium-doped fiber

Eq.s (7) and (8) of this chapter indicate that only four parameters, $\alpha(\lambda)$, $l(\lambda)$, and $g^*(\lambda)$, and ξ, have to be measured in order to use a spectrally resolved, large-signal amplifier model that included the effects of amplifier self-saturation on ASE. A white-light source was used in fiber cutback measurements of $\alpha(\lambda)$ and $l(\lambda)$ around 1400-1650 nm. The value of $\alpha(\lambda)$ at 980 nm was provided by the fiber provider. The experimental setup for measuring the absorption spectrum is shown in Fig. 3.A.2.

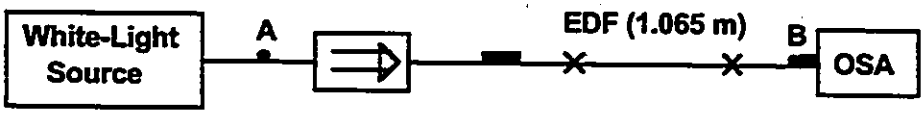

Fig. 3.A.2. Experimental setup for measurement of absorption spectrum

The fiber excess losses, $l(\lambda)$, were measured at wavelengths between the erbium absorption peaks using cutback method.

The emission cross-section profile of EDF can be measured by using a short piece of EDF (7 cm) pumped at 980 nm. A high power on the order of 70 mW can generate a broadband fluorescence spectrum in the 1500 nm band.

An experimental setup for measuring the fluorescence spectra of EDF is shown in Fig. 3.A.3. As seen, the backward ASE spectra were measured by this method.

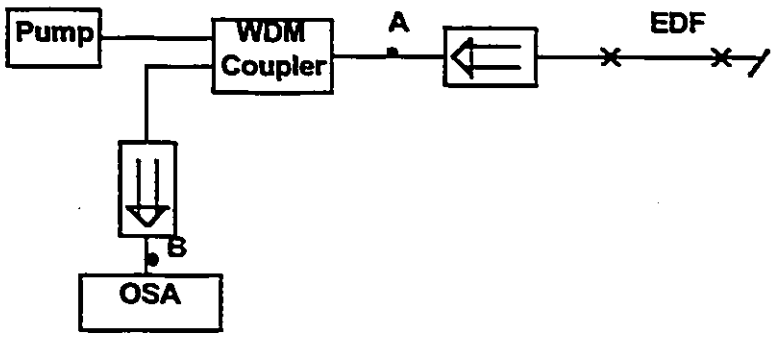

Fig. 3.A.3. Experimental setup for measurement of fluorescence spectrum

Since the WDM coupler used in Fig. 3.A.3 has a nonflat frequency response, we measured the spectra in points *A* and *B* (Fig. 3.A.4) to calibrate the measured ASE spectra. Eq. (7) of this chapter describes the spatial development of the spontaneous emission powers copropagating to the pump in the EDF. The same equation with negative signs can be used for describing the spatial development of the spontaneous emission counter propagating to the pump in the EDF. Eq. (7) can be rewritten as

$$\frac{dP_k}{dz} = P_k(z)\Gamma_k(\sigma_{ek}N_2 - \sigma_{ak}N_1) + 2\sigma_{ek}N_2\Gamma_k h\nu_k\Delta\nu_k - (\alpha_k + l_k)P_k(z) \quad (2)$$

When the EDF length is short enough, the attenuation of the pump power is negligible and can be assumed to be a constant along the EDF, and for a highly doped EDF the intrinsic fiber loss is negligible when compared with the other two terms. Thus the fluorescence power $F(\lambda)$ can be approximated as

$$P_k = 2\sigma_{ek}N_2\Gamma_k h\nu_k\Delta\nu_k L \quad (3)$$

where L is the length of EDF. Eq. (3) indicates that the fluorescence power is linearly proportional to σ_{ek}, thus the profile of the emission crosssection spectrum can be measured by normalizing the fluorescence power spectrum with $\nu\Delta\nu$ or $\Delta\lambda/\lambda^3$.

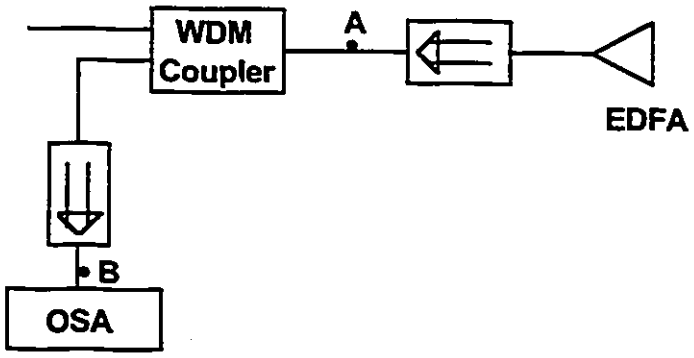

Fig. 3.A.4. Experimental setup for calibration of fluorescence spectrum

The normalized fluorescence spectra, $F(\lambda)$, were calibrated in terms of $g^*(\lambda)$ by measuring the dB change in output signal power, $\Delta G(\lambda_s)$, in the amplifier that was first unpumped, then completely inverted by pumping at 980 nm. The input

signal power was $P_s = 1\mu$W at $\lambda_s = 1557$ nm. Then, the gain spectra obtained from $F(\lambda)$ were

$$g^*(\lambda) = [\Delta G(\lambda_s)/L - \alpha(\lambda_s)]F(\lambda)/F(\lambda_s) \tag{4}$$

where L is the Er-doped fiber length.

The fiber saturation parameter, $\xi = A_{eff}n_t/\tau$, is another important fiber parameter. Since the values of τ, b, and n_t were known, ξ was easily calculated.

From eq. (6) of chapter III, if Γ and N_t are known, from $\alpha(\lambda)$ and $g^*(\lambda)$, we can directly calculate the absorption and emission cross-sections. The cross sections can also be obtained indirectly, with the Ladenberg-Fuchbauer (LF) equation, which calculates the peak cross section from integrated spectrum [81].

Fig. 3.A.1 shows the evaluated absorption and emission cross sections from the gain and loss spectra measurements described earlier.

A theory/experiment comparison of pump-induced changes in both forward and backward ASE power spectra was used to normalize the cross section values. This is the most appropriate test for cross section measurements.

Chapter IV

Amplified Spontaneous Emission

IV.1 Introduction

In chapter 2, amplified spontaneous emission (ASE) was neglected in the solution of the rate equations. As mentioned, this assumption is valid for fiber amplifiers with a gain of less than 20 dB, or an input signal power of more than -20 dBm. However, in many situations, for example preamplificaton, EDFAs are required to have a gain of more than 20 dB, and an input signal power of less than -20 dBm. In the preamplifier application, the EDFA increases the receiver sensitivity by amplifying the signal power to render the receiver thermal noise power negligible. The improvement of the receiver sensitivity is less than preamplifier gain because of the excess ASE noise generated in the amplifier. In chapter 3, the amplifier model is refined to include the effects of ASE, where the EDFA is modeled with the rate equations using a two-level approximation.

In this chapter, we describe modelling the generation of ASE. The phenomenon of amplification of spontaneous emission is an important issue, which occurs concurrently with signal amplification and degrades the signal-to-noise ratio (SNR). The number of EDFA repeaters that could be placed in a long-haul fiber link, or performance of EDFA as a preamplifier, depends on the EDFA noise characteristics.

This chapter is organized as follows. Modelling the generation of ASE is described in section 2. The ASE model is used to describe the optical signal-to-noise ratio (SNR) and noise figure (NF) of the optical fiber amplifier, in section 3. In section 4, the electrical SNR and NF are described. It is explained how some key parameters can be extracted experimentally from measured values. The BER performance of an amplitude modulated signal is also described. Experimental results are presented on the shape of ASE spectra in section 5 and conclusions are given in section 6.

IV.2 Amplified Spontaneous Emission

In the previous chapter, we described the absorption and emission cross sections of erbium, which govern the ASE spectrum.

Recall that the absorption of pump radiation produces a population inversion ($\Delta N = N_2 - N_1 > 0$) which decreases in the pump propagation direction. The signal and spontaneous emission are then amplified by stimulated emission from the population inversion according to eq.(4) of chapter 3:

$$\frac{dP(\lambda, z)}{dz} = \Gamma[N_2(z)\sigma_e(\lambda) - N_1(z)\sigma_a(\lambda)]P(\lambda, z). \tag{1}$$

Defining

$$\gamma(\lambda, z) = N_2(z)\sigma_e(\lambda) - N_1(z)\sigma_a(\lambda), \tag{2}$$

it can be seen that amplification occurs when $\gamma(\lambda, z) > 0$ and absorption occurs, otherwise.

Assuming a uniform distribution of erbium ions in the core of a single mode fiber, that supports only two fundamental modes, with N_2 ion density in the metastable level, spontaneously emits $2N_2\sigma_e(\lambda)\Delta\nu dz$ photons per second within

the bandwidth $\Delta\nu$, centered at λ over the length dz. The added spontaneous emission power within length dz of fiber is $2N_2\sigma_e(\lambda)h\nu\Delta\nu dz$. Thus,

$$\frac{dP_{ASE}(\lambda)}{dz} = 2N_2(z)\sigma_e(\lambda)h\nu\Delta\nu \tag{3}$$

From (2),

$$\sigma_e(\lambda) = \frac{\eta\gamma(\lambda)}{\eta N_2 - N_1} \tag{4}$$

where $\eta = \sigma_e(\lambda)/\sigma_a(\lambda)$. This gives:

$$\frac{dP_{ASE}(\lambda)}{dz} = 2n_{sp}\gamma(\lambda)h\nu\Delta\nu \tag{5}$$

where we have introduced the amplifier *spontaneous emission factor*:

$$n_{sp} = \frac{\eta N_2}{\eta N_2 - N_1}. \tag{6}$$

At full medium inversion, where all the atoms are in the excited state, i.e., $N_1 = 0$, the spontaneous emission factor n_{sp} reaches its minimum value of unity. In the general case where the coefficient η depends on the frequency and N_1 and N_2 are a function of z, the spontaneous emission factor can be defined through

$$n_{sp}(\lambda, z) = \frac{\eta(\lambda)N_2(z)}{\eta(\lambda)N_2(z) - N_1(z)} \tag{7}$$

The power of the amplified spontaneous noise ASE at wavelength λ leaving the fiber section dz, within a frequency band of $\Delta\nu$ is given by

$$dP_{ASE}(z + dz) = \gamma(z)[2n_{sp}(z)h\nu\Delta\nu] \tag{8}$$

The differential equation (5) is solved with integrating factor $exp\int_0^z \gamma(z')dz' = G(z)$ to give the output ASE power within a frequency band $\Delta\nu$ at frequency ν from a fiber length of L

$$P_{ASE}(L) = n_{sp} h\nu \int_0^L \gamma(z) dz + ctc \tag{9}$$

Assuming n_{sp} is constant throughout the fiber and the fact that the ASE noise power is zero at $z = 0$ where the gain of amplifier is 1 ($G = 1$) one obtains the mean output noise power in bandwidth $\Delta\nu$:

$$P^{\pm}_{ASE} = n^{\pm}_{sp} h\nu \Delta\nu (G - 1) = n^{\pm}_{eq} h\nu \Delta\nu G \tag{10}$$

where the corresponding number of ASE photons within the frequency band $\Delta\nu$ at frequency ν is

$$N(z) = n_{sp} G \Delta\nu. \tag{11}$$

n_{eq} is, by definition, the equivalent input noise, corresponding to forward and backward propagation directions. Eqs. (10) and (11) show that the generation of ASE noise power is equivalent to the amplification of n_{sp} or n_{eq} fictious input photons. In the high gain regime and complete inversion limit, the equivalent noise input becomes $n^{\pm}_{sp} \approx n^{\pm}_{eq} \approx 1$, representing a single photon in bandwidth $\Delta\nu$. In this limit, the ASE power increases linearly with the gain.

As the gain is increased, the stimulated emission by ASE is enhanced to the point where it eventually competes with the pumping rate. This competition occurs in regions located near the fiber ends (where the ASE is the highest). In these regions, the medium inversion is reduced and the amplifier gain saturates even in the absence of any input signal.

Contrary to the case of saturation by amplified signal, the effect of amplifier self-saturation by ASE cannot be entirely suppressed by increasing the pump power. This is because, according to eq. (10), any increase in the gain results in

an almost proportional increase in ASE. However, even when saturated, the amplifier gain can be increased with higher pump power. In this regime, the maximum gain eventually becomes limited by the effect of laser oscillation. Oscillation occurs when the amplifier gain is high enough to compensate for the return loss of any reflecting element of ASE. Reflections from the surface of different optical components and from Rayleigh back scattering in the fiber cannot be totally suppressed. Thus, the laser oscillation effect ultimately limits the gain. However, the amplifier gain is limited to much smaller values, for high speed (Gb/s) systems, before the power penalty due to reflection becomes unacceptable. In chapter 6, we develop a simple formula to evaluate the power penalty associated with each amplifier. In chapter 7, we discuss how a two-stage amplification where both bandpass optical filters and isolators are placed between two stages of amplifiers is the most efficient way to suppress the self-saturation in bidirectional amplifiers and to render the associated power penalty negligible.

IV.3 Optical SNR and Noise Figure

IV.3.1 Derivation of Noise Terms

The noise figure (NF) is a measure of SNR degradation from the input to the output of an amplifier. In system applications, the received SNR at the receiver end should be more than a particular value. For this reason, the ASE and NF of EDFAs should be carefully studied, whether they are used as power boosters, in-line repeaters, or preamplifiers. The ASE noise falling in the operating signal bandwidth is a major parameter in determining the overall system performance, i.e., the maximum transmission distance and bit rate.

The NF is defined through the ratio

$$NF = \frac{SNR_o^{in}}{SNR_o^{out}} \tag{12}$$

where SNR_o^{in} is the amplifier input optical SNR. An ideal detector of unity quantum efficiency, without considering the effect of electrical bandwidth, has an identical electrical SNR because the electrical quantities are proportional to the squared optical quantities. Optical SNR is useful for characterizing the EDFA performance, eventhough in real communication systems only electrical SNR is relevant. The NF of the optical amplifier is always more than unity, since the amplifier introduces ASE noise within the amplifier, $SNR_o^{out} < SNR_o^{in}$.

There are several methods of calculating the amplifier noise figure. The output of the amplifier can be treated as the superposition of the signal and white Gaussian noise [67]. To describe the electrical SNR and NF, we use this approach to calculate the BER performance of an amplitude modulated signal, in the next section. The present approach is based on the master equation approximation that calculates the noise figure for a two level system without considering the length dependence of n_{sp} [66].

For coherent light such as that from a laser operating far above the threshold, the average number of emitting photons is constant while the emission time is random. Assuming that photon emissions are independent, the statistics of photon emission is, indeed, Poisson. The photon statistics master equation describes the change of the photon number probability along the length of the amplifier. This equation can be solved through probability generation function (PGF) method [20] and [90]. Mean and variance of the number of output photons, $n(z)$ can be evaluated by calculating the first two moments. For Poisson input statistics these terms are

$$< n(z) >= G(z) < n(0) > + MN(z) \tag{13}$$

$$\sigma^2(z) = G(z) < n(0) > + MN(z) + 2G(z)N(z) < n(0) > + MN^2(z) \tag{14}$$

where $\sigma^2(z) =< n^2(z) > -[< n(z) >]^2$ is the output photon statistics variance, $< n(0) >$ is the input mean, and M is the number of modes. The results of eq. (13) and (14) are obtained for a linear amplifier. The terms G and N are functions of z and correspond to the amplifier gain and output ASE noise photon number as defined in eq. (11). In eq. (14), the first two terms contributing to the output variance are called shot noise and the last two terms are usually called beat noise. We notice this output noise is associated with the statistics of the amplified light, and not related to the square law detection.

IV.3.2 Optical SNR and NF

Consider digital communication systems. The input signal to the amplifier is a modulated signal at a bit rate $B = 1/T$. The mean of the number of the output photons is the sum of the average number of photons contributed by the signal and that contributed by the ASE noise. Thus, if the average number of ASE noise photons are subtracted from the mean output photons $< n(z) > - < n(z) >_{sp}$, the result corresponds only to the signal contribution. At the receiver end, the optical power is converted to electrical current where $P_{phot.} = P_{sig}^2$. The associated noise power is approximated by $P_{noise} = \sigma^2$. Therefore, the optical signal-to-noise ratio is defined by;

$$SNR_o(z) = \frac{<< n(z) > - < n(z) >_{sp}>_T^2}{\sigma^2(z)} = \frac{G^2(z) < n(0) >^2}{\sigma^2(z)} \tag{15}$$

In eq. (15), $< ... >_T$ denotes a time average over the bit period T, and the quantity $\sigma^2(z)$ is the noise power measured over this period. It can be seen that an ideal

detector of unity quantum efficiency, without electrical filtering, has an SNR equal to optical SNR. This means, outside the presence of thermal noise, optical SNR cannot be improved by preamplification. Thus, optical SNR provides an upper limit on the system performance.

For input signals with Poisson statistics, we have $\sigma^2(0) =< n(0) >$, and the $SNR_o(z)$ at $z = 0$ is equal to the mean, i.e.,

$$SNR_o(0) =< n(z) > \tag{16}$$

Eq. (16) shows that larger SNRs are achieved by larger input signal powers of the EDFA. This is the main reason that larger input signal powers are preferable for EDFAs as in-line repeaters. From eq. (13) and (14), the output SNR, $SNR_o(z)$ and optical noise figure can be calculated

$$\frac{1}{SNR_o(z)} = \frac{1}{< n(0) >}(\frac{1+2N(z)}{G(z)} + \frac{MN(z)[N(z)+1]}{G^2(z) < n(0) >}) \tag{18}$$

$$F_0(z) = \frac{1+2N(z)}{G(z)} + \frac{MN^2(z)}{G^2(z) < n(0) >} + \frac{MN(z)}{G^2(z) < n(0) >} \tag{17}$$

If we assume an input high enough such that $[G < n(0) >] \gg N$, the optical SNR and NF in eqs. (17) and (18) reduce to:

$$SNR_o(z) = \frac{G(z) < n(0) >}{1+2N(z)} \tag{19}$$

$$F_o(z) = \frac{1+2N(z)}{G(z)} = \frac{1+2n_{sp}(z)[G(z)-1]}{G(z)} \tag{20}$$

where n_{sp} is defined in eq. (6).

Eq. (19) indicates that the optical SNR can be simply measured by the ratio of signal power to noise power, when the noise is not too strong. And that, the

SNR even at the input of the amplifier is limited and is determined by the statistics of the amplified light.

In the high gain limit $G \gg 1$, the optical noise figure reduces to

$$F_o(z) = 2n_{sp} \tag{21}$$

Since n_{sp} is equal to or greater than unity, the optical NF of a high gain amplifier is always more than 3 dB. The 3 dB lower limit for the optical noise figure at high amplifier gains is commonly referred to as the quantum limit.

It was shown by Desurvire [19] that the spontaneous emission factor at signal wavelength λ_k decreases with increasing pump power to a minimum limit n_{sp}^{min} given by

$$n_{sp}^{min}(\lambda_p, \lambda_k) = \frac{1}{1 - \frac{\sigma_e(\lambda_p)\sigma_a(\lambda_k)}{\sigma_a(\lambda_p)\sigma_e(\lambda_k)}} \tag{22}$$

Before moving to the description of electrical SNR and NF, we mention how n_{sp} and optical NF can be calculated by easily measurable parameters, experimentally. By determining the gain G and $P_{ASE}^{out}(forward, \lambda)$ in a narrow bandwidth (e.g., $\Delta\nu = 1$ nm), the n_{sp} and n_{eq} can be evaluated. From (10), these two parameters are given by

$$n_{sp} = \frac{1}{G(\lambda) - 1} \frac{P_{ASE}^{out}(forward, \lambda)}{2h\nu\Delta\nu} \tag{23}$$

$$n_{eq} = \frac{1}{G(\lambda)} \frac{P_{ASE}^{out}(forward, \lambda)}{2h\nu\Delta\nu} \tag{24}$$

From (20), the EDFA optical NF can be determined from calculation of $G(\lambda)$ and $n_{sp}(\lambda)$

$$F_o(\lambda) = \frac{1 + 2n_{sp}(\lambda)[G(\lambda) - 1]}{G(\lambda)} = \frac{1}{G(\lambda)} + 2n_{sp}(\lambda) \tag{25}$$

IV.4 Electrical SNR and Bit Error Rate

IV.4.1 Electrical SNR

Optical SNR provides an upper limit on the system performance. It does not provide the power penalty and bit error rate floor induced by the noise while electrical SNR provides these informations.

In this section, the output of the amplifier can be treated as the superposition of the signal and white Gaussian noise [67]. The photodetector is a squaring-law device that yields a photocurrent proportional to the mean optical power. The noise to the mean power $P_{ASE} = Nh\nu B_o$ is added to the signal. From (11), the number of ASE photons at the amplifier output is given by

$$N = n_{sp}(G-1)\Delta\nu = n_{eq}G\Delta\nu.$$

The process of square-law detection and the determination of photocurrent noise spectral density is a well-known problem in electrical engineering [67].

In the following, we will write the optical powers as their photocurrent equivalent, i.e., as the photocurrent that would be generated by detecting the optical power with a detector with a quantum efficiency η.

The photocurrent equivalent of the spontaneous emission power, at the receiver is

$$I_{sp} = \eta e P_{sp}/h\nu = \eta N(G-1)eB_o \qquad (26)$$

where P_{sp} is the received ASE noise power. After square law detection in the

receiver, the received signal power is given by:

$$P_s = (I_s)^2.$$

The noise terms are:

$$N_{shot} = 2B_e e(I_s + I_{sp}) \tag{27}$$

$$N_{s-sp} = 4I_s I_{sp} B_e / B_o \tag{28}$$

$$N_{sp-sp} = I_{sp}^2 B_e (2B_o - B_e)/B_o^2 \tag{29}$$

$$N_{th} = I_{th}^2. \tag{30}$$

Thus, the total noise is:

$$N_{tot} = N_{shot} + N_{s-sp} + N_{sp-sp} + N_{th} \tag{31}$$

In equations (27) to (31), N_{shot}, N_{s-sp}, N_{sp-sp}, and N_{th} indicate the shot noise, signal-spontaneous beat noise, spontaneous-spontaneous beat noise, and thermal noise. Electrical and optical bandwidths are expressed by B_e and B_o, respectively.

Since in high-speed amplified systems, signal-spontaneous beat noise is the dominant noise component, it is useful to describe how it can be experimentally extracted from measured optical SNR. If the optical SNR is measured in optical band B_o, for the received optical signal P_s, $P_{sp} = P_s/SNR$, and

$$N_{s-sp} = (4P_s^2 e^2/SNRh^2\nu^2)(B_e/B_o). \tag{32}$$

Since $P_{ASE} = n_{sp}h\nu B_o$, the variance of the signal-spontaneous beat noise can also be expressed by

$$N_{s-sp} = 4P_s n_{sp} B_e/h\nu. \tag{33}$$

IV.4.2 Bit Error Rate (BER)

For an amplitude modulated signal, the BER analysis based upon the Gaussian assumption was developed by S. D. Personick [71]. In this analysis, the BER is given by:

$$BER = \frac{1}{\sqrt{(2\pi)}} \frac{exp(\frac{-Q^2}{2})}{Q} \tag{34}$$

where Q (which we shall refer as Personick's Q factor) is given by:

$$Q = \frac{< i_1 > - < i_0 >}{\sqrt{N_{tot}(1)} + \sqrt{N_{tot}(0)}}. \tag{35}$$

The quantities $< i_1 >$, $< i_0 >$ are the mean photocurrents associated with a '1' and '0'; $N_{tot}(1)$, $N_{tot}(0)$ are the averaged standard deviation from the mean values. A BER of 10^{-9} requires $Q = 6$. Equations (26)-(35) form the basis on which the performance of the amplifier systems is evaluated.

IV.5 Experimental ASE Spectra

The ASE power spectrum closely emulates the amplifier gain spectrum. Thus, it provides useful information on the EDFA operating characteristics depending on , for example, the pump and signal power. In this section, we demonstrate the ASE spectra of an EDFA under different operating conditions corresponding to moderate- and high-inversion levels. The experimental results show that, within the 1550 nm window, the gain slope could be positive or negative depending on the inversion level (Figs 4.1-4.6).

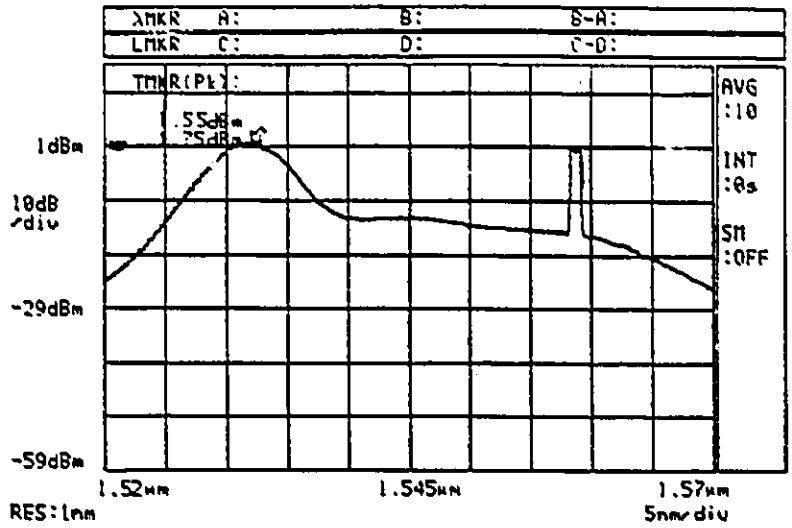

Fig. 4.1. ASE spectrum for $P_s = -30$ dBm.

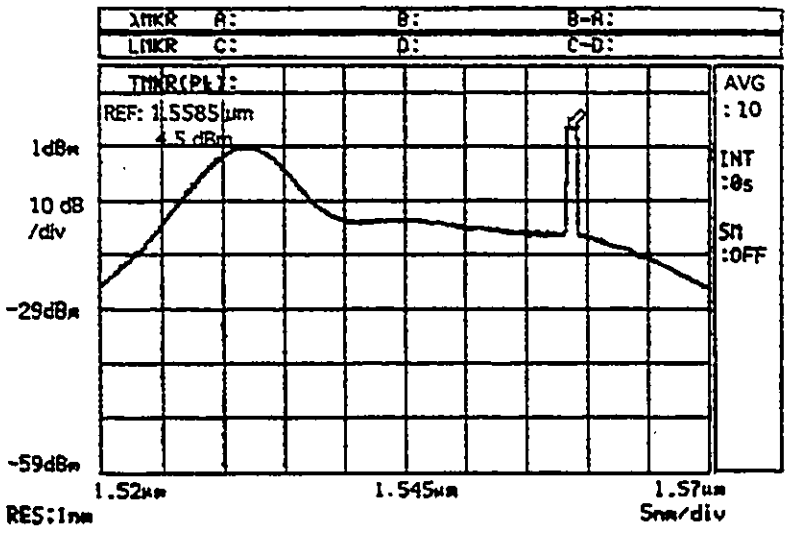

Fig. 4.2. ASE spectrum for $P_s = -25$ dBm.

As seen, there is a strong peak around 1530 nm, when EDFA is operating at high-inversion regime. Small input powers correspond to high-inversion levels. As the input power increases the 1530 nm peak vanishes.

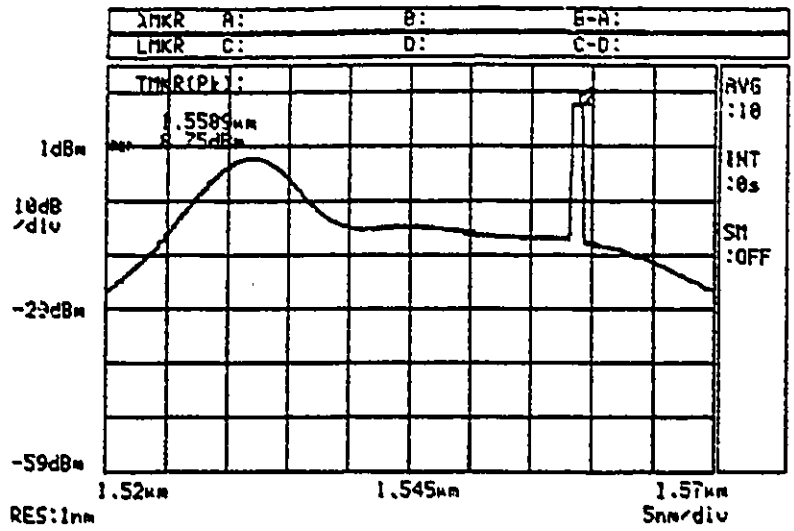

Fig. 4.3. ASE spectrum for $P_s = -20$ dBm.

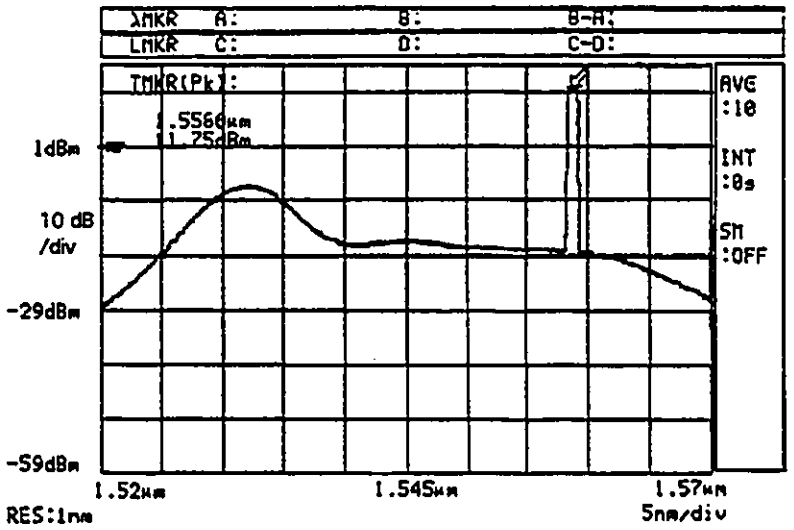

Fig. 4.4. ASE spectrum for $P_s = -15$ dBm.

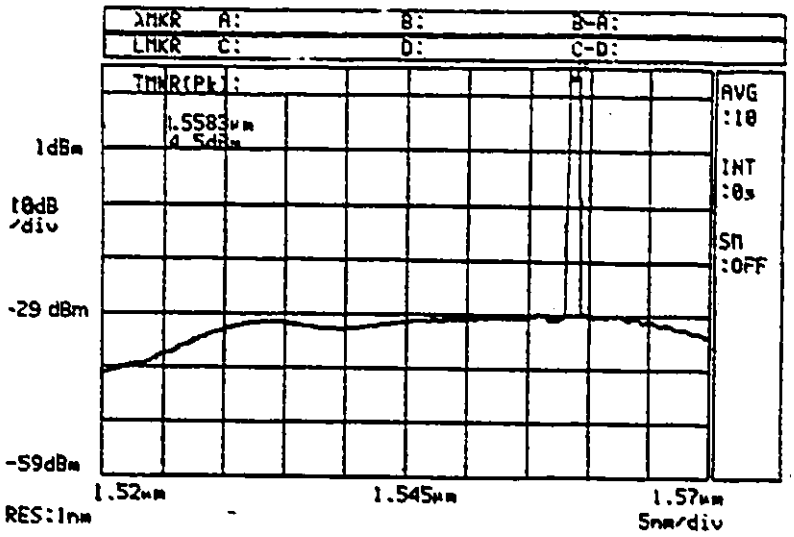

Fig. 4.5. ASE spectrum for $P_s = 0$ dBm.

High input power levels, such as in Fig. 4.5, correspond to the low medium inversion. In this regime, ground level absorption dominates at short wavelengths ($\lambda = 1.52 - 1.54\mu$m), resulting in the vanishing of the main peak near $\lambda = 1.53$ nm (see Fig. 4.1 and 4.2, for example).

We also measured the ASE spectra for two wavelength-division multiplexed (WDM) signals at 1552 and 1542 nm (Fig.s 4.6, and 4.7). The same trend was observed. This observation is the basis of the proposed method for equalizing both amplifier gain and SNR within the 1550 nm window. This method is discussed in the next chapter.

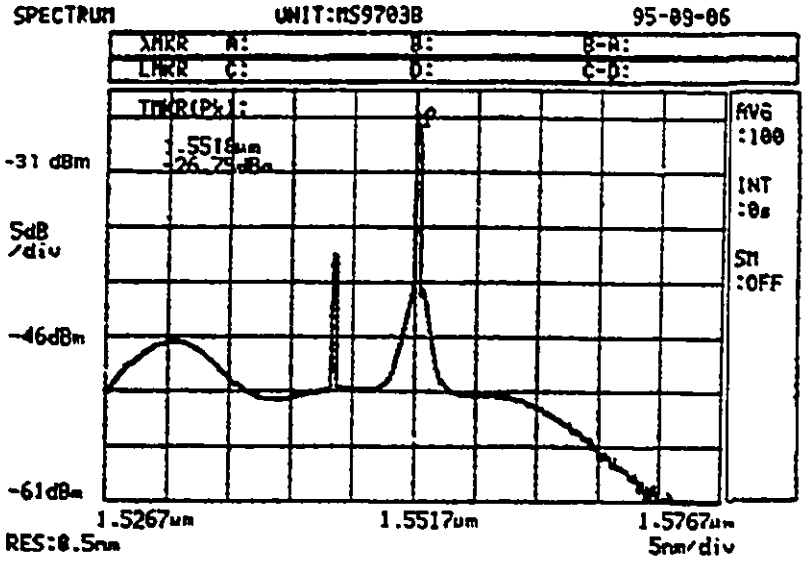

Fig. 4.6. ASE spectrum for $P_s = -30$ dBm at both wavelengths.

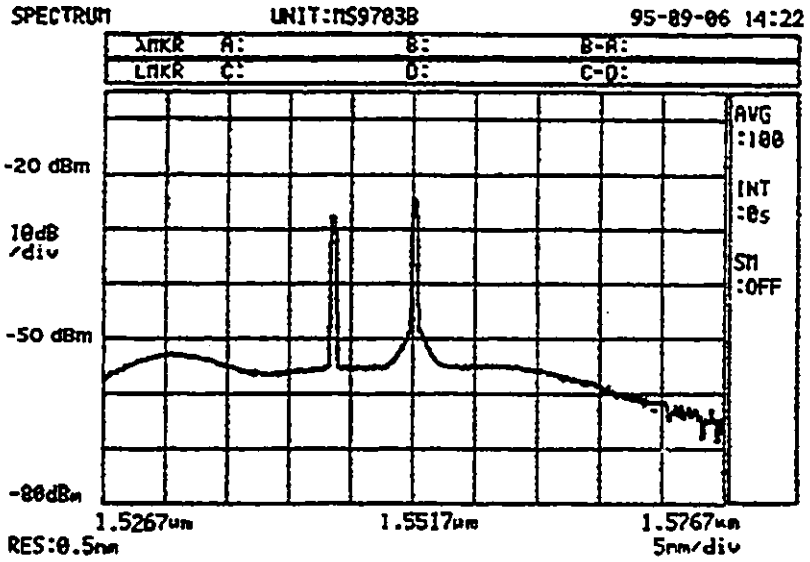

Fig. 4.7. ASE spectrum for $P_s = -20$ dBm at both wavelengths.

IV.6 Conclusions

In this chapter, expressions are given for the ASE power of the EDFA, its spontaneous emission factor, and the noise figure. As the gain increases, n_{sp} decreases to unity, and the NF approaches 3 dB. A simple expression is given for the BER performance evaluation of an amplitude modulated signal. The BER performance depends on the ASE noise power, signal power, receiver noise, and receiver electrical bandwidth. The ASE spectra emulates the spectrum of the amplifier gain. This feature is used to demonstrate that the gain slope in 1550 nm wavelength window is a function of the inversion level. The experimental results are demonstrated.

Chapter V

Gain Equalization II

V.1 Introduction

The ASE power spectrum closely emulates the gain spectrum, so it provides useful information on the EDFA operating characteristics in various pump and signal power regimes. The NF at each wavelength, on the other hand, provides a measure of optical SNR degradation from the input to the output of the amplifier at that wavelength. System applications require that a certain level of SNR be achieved at the receiver end, to guarantee a certain BER. For this reason, for WDM transmission systems, it is important that not only the gains at different wavelengths are equalized, but also all wavelength channels experience similar SNR degradations. In this chapter, we introduce a simple method that equalizes both signal power and SNR of multiple wavelength channels in WDM transmission systems. This method is based on the fact that regardless of the operating point of the amplifier (fiber length, pump power, signal power, etc.), there always exists a peak in an EDFA gain profile [101]. The existence of a peak causes the so called self-filtering effect in the amplifiers. The same phenomenon is used in single-channel long distance transmission systems without in-line optical filters. However, it degrades the performance of WDM systems due to the great imbalance of signal power and SNR among the multiple channels. It has been shown [101] that, although the gain peak can be shifted to a different wavelength by changing the inversion level of the amplifier, it seems impossible to get an absolute flat

gain spectrum by a single EDFA. We introduced the ASE spectra of an EDFA under different operating conditions corresponding to moderate- and high-inversion levels. The experimental results show that, within the 1550 nm window, the gain slope could be positive or negative depending on the inversion level.

This chapter is organized as follows. The principle of gain equalization by alternatively using high and moderate-inversion EDFAs is discussed in section 2. The performance of the compensated system is compared with that of uncompensated systems with only high-inversion or moderate-inversion EDFAs in section 3. The results show that the uncompensated system with only high or moderate-inversion amplifiers employed have different gain peaks and result in self-filtering at different wavelengths. Neither of these can satisfy the requirements of long distance WDM transmission. The proposed compensated system can mitigate the self-filtering effect and exhibits a flatter gain. The compensated system also shows potential for a longer transmission distance and signal channels upgrade. Our conclusions are presented in section 4.

V.2 Principle

In this section, we will discuss the basic principle of our proposed gain equalization approach. From eq. (5) of Chapter 3, gain $G_{dB}(\lambda)$ of a length L EDFA at a wavelength λ can be described in dB as follows [25]:

$$G_{dB}(\lambda) = 0.43\Gamma N_t L[(\sigma_a(\lambda) + \sigma_e(\lambda))\bar{n_2} - \sigma_a(\lambda)] \qquad (1)$$

where N_t is the total ion density, $\bar{n_2}$ represents the upper level population

average along the entire length of the amplifier, and $\sigma_a(\lambda)$ and $\sigma_e(\lambda)$ are the absorption and emission cross-sections of the erbium-doped fiber, respectively. The overlap between the optical mode and erbium-doped fiber core is shown by Γ. The gain difference ΔG_s of an EDFA between two signal wavelengths can be expressed as:

$$\begin{aligned}\Delta G_s &= G_{dB}(\lambda_1) - G_{dB}(\lambda_2) \\ &= 0.43\Gamma N_t L[(\sigma_a(\lambda_1) - \sigma_a(\lambda_2) + \sigma_e(\lambda_1) - \sigma_e(\lambda_2))\bar{n_2} - (\sigma_a(\lambda_1) - \sigma_a(\lambda_2))].\end{aligned} \tag{2}$$

In the cascaded optical amplifier systems, the gain profile changes along the amplifier chain due to the accumulation of ASE from stage-to-stage. If the inversion status is identical for all amplifiers, the gain difference ΔG_s among the multichannels can have little change in the case where the number of cascaded amplifiers is not too large. Therefore, we can adopt the same assumption as (1b) in [2] to illustrate our basic idea. The total gain difference $\Delta G_{cascade}$ in a cascade of EDFAs is approximately equal to:

$$\Delta G_{cascade} = N.\Delta G_s \tag{3}$$

where N is the number of amplifiers in the system.

It can be seen from eq. 3 that although the gain difference $\Delta G_{cascade}$ in a solitary amplifier can be small, the total gain variation through successive amplifiers will be large due to the accumulation of ΔG_s by the large number of EDFAs used in the system, and results in exponentially increasing inter-channel power spread [32]. This is the situation for the system with the same inversion level

cascaded EDFAs. According to [101], no matter which inversion status the EDFA operates at, a gain peak always exists at some wavelength. Hence, the gain difference between the channel at the gain peak and other channels will accumulate along the amplifier chain. In other words, there is no compensation mechanism to prevent increased gain differences in this system.

If there is a signal at the gain peak wavelength, it will become stronger and stronger, while other wavelength signals lose gain rapidly and self-filtering occurs. This effect has some benefits for single channel transmission over long distance because it can automatically compress ASE power at other wavelengths without using the optical filters. However, it is harmful to WDM applications due to its sharp and narrow self-filtering peak.

We show here that the self-filtering can be mitigated and gain difference can be reduced by alternatively using the high- and moderate-inversion EDFAs in the system. At high-inversion regime, the upper level population average $\bar{n_2}$ of an EDFA operating at high-inversion status is close to one. Suppose $\lambda_1 < \lambda_2$. Since $\sigma_e(\lambda_1) > \sigma_e(\lambda_2)$ in the wavelength region from 1550 to 1560 nm for the alumino-germania-silica fiber, then the gain difference ΔG_h between λ_1 and λ_2 in a high-inversion amplifier is larger than zero, i.e., the gain in the shorter wavelengths is larger than that in the longer ones. If the EDFA operates at moderate-inversion status, $\bar{n_2}$ is less than unity. Then, $\bar{n_2}$ can be so small to make the gain difference ΔG_m in a moderate-inversion amplifier less than zero. This means, the gain in the shorter wavelength will be less than that in the longer wavelength. Therefore, when we combine N_1 high-inversion and N_2 medium-inversion EDFAs, the gain difference ΔG_{hm} can be less than the gain difference of $N_1 + N_2$ cascaded EDFAs with the same inversion status in series (because ΔG_h and ΔG_m have opposite

signs), i.e.:

$$\Delta G_{hm} = N_1.\Delta G_h + N_2.\Delta G_m < (N_1 + N_2).\Delta G_s. \quad (4)$$

Then the total gain difference ΔG_{hm}^{tot} by alternative use of high- and moderate-inversion EDFAs will be less than the total gain difference $\Delta G_{cascade}$ by using EDFAs at the same inversion status, i. e.,

$$\Delta G_{hm}^{tot} = \frac{N}{N_1 + N_2}\Delta G_{hm} < N.\Delta G_s = \Delta G_{cascade}. \quad (5)$$

Basically, we propose a simple scheme for gain and SNR equalization in a chain of cascaded EDFAs. We show that the gain imbalance of high-inversion and medium-inversion EDFAs can compensate one another, when they are employed, alternatively. Therefore, the signal power spread and the optical SNR differentials among the channels would vary by a small value, even in a system with a large number of amplifiers.

V.3 Discussion

V.3.1 Gain Equalization by Mitigating Self-Filtering

The performances of the systems with moderate- or high-inversion EDFAs are studied and compared with the compensated systems. The evolution of signal power and optical SNR through the amplifier stages is investigated for three different systems. Here, we estimate the noise power by calculating the ASE power

within 0.1 nm optical bandwidth around the signal wavelength. This is because the ASE is the dominant noise source in lightwave communication systems that use optical amplifiers. In our numerical analysis, we use the amplifier model described in chapter III. Alumino-germania-silica fiber is assumed in this model, with a $NA = 0.18$, a fiber core radius of 2 μm, an erbium ion radius of 1.6 μm with the absorption and emission cross-sections being the same as those of the Al-Ge-Si fiber in Fig. 2.3. All our calculations in this chapter apply to this specific type of fiber. However, the conclusions can be extended to other types of silica EDFAs.

A four-channel WDM system with 2 nm inter-channel spacing is studied for comparison of three different systems. At the input of the first EDFA, the total input signal power is -7 dBm (-13 dBm per channel). The span loss between the amplifiers is assumed to be 15 dB, corresponding to 70 km transmission loss (assuming a 0.21 dB/km average fiber attenuation). All EDFAs are pumped by 980 nm lasers.

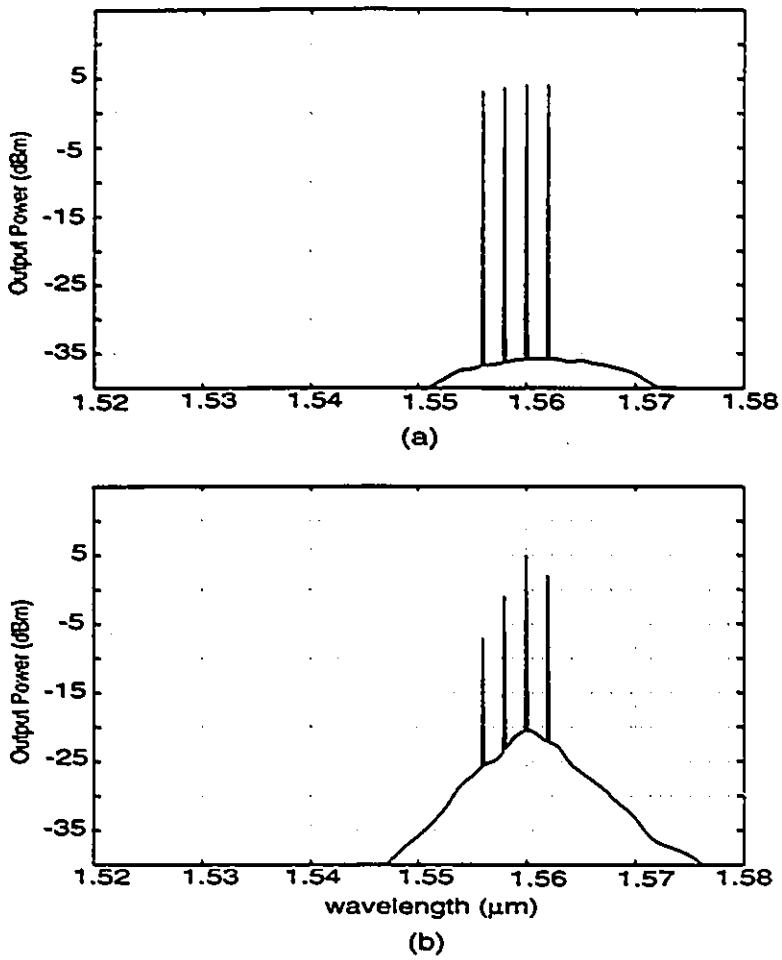

Fig. 5.1. Output spectrum of moderate-inversion EDFAs. (a) After one stage. (b) After 15 stages.

V.3.2 Systems With Cascaded Moderate-Inversion EDFAs

The moderate-inversion amplifiers are usually employed in lightwave communications systems. There are two advantages in using such systems: 1) the signal power can be automatically regulated through the cascaded moderate-inversion amplifiers; 2) the ASE peak around 1532 nm can be suppressed. However, such systems are not suitable for WDM applications due to a large signal power spread among the WDM channels.

The gain peak is around 1560 nm for a typical moderate-inversion amplifier with a fiber length of 45 m and a pump power of 60 mW. Therefore, the signal wavelengths are arranged in the region of 1556 to 1562 nm. The signal gain is wavelength-dependent. The highest gain at 1560 nm is 17.05 dB, and the lowest gain at 1556 nm is 16.2 dB. We assume a span loss of 15 dB between the amplifiers.

Fig. 5.1 (a) and (b) show the output spectrum after the first and the 15th stage moderate-inversion EDFAs. Because the gain peak is at 1560 nm, the signal at this wavelength has a higher gain and becomes much stronger than the other signal channels after cascaded amplifiers. Hence, the self-filtering occurs at 1560 nm, and the ASE peak around 1532 nm does not exist in this case.

Figs 5.2 (a) and 5.3 (a) show the changes of signal power and optical SNR along the amplifier stages, respectively. Although the gain difference in a single EDFA is only 0.85 dB, it becomes as large as 12.3 dB (close to the estimated result of 12.75 dB by equation (3) in section 2) after 15 stages of amplifiers. The SNR at 1560 nm self-filtering wavelength is 25.5 dB, while the SNR at 1556 nm becomes worse than 18.5 dB.

Consequently, systems with moderate-inversion amplifiers as in Fig.1 (a), (b) produce signal spectra with a large gain variance as the number of amplifiers grows. It has been found that the self-filtering peak will be sharper and sharper with an increase in the number of amplifiers. Therefore, systems with moderate-inversion amplifiers do not qualify for WDM applications.

V.3.3 Systems With Cascaded High-Inversion EDFAs

It has been reported that the inter-channel power spread can be suppressed when the amplifiers in the systems are operated in high-inversion status [31]. A high-inversion EDFA can produce a gain spectrum whose shape essentially follows that of the emission cross-section. Here, we arrange the four signal wavelengths in the region from 1544 to 1550 nm, which is the instinctive flat region for emission cross-section of alumino-germano silica fibers. For this high-inversion amplifier, the fiber length is shortened to 9 m and the pump power is 60 mW. The signal gain at the worst wavelength channel at 1550 nm is 17.8 dB, which can compensate the span loss of 15 dB between two amplifiers.

Fig.s 5.4(a) and (b) show the spectra after the first and the 10th stage amplifiers. Because the gain peak is at 1532 nm, the ASE peak around this wavelength becomes dominant after 10 stages of amplifiers. The evolution of signal power and SNR is given in Fig. 5.2(b) and Fig. 5.3(b), respectively. The signal power spread is only 0.3 dB after 10 stage amplifiers, but the signal power decreases greatly, resulting in SNR degrading from 40.03 dB to 12.4 dB. For a 10 Gb/s transmission system with a bit-error ratio (BER) of 10^{-14}, the optical SNR must be more than 14.5 dB [2]. Hence, the signals cannot be allowed to propagate over longer spans.

It is true that the inter-channel power spread is greatly reduced when the amplifiers are operated in a high-inversion status. However, the performance of this system shows a rapid decline in all the signals. This is because the ASE peak around 1532 nm increases very fast and eventually dominates. The self-filtering at 1532 nm compresses the ASE and signals at other wavelengths. As a

result, the system with high-inversion amplifiers is limited by the number of few EDFAs employed, unless additional optical filters are introduced, however that will increase the cost. In our calculations, the number of amplifier stages cannot be over 10 in such a system.

V.3.4 Compensated Systems With Alternatively Used High and Moderate-Inversion EDFAs

A compensated system, using alternative high and moderate-inversion amplifiers, is proposed to overcome the limit in the WDM systems where only high or moderate-inversion EDFAs are employed. It is noticed that the slopes of the gain curves are opposite for high and moderate-inversion EDFAs in the region of 1550 to 1560 nm. This implies that it is possible to get a flat gain over this wavelength area by alternatively using these two different inversion amplifiers.

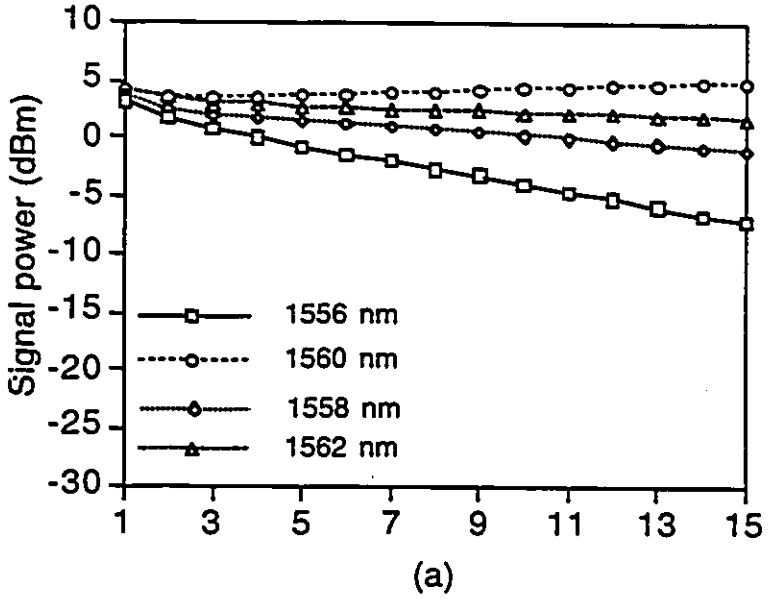

Fig. 5.2.(a) Evolution of signal power with the number of amplifiers operating at medium-inversion regime.

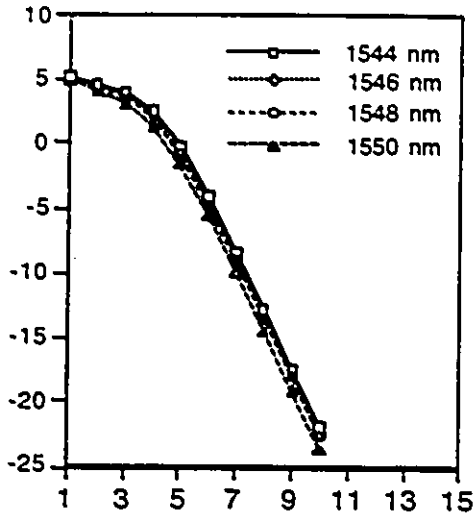

Fig. 5.2.(b) Evolution of signal power with the number of amplifiers operating at high-inversion regime.

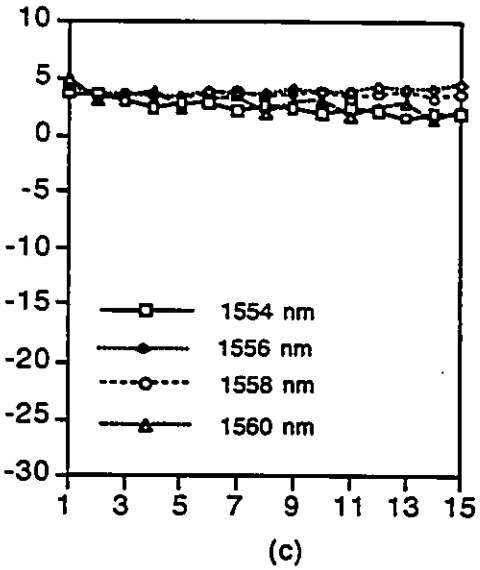

Fig. 5.2.(c) Evolution of signal power with the number of amplifiers operating at moderate- and high-inversion regime, alternatively.

It is well known that the gain profile of EDFAs is not linear. By changing the inversion status of an EDFA, its gain peak wavelength can sweep the 1550-1560 nm window [101]. Thus the gain imbalance of the EDFAs over this window can be compensated by cascading amplifiers at different inversion status. A careful design for suitable inversion status is necessary to make the gain curve similarly linear among the multichannels in order to obtain the optimum compensation effect. When the upward (moderate-inversion status) and the downward (high-inversion status) slant gain curves are combined together, a relatively flat curve can be expected.

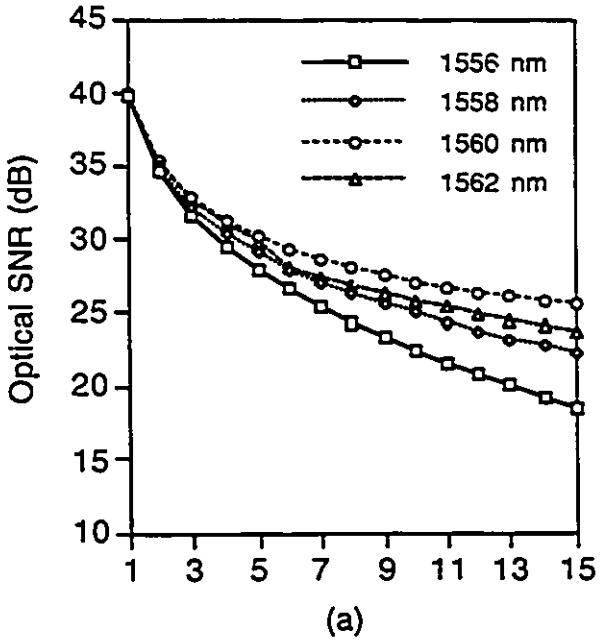

Fig. 5.3.(a) Evolution of SNR with the number of amplifiers operating at moderate-inversion regime.

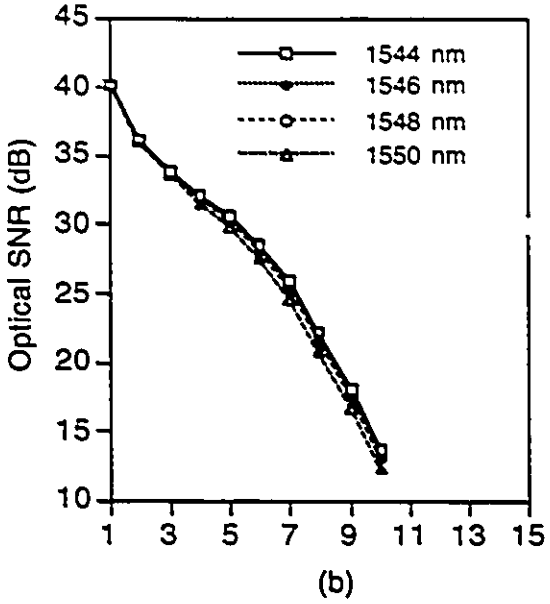

Fig. 5.3.(b) Evolution of SNR with the number of amplifiers operating at high-inversion regime.

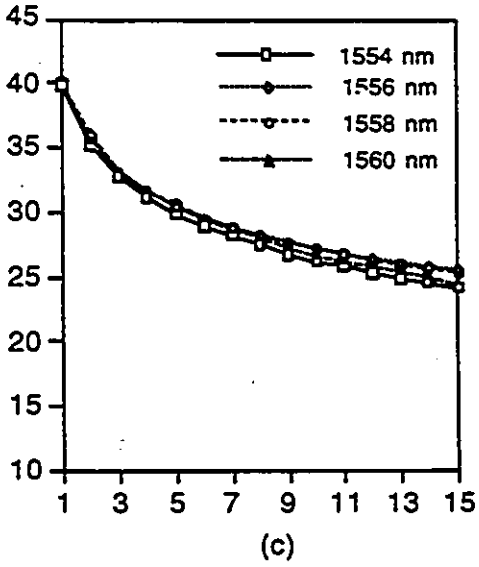

Fig. 5.3.(c) Evolution of SNR with the number of amplifiers operating at moderate- and high-inversion regime, alternatively.

There are three factors that should be considered when the compensated systems are designed. First, the suitable high- and moderate-inversion levels of EDFAs need be carefully selected to have a linear gain profile. The fiber length and pump power are chosen by calculation to be 9 m and 60 mW for the high-inversion amplifier, and 40 m and 60 mW for the moderate-inversion amplifier, respectively.

Second, the signal wavelength should be at the region where the gain curves of high and moderate-inversion amplifiers are closest to a linear shape. Therefore, the signals are arranged from 1554 to 1560 nm in this compensated WDM system.

Third, the slopes of gain curve of high and moderate-inversion amplifiers are usually unequal, so it is necessary to find the optimum ratio for the number of high-inversion EDFAs to the number of moderate-inversion EDFAs used in the compensated systems. It is found by calculation that when one high-inversion EDFA is combined with two moderate-inversion EDFAs, the gain difference can be reduced to a minimum in this compensated system.

Fig. 5.5 shows the output spectrum in the compensated system after 15 stages of high and moderate-inversion amplifiers are alternatively used. The high-inversion EDFAs are used in the 2nd, 5th, 8th, 11th and 14th stage of the EDFA chain, and others are moderate-inversion EDFAs. It can be seen that the favorite gain wavelength is neither at 1532 nm that was most favored by the cascaded high-inversion amplifiers, nor at 1560 nm that was most favored by the cascaded moderate-inversion amplifiers, but it is around 1556 and 1558 nm. A flat gain profile among the multichannels is obtained, as expected.

The evolution of signal power variations along the amplifier stages in the compensated systems is shown in Fig. 5.2(c). The maximum signal power is 4.42

dBm at 1556 nm, while the minimum signal power is 1.95 dBm at 1554 nm, only 2.47 dB signal power difference after 15 stages of amplifiers in this system. Fig. 5.3(c) shows the changes of SNR differentials with the amplifier stages. The highest SNR at 1556 nm is 25.4 dB, and the lowest SNR at 1554 nm is 24.1 dB, the SNR difference is 1.3 dB after 15 stages of amplifiers.

It can be seen from Fig. 5.2(c) and Fig. 5.3(c) that a longer transmission distance is possible for the compensated system. When the optical SNR is decreased with the transmission distance to 14.5 dB, required for a 10^{-14} BER in a 10 Gb/s communication system, the number of amplifiers is allowed to be larger than 30 in the compensated systems, corresponding to over 2000 km propagation distance (assuming 0.21 dB/km fiber loss). In this case, the inter-channel power spread is 5.4 dB.

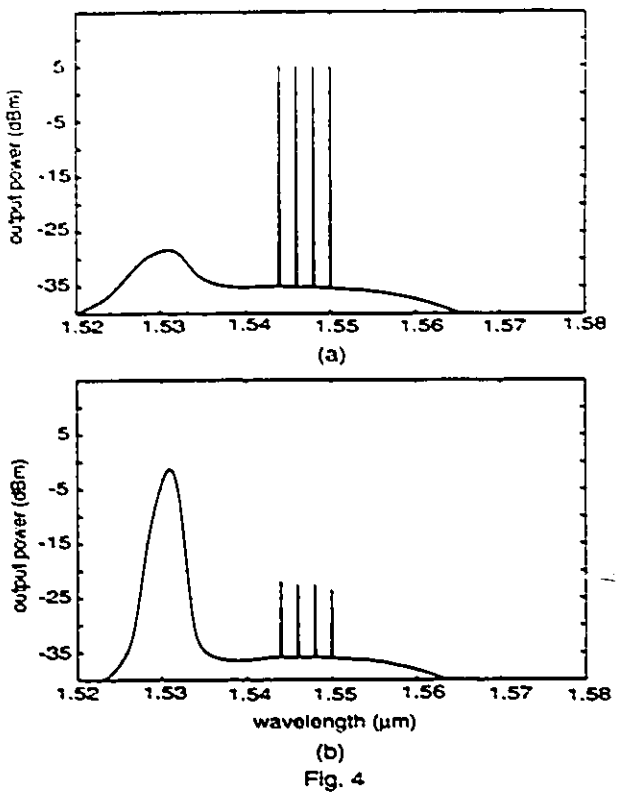

Fig. 5.4. Output power spectrum of cascaded high-inversion EDFAs. (a) After one stage EDFA. (b) After 10 stages of EDFA.

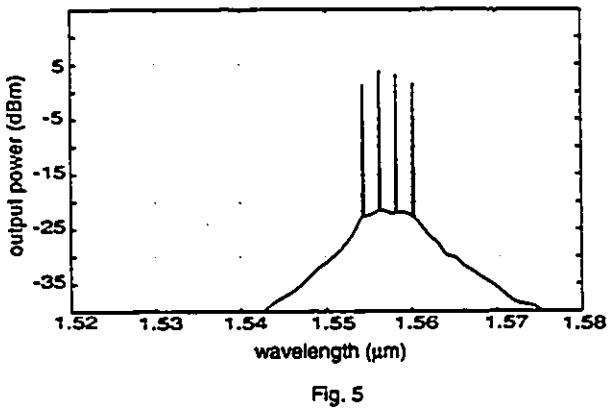

Fig. 5.5. Output power spectrum of 15 cascaded high- and medium-inversion EDFAs.

In order to compare the performance of the compensated system to uncompensated ones where only high-inversion amplifiers or moderate-inversion amplifiers are employed, we define the criteria that signal power spreads of more than 10 dB or optical SNRs less than 14.5 dB are not acceptable. Based on these criteria, the number of amplifiers in the systems with high-inversion amplifiers is limited to 10, and limited to 15 in the systems with moderate-inversion amplifiers. However, this number can be extended to more than 30 in the compensated system.

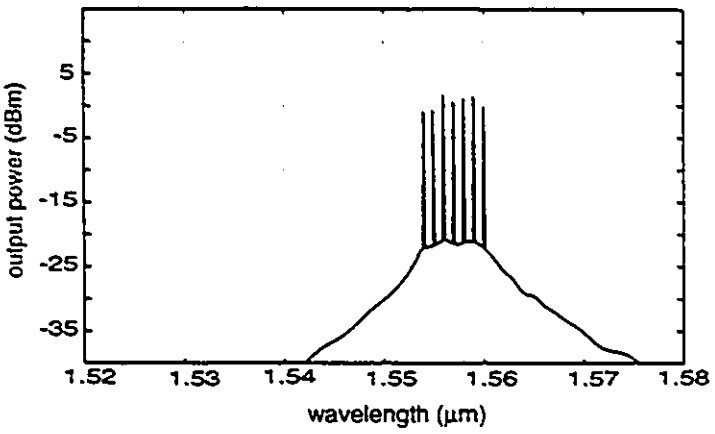

Fig. 6

Fig. 5.6. Output power spectrum of cascaded high-inversion EDFAs, for more signal channels.

The ability to increase the number of the signal channels in the compensated systems is also studied. Fig. 5.6 shows the output spectrum after 15 stages of amplifiers when three additional channels are added into the compensated system. The signal power spread only increases to 2.7 dB, while the optical SNR degrades

to 21 dB. This means that the compensated system has potential for upgrading the signal channels.

In summary, there are two obvious advantages for using EDFAs with two inversion status instead of the same in the cascaded amplifier systems: 1) the self-filtering effect is mitigated, leading to equalization of the signal power and SNR among the multichannls; 2) the 1530 nm ASE peak is removed with no additional optical filtering.

V.4 Conclusions

A simple method, using alternative moderate-inversion and the high-inversion EDFAs, has been proposed to mitigate the self-filtering effects and equalize the signal powers and SNR in WDM transmission systems with cascaded amplifiers. Compared with the uncompensated systems with only high-inversion or moderate-inversion amplifiers, the compensated system shows less signal power spread and optical SNR difference. A signal power spread of 2.47 dB and an optical SNR difference of 1.3 dB (SNR over 24 dB) are obtained in the compensated system after 15-stage amplifiers, corresponding to about 1000 km transmission. The calculations show that longer transmission up to 2000 km with more than 30 amplifiers is possible using this compensated system. The potential to upgrade the system to accommodate more signal channels is also demonstrated.

Chapter VI

Interferometric Conversion of the Laser Phase Noise to Intensity Noise

VI.1 Introduction

In this chapter, we present a model for the interferometric conversion of phase noise to intensity noise. In multi-tap filters, we model this phenomenon and evaluate the effect of this noise on the response of the filter. Primarily, the purpose is to apply the derivations to the filter design of chapter III. We discuss the conditions under which the probability density function (pdf) of the intensity noise at the filter output can be expressed by a Gaussian distribution.

It is known that the detection performance of a coherent lightwave transmission link can be sharply degraded by the laser phase noise. In the presence of phase noise, the BER performance of some gigabit-per-second fiber systems is also degraded. This is attributed to interferometric conversion of laser phase noise to intensity noise by multiple reflections at connectors and splices. We address this problem in chapter 7. Here, we first calculate the pdf of the intensity noise at the filter output and estimate the filter performance degradation. The BER performance degradation due to this intensity noise is also calculated. In this work, the modulation scheme examined is on-off-keying (OOK), which is equivalent to binary amplitude-shift-keying (ASK). The effect of the laser phase noise has been investigated on the performance of the optical systems [21], [22], [61] and [62].

There are three features which, taken together, distinguish this study from previous ones: 1) it adheres fully to the model of phase noise as Brownian motion, i.e., the integral of white Gaussian noise (rather than regarding the frequency deviation as random but fixed during each interval), 2) the probability density function of the intensity noise is estimated by a normal distribution where the conditions under which these calculations are valid are examined, and 3) a simple method is developed to evaluate the BER performance in the presence of this noise.

This chapter is organized as follows. In section 2, the statistics of the laser phase noise are examined. In section 3, the pdf of the intensity noise at the output of a coherent filter is derived. The variance of this noise is calculated. In section 4, the power penalty associated with this noise is calculated. These derivations are applied to the designed coherent filter in Chapter 3. Results indicate that under normal conditions, the filter response degradation due to the laser phase noise is negligible. In section 5, we extend our power penalty calculations to the case of reflections. Finally, conclusions are presented in section 6.

VI.2 Statistics of the Phase Noise

To account for the laser phase noise, the model for a laser tone in complex form $e^{j2\pi f_c t}$ is refined to $e^{(j2\pi f_c t+\phi(t))}$ where the random fluctuation $\phi(t)$ is a continuous-path Brownian motion process with zero mean and variance [72]

$$E(\phi^2(t)) = 2\pi\Delta\nu t \tag{1}$$

The resulting power spectrum is Lorentzian. The parameter $\Delta\nu$ is the frequency spacing between the 3-dB points of the power spectral density function. The fact

that the random phase fluctuations of the laser light are modeled by the Brownian motion (or Wiener-Levy random process) explains many of the properties involving statistics of the phase.

According to the Wiener-Levy model [72], the phase itself is a nonstationary zero-mean Gaussian random process. Denoting it by $\phi(t)$, its mean and autocorrelation are given by:

$$E\{\phi(t)\} = 0 \quad and \quad R(t_1, t_2) = \begin{cases} \alpha t_2 & \text{if } t_1 \geq t_2; \\ \alpha t_1 & t_1 \leq t_2. \end{cases} \tag{2}$$

The process $\phi(t)$ can be written as the integral of white noise with $n(t)$ a stationary normal process with zero mean and flat spectrum,

$$S_n(\omega) = \alpha$$

where $\phi(t) = \int_0^t n(\tau)d\tau$.

The one-dimensional density of $\phi(t)$ can simply be found from these properties. The random variable (r.v.) $\phi(t)$ has a zero mean and variance

$$R(t, t) = \alpha t. \tag{3}$$

By comparing (1) and (3), we find that α which is a proportionality constant is determined by the laser linewidth $\alpha = 2\pi\Delta\nu$.

It can also be expressed in terms of laser coherence time τ_c, where $\tau_c = 1/(\pi\Delta\nu)$.

It is easily seen that, the r.v. $\phi(t)$ has independent increments. For $t_1 > t_2$, $\Delta\phi = \phi(t_1) - \phi(t_2)$ has a zero mean and its variance

$$\sigma^2_{\Delta\phi} = E\{[\phi(t_1) - \phi(t_2)]^2\} = \alpha t_1 + \alpha t_2 - 2\alpha t_2 = \alpha(t_1 - t_2) \tag{4}$$

depends only on $(t_1 - t_2)$. Therefore, $\Delta\phi$ is a stationary normal process. Hence, its density is given by:

$$p_{\Delta\phi}(\Delta\phi) = \frac{1}{\sqrt{2\pi}\sigma_{\Delta\phi}} e^{-\left[\frac{(\Delta\phi)^2}{2\sigma_{\Delta\phi}^2}\right]} \tag{5}$$

VI.3 Effects of Phase Noise on the Performance of Coherent Filters

VI.3.1 The pdf of Relative Intensity Noise at the Output of a 2-Tap Coherent Filter

Consider a 2-tap filter in Fig. 6.1, where c_0 and c_1 are the complex coefficients, and τ is the corresponding delay-time between the two taps.

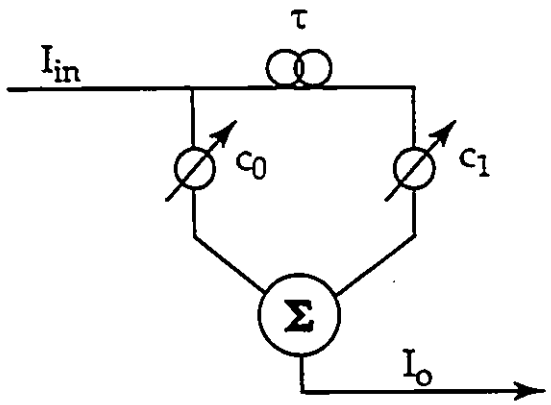

Fig. 6.1. Schematic diagram of a 2-tap filter

Initially, we consider the case of a laser operating under CW condition, for which we can consider the input optical field into the filter as:

$$e(t) = A \exp\,(j2\pi f_c t)$$

where f_c is the laser center frequency. In this case, where there are no random phase fluctuations in the laser output, the normalized light intensity at the filter output is :

$$U_R^2 = U_0^2 + U_1^2 + 2U_0U_1\cos\theta \tag{6}$$

$U_R^2 = I_0/I_{in}$ is the normalized output power, $U_0 = |c_0|$, $U_1 = |c_1|$, and $\theta = \angle c_1 - \angle c_0 + 2\pi f_c\tau$. The input optical intensity, without any loss of generality, is normalized to one,

$$|c_0|^2 + |c_1|^2 = 1.$$

It is easily seen that the normalized output intensity of the filter in the presence of phase noise is expressed by

$$U_R'^2 = U_0^2 + U_1^2 + 2U_0U_1\cos(\theta + \Delta\phi_{01}) \tag{7}$$

where $\Delta\phi_{01} = \phi(t+\tau) - \phi(t)$ has a zero mean and a variance of $\alpha\tau = 2\pi\Delta\nu\tau = 2\tau/\tau_c$, where τ_c is the coherence time of the laser.

From (5), we know that the probability of $|\Delta\phi|$ being greater than $5\sigma_{\Delta\phi}$ is extremely small

$$Pr[|\Delta\phi| > 5\sigma_{\Delta\phi}] \approx 0.0001$$

We also know that the functions $\cos\alpha$ and $\sin\alpha$ can be almost accurately estimated to 1 and α, where α is smaller than $1^\circ = \pi/180$ rad. Therefore, $\sigma_{\Delta\phi} = 2\tau/\tau_c$ should be less than $\pi/(180\times 5)$ or $\tau_c > (1800/\pi)\tau$. The delay time τ corresponds

to delay length of 80μm is 26.7×10^{-14} sec. Hence, the laser coherence time τ_c should be greater than 1.53×10^{-11} sec. In other words, the laser should have a linewidth less than 2.08 GHz which is very practical. Based on these assumptions, for small values of τ/τ_c, the intensity noise which is the difference between the intensity expressed by (6) and (7) can be expressed as:

$$\begin{aligned} I_n &= 2U_0U_1[\cos\theta - \cos(\theta + \Delta\phi)] \\ &= 2U_0U_1[\cos\theta - \cos\theta + \sin\theta\ \Delta\phi] \\ &= 2U_0U_1 \sin\theta\ \Delta\phi \end{aligned} \tag{8}$$

In (8), without loss of generality we have dropped the subscript for θ and $\Delta\phi$. Since $2U_0U_1 \sin\theta$ is a constant, the power spectral density of the intensity noise at the output is Gaussian with a zero mean and a variance which is directly a function of the input light intensity and also is related to the filter parameters. The variance of the "normalized" noise obviously cannot be more than the variance of $\Delta\phi$ itself. The exact noise pdf for the general case is derived in Appendix VI.A.

VI.3.2 The pdf of Relative Intensity Noise at the Output of a Multi-Tap Coherent Filter

The normalized intensity at the output of a multi-tap filter outside and in the presence of phase noise are expressed:

$$U_R^2 = \sum_i U_i^2 + 2\sum_i \sum_j U_iU_j \cos\theta_{ij} \tag{9}$$

where $U_i = |c_i|$ and $\theta_{ij} = \angle c_j - \angle c_i + 2\pi f_c\tau(j-i)$. In the presence of phase noise, the filter output intensity is expressed:

$$U_R'^2 = \sum_i U_i^2 + 2\sum_i \sum_j U_iU_j \cos(\theta_{ij} + \Delta\phi_{ij}) \tag{10}$$

where $\Delta\phi_{ij} = \phi(t_0 - j\tau) - \phi(t_0 - i\tau)$. The initial time t_0, without loss of generality can be set to zero. Therefore, $\Delta\phi_{ij} = \phi(j\tau) - \phi(i\tau)$. For small values of $\tau < \tau_c$, based on the same assumptions stated for the 2-tap filter, one can express the normalized intensity noise by:

$$I_n = 2\sum_i \sum_j U_i U_j \sin\theta_{ij}\ \Delta\phi_{ij} \tag{11}$$

$\Delta\phi_{ij}$: $\forall i, j$ are not necessarily independent, and the correlation factor can be found:

$$\begin{aligned} c &= E\{\Delta\phi_{ab},\ \Delta\phi_{a'b'}\} \\ &= E\{[\phi(t_a) - \phi(t_b)][\phi(t_{a'}) - \phi(t_{b'})]\} = \alpha t_{overlap} \end{aligned}$$

therefore, $\Delta\phi_{ij}$'s are independent if and only if $(\tau_j - \tau_i)$'s do not overlap. By breaking $\Delta\phi_{ij}$'s into single pieces corresponding to only one delay time τ, we would have:

$$I_n = 2\sum_{i=0}^{N-1} U_i \sum_{j=i+1}^{N} U_j \sin\theta_{ij}\ \Delta\phi_{i\ i+1}. \tag{12}$$

$\Delta\phi_{i\ i+1}$ $\forall i$ are iid random variables. Thus, the variance of I_n is

$$\sigma^2_{I_n} = [2\sum_{i=0}^{N-1} U_i \sum_{j=i+1}^{N} U_j \sin\theta_{ij}]^2 \sigma^2_{\Delta\phi} \tag{13}$$

The upper bound for the variance of normalized noise intensity I_n can be found by evaluating the maximum value of the constant coefficient in eq.(12). The constant $[2\sum_{i=0}^{N-1} U_i \sum_{j=i+1}^{N} U_j \sin\theta_{ij}]^2$ for the N-tap filter is maximized when $U_i = \frac{1}{\sqrt{N}}$, $\forall i$ and $\sin\theta_{ij} = 1$, $\forall i, j$. Therefore, the variance of I_n is upper limited by $[(N-1)\frac{2\pi}{\tau_c}]^2$. Since θ_{ij} is a function of the center frequency f_c, the variance of the noise is a function of the input frequency.

VI.4 System Performance Degradation

VI.4.1 Coherent Filter Performance Degradation

The intensity noise increases in proportion to signal power, where I_n is the normalized intensity noise. From (12), one cannot predict the shape of noise spectral density. The variance of the relative intensity noise $\sigma_{I_n}^2$ evaluated by eq. (13) is equivalent to the integral of the noise spectral density over the entire spectrum. For high bit rate systems, for which the system bandwidth B is substantially greater than the source linewidth $\Delta\nu$, almost all of the noise passes through the receiver bandwidth and the noise power (noise variance in the case of Gaussian noise) is equivalent to the total integral of $RIN(f)$ or the variance calculated in the last section. For low speed systems, the integral of $RIN(f)$ over the receiver bandwidth is likely to remain much less than the integral over the entire spectrum. Therefore, for these systems, the results obtained by eq.s (12) and (13) provide a pessimistic prediction of the system performance degradation.

To estimate system penalties resulting from interferometric noise, we consider a fiber transmission system based on binary on-off keying of the laser transmitter. We will assume non-return-to-zero (NRZ) formatted data, with the laser pulse waveform for an isolated "one" given by

$$b(t) = 1, \quad 0 \leq t \leq T$$

$$= 0, \quad otherwise$$

where T is the bit duration. The optical intensity measured at the receiver is given

by (see (10) and (11))

$$I(t) = [U_R{}^2 + I_n + n(t)] * h_r(t) \tag{14}$$

where $h_r(t)$ is the receiver impulse response function. In (14), $n(t)$ represents the thermal noise introduced at the optical receiver. In the case of coherent filter, the total delay $N\tau$ is much less than bit duration T. Therefore, regardless of the data sequence, the tapped signals beat with one another and generate the intensity noise. As mentioned before, we shall consider the case of high bit rate systems where all the intensity noise is assumed to fall within the receiver bandwidth. This assumption may not be valid for isolated "one" bits, if the laser undergoes fast fluctuations due to frequency chirp at the leading and trailing edges of the pulse. In such a case, the interferometric noise will fall outside the receiver bandwidth. However, the interferometric noise for sequences with several consecutive ones will contribute to the system degradation, and the power penalty might not be expected to decrease significantly. The same argument is true even in such a case that $N\tau$ is larger than T. That is, the consecutive "one" bits will interfere and generate intensity noise.

VI.4.2 Coherent Filter Performance: Example

We use the values of the taps of the coherent filter designed in chapter III, to evaluate its response degradation due to the presence of the laser phase noise. The variance of the output power from its nominal value is computed at each wavelength, using eq. (13). Fig. 6.2 depicts the variance of the output power where $2\tau/\tau_c = \pi/180$. The corresponding delay length in the filter was 80 μm. Hence, these results are given for a laser of linewidth 10.4 GHz.

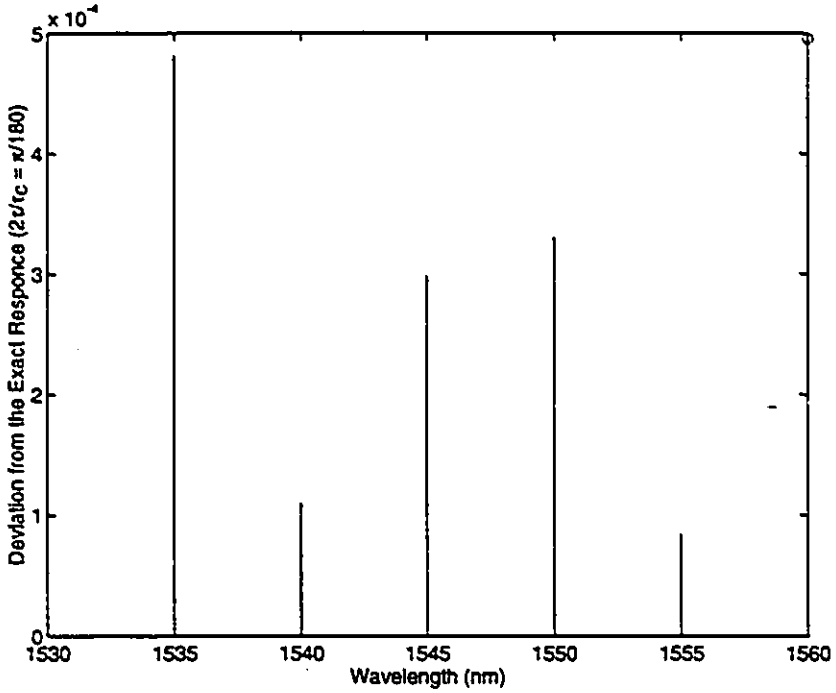

Fig. 6.2. Deviation of the filter response from the exact value at different wavelengths for $\tau/\tau_c = \pi/180$

As seen, even for such a large linewidth, the performance of the filter is acceptable. Fig. 6.3 depicts the same results for a laser of linewidth 2.08 GHz. Such lasers are readily available.

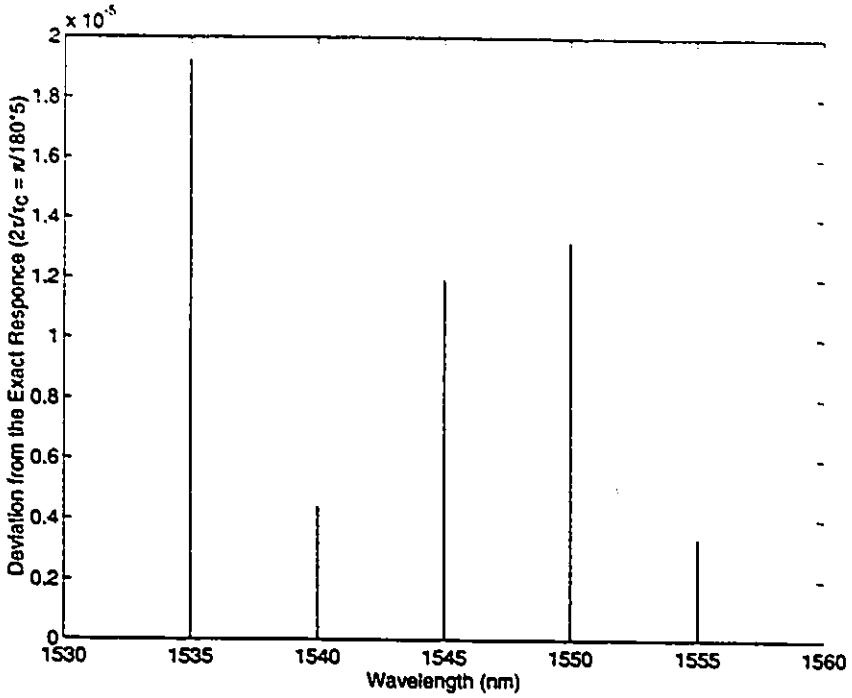

Fig. 6.3. Deviation of the filter response from the exact value at different wavelengths for $\tau/\tau_c = \pi/(5 \times 180)$

VI.4.3 Power Penalty Analysis

Let μ_1 and μ_0 denote the average values , and ${\sigma_1}^2$ and ${\sigma_0}^2$ the noise variances of the signal $I(t)$ for "ones" and "zeros", respectively. For a threshold value of D and the Gaussian-distributed noise, the probability of making a decision error is given by

$$P_e = \frac{1}{2}Q[\frac{\mu_1 - D}{\sigma_1}] + \frac{1}{2}Q[\frac{D - \mu_0}{\sigma_0}] \tag{14}$$

where

$$Q(X) = \int_X^\infty \frac{1}{\sqrt{2\pi}} e^{-x^2/2} dx. \tag{15}$$

In the absence of signal-dependent noise sources, the noise variances of the signal $I(t)$ are the same for both "ones" and "zeros" ($\sigma_1{}^2 = \sigma_0{}^2 = < n >^2$). In this case, the optimum threshold value is midway between expectations μ_1 and μ_0. In the case of OOK, $\mu_0 = 0$, and $D = \frac{\mu_1}{2}$. The interferometric noise represented by I_n in (12) affects only the "one" bits. If the threshold is fixed at $D = \frac{\mu_1}{2}$ in the presence of intensity noise, the error probability P_e is given by

$$P_e = \frac{1}{2}Q[\frac{\mu_1}{2\sigma_0}] + \frac{1}{2}Q[\frac{\mu_1}{2\sigma_1}] \tag{16}$$

The noise variance for $\sigma_1{}^2$ for "ones" is determined from (13):

$$\sigma_1{}^2 = \sigma_0{}^2 + \sigma_{I_n}{}^2 \tag{17}$$

$$\sigma_1{}^2 = \sigma_o{}^2 + \sigma_{I_n}{}^2\mu_1{}^2 \tag{18}$$

For moderate error probabilities, P_e will be dominated by the second term in (16). From (16) and (18), the power penalty due to interferometric noise is given by

$$penalty = -5log[1 - 144\sigma_{I_n}{}^2] \tag{19}$$

where for $P_e = 10^{-9}, q \approx 5.9$ satisfies $\frac{1}{2}Q(q) = 10^{-9}$.

Figs 6.4 and 6.5 show the corresponding power penalties for different wavelength channels where lasers of linewidth 10.4 and 2.08 GHz are used, respectively.

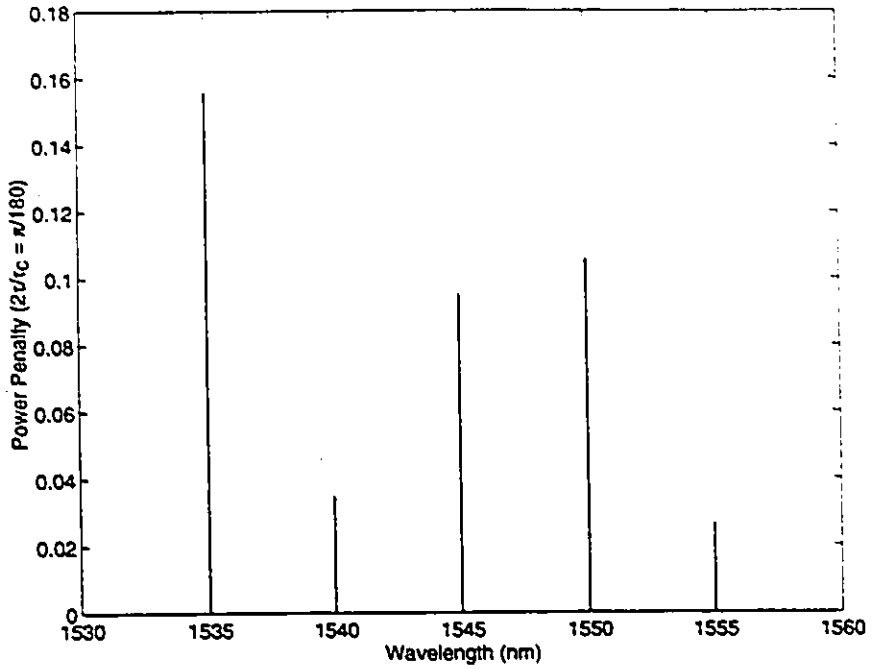

Fig. 6.4. Power penalty at different wavelengths for $\tau/\tau_c = \pi/180$

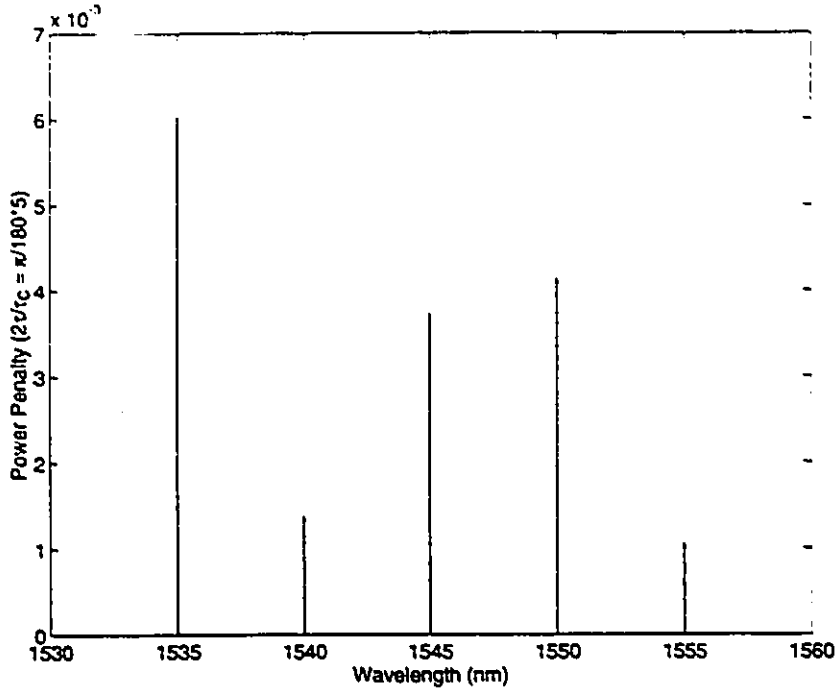

Fig. 6.5. Power penalty at different wavelengths for $\tau/\tau_c = \pi/(5 * 180)$

VI.5 Power Penalty due to Phase-to-Intensity Conversion by Reflections

Consider an interferometer formed by two reflectors. In this filter, the signal field is added to its doubly reflected field. If the intensity reflection coefficients are R_1 and R_2, and the round-trip path delay time is τ, the effective tap coefficients are "one" and $R = R_1 R_2$, and the corresponding delay time is τ. In other words, in Fig. 6.1, $U_0 = 1$ and $U_1 = R$. Thus, the output of such an interferometer can be expressed by eq. (7), where the second term U_1^2 can be neglected, since R is typically very small. Assuming the round-trip path delay time is longer than the laser coherence time τ_c, Φ_{01} will be uniformly distributed over the interval$[-\pi, \pi]$, and $cos(\theta + \Delta\Phi_{01})$ will have the variance 1/2. Therefore, the variance of the intensity noise at the output of this interferometer is $2U_0^2U_1^2 = 2R^2$.

This result should be applied to the eq. (19), in order to calculate the power

penalty due to the interferometric conversion of the phase noise to the relative intensity noise due to reflection. Thus,

$$penalty = -5log[1 - 144R^2] \tag{20}$$

If the reflected signal passes through a gain medium of gain G, then the power penalty increases,

$$penalty = -5log[1 - 144G^2R^2] \tag{21}$$

VI.6 Conclusions

We have developed a very simple formula to calculate the variance of the intensity noise generated by interferometric conversion of the phase noise. We showed the pdf of the intensity noise can be estimated by a Gaussian distribution, under certain conditions which we stated. The power penalty associated with this noise was also calculated for an OOK modulated signal. These findings were applied to the gain equalizer designed in chapter III. The results assure that the degradations due to the laser phase noise can be rendered negligible by choosing a reasonably narrow linewidth laser. Finally, the power penalty due to the interferometric conversion of phase-to-intensity noise due to reflection was evaluated.

Appendix VI.A

Exact pdf of Intensity Noise at the Output of a 2-Tap Coherent Filter

In this appendix, the exact pdf of the intensity noise at the output of a two-tap filter is derived. U_R^2 and $U_R'^2$ are the output powers in the absence and presence of the phase noise.

$$\begin{cases} U_R^2 = U_1^2 + U_2^2 + 2U_1U_2\cos\theta \\ U_R'^2 = U_1^2 + U_2^2 + 2U_1U_2\cos(\theta+\Delta\phi) \quad \Delta\phi > 0,\ x > 0 \end{cases}$$

$$|U_R^2 - U_{R'}^2| < x \rightarrow 2|U_1U_2|\ |\cos\theta - \cos(\theta+\Delta\phi)| < x$$

$$\cos\theta - \cos(\theta+\Delta\phi) < \frac{x}{2U_1U_2}$$

$$\cos(\theta+\Delta\phi) > \cos\theta - \frac{x}{2U_1U_2}$$

$$\Rightarrow \theta + \Delta\phi < \cos^{-1}\left(\cos\theta - \frac{x}{2U_1U_2}\right)$$

$$\Delta\phi < \cos^{-1}\left(\cos\theta - \frac{x}{2U_1U_2}\right) - \theta$$

$$P_r\{(U_R^2 - U_R'^2) < x\} \Rightarrow P_r\{\Delta\phi < \cos^{-1}\left(\cos\theta - \frac{x}{2U_1U_2}\right) - \theta\}$$

$$= \int_0^{\cos^{-1}\left(\cos\theta - \frac{x}{2U_1U_2}\right) - \theta} P_{\Delta\phi}(\Delta\phi)d\Delta\phi = \text{erf}\left(\cos^{-1}\left(\cos\theta - \frac{x}{2U_1U_2}\right) - \theta\right)$$

If $\Delta\phi < 0$ and $x > 0$

$$|U_R^2 - U_{R'}^2| < x \rightarrow U_R^2 - U_{R'}^2 > -x$$

$$2U_1U_2|\ \cos\theta - \cos(\theta + \Delta\phi)| > -x$$

$$2U_1U_2\ [\cos\theta - \cos(\theta + \Delta\phi)] - n$$

$$\cos\theta - \cos(\theta + \Delta\phi) > \frac{-x}{2U_1U_2}$$

$$\cos(\theta + \Delta\phi) < \cos\theta + \frac{x}{2U_1U_2}$$

$$\Delta\phi > \cos^{-1}\left(\cos\theta + \frac{x}{2U_1U_2}\right) - \theta$$

$$\int_{\cos^{-1}\left(\cos\theta + \frac{x}{2U_1U_2}\right) - \cos\theta}^{0} P_{\Delta\phi}(\Delta\phi)d\Delta\phi = \text{erfc}\left(\theta - \cos^{-1}\left(\cos\theta + \frac{x}{2U_1U_2}\right)\right)$$

$$P_t\{|U^2 - U'^2| < x\} = \frac{1}{2}\left[\text{erfc}\left(\cos^{-1}\left(\cos\theta - \frac{x}{2U_1U_2}\right) - \theta\right)\right.$$
$$\left. - \text{erfc}\left(\cos^{-1}\left(\cos\theta + \frac{x}{2U_1U_2}\right) - \theta\right)\right]$$

Chapter VII

Bidirectional Optical Amplifiers

VII.1 Introduction

Erbium-doped fiber amplifiers have succeeded in a wide range of applications as postamplifiers, preamplifiers, and in-line repeaters in optical fiber communications systems. However, the great majority of these systems are configured for transmission in a single direction only and use unidirectional EDFAs with optical isolators on both the input and output. Bidirectional operation of an EDFA is desired since this has the advantage of reducing not only the number of fiber links by a factor of two, but also, the number of passive components such as splitters in bidirectional multichannel passive optical networks, e.g., fiber-to-the-home/curb/business systems. Bidirectional amplification allows the bidirectional transmission of tree distributed networks by compensating the splitting and transmission losses.

It is known that, the EDFA is at lasing threshold when the round-trip gain equals one, i.e., $G_{max}^2 R_1 R_2 = 1$, where R_1 and R_2 are reflection coefficients on either side of the EDFA, and G is the gain peak of the amplifier (Fig. 7.1). However, the maximum amplifier gain is restricted to much smaller values before the system degradation becomes unacceptable.

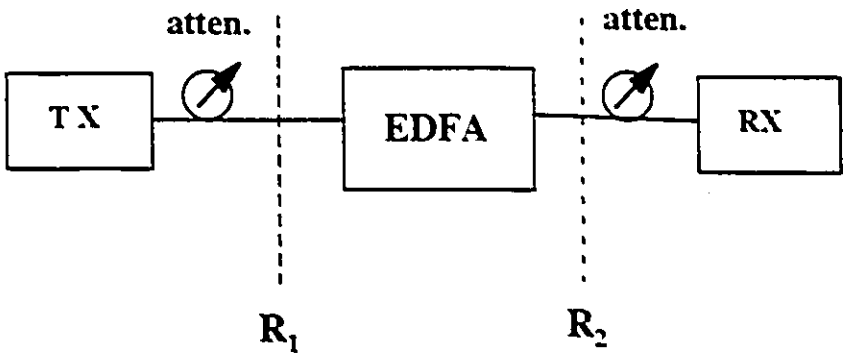

Fig. 7.1. Transmission link with an EDFA and two-way reflections

For bidirectional transmission systems with optical amplifiers, severe system degradations are due to multiple reflections which interferometrically convert laser phase noise into intensity noise. The presence of reflections due to Rayleigh backscattering (reflection power typically is of the order of -31 to -34 dB for a long length of fiber) limits the maximum tolerable gain to about G=19 dB if no optical isolator is incorporated in the amplifiers [28]. The interferometric noise from multiple reflections increases proportionally with amplifier gain, i.e., a factor of 20 dB gain requires a reduction in reflectance by the same 20 dB over the previously tolerable reflectance.

This chapter is organized as follows. In section 2, we give the power penalty associated with both interferometric and signal-spontaneous noise for an amplifier. In section 3, we introduce a new bidirectional EDFA that introduces a negligible power penalty while producing a large gain. The experimental setup is also described in this section. In section 4, the experimental results are presented on the amplifier performance. Possible improvements are investigated using computer simulation of the amplifier. In section 5, alternative configurations of the bidirectional EDFA are discussed, and conclusions are presented in section 6.

VII.2 Maximum Allowable Gain and Power Penalty

Fig. 7.1 depicts a transmission link with an erbium-doped fiber amplifier and two reflections on either side of the EDFA. As discussed in chapter 6, the interference between the transmitted and doubly reflected optical fields introduces the interferometric noise. For Gbit/s transmissions where the modulation data rate is much higher than the CW laser linewidth $\Delta\nu$ ($\Delta\nu$ typically $\approx$ 10-100 MHz), most of this noise falls within the receiver bandwidth. Typically, the length of EDF exceeds the coherence length of DFB lasers. Therefore, the two optical fields add incoherently, and the variance of the reflection-induced intensity noise can be easily calculated by [29]:

$$\sigma^2 = \alpha^2 G^4 R^2 (P/h\nu B)^2 \tag{1}$$

where α is the attenuation between the amplifier and the receiver, G is the amplifier gain, $R^2 = R_1 R_2$ for maximally aligned states of polarization, P is the peak input power into the amplifier and B is the bit-rate. This noise and signal-spontaneous emission beat noise which is the dominant amplifier-related noise together introduce a power penalty for high-bit rate systems. The variance of the signal-spontaneous beat noise in photons per bit is given by eq. (32) of chapter 4: $4P_s P_{sp}/(h^2\nu^2)\frac{B_e}{B_o}$, where P_s is the signal input power to the amplifier, $h\nu$ is the photon energy, and B_e is the electrical bandwidth. We know $P_{sp} = n_{sp} h\nu B_o$ where n_{sp} is the amplifier spontaneous noise factor ($n_{sp} = 1$ for an ideal amplifier). Therefore, the variance of the beat noise can also be given by $2P_S n_{sp} B/h\nu$ (eq. (33) of chapter IV) where B is the bit rate and $B_e = 2B$. Approximating the signal-spontaneous beat noise and the intensity noise density as being Gaussian, the power penalty for an OOK modulated signal can be computed as eq. (21) of

chapter VI.

$$penalty(\lambda) = -5log[1 - 144(N_{sp}h\nu B/P_{in} + G^2R^2)] \quad (2)$$

where $P_{in}(\lambda)$ is the time-average input power of the amplifier at wavelength λ. For a given value of P_{in}, GR must be limited to a certain value to maintain a tolerable power penalty. We introduce a two-stage bidirectional EDFA (BEDFA) where the reflected signals are attenuated so that the gain for the transmitted signals can be increased.

VII.3 Increasing Repeater Span in High-Speed Bidirectional WDM Systems Using a New Bidirectional EDFA Configuration

VII.3.1 Bidirectional Optical Amplifier Configuration

Fig. 7.2 depicts the two-stage bidirectional optical amplifier unit that consists of two EDFAs and one frequency-tunable reflection attenuator (FTRA) that is inserted between the two amplifiers. This configuration allows bidirectional signals transmitted on a single optical fiber to be amplified by both EDFAs while they are blocked from propagating in the opposite direction by the FTRA. Each signal is amplified by a co- and then a counter-propagating EDFA. Signals within the first frequency band f_1 after being amplified by a pump co-propagating EDFA, propagate through the FTRA in one direction and are prevented from propagating in the reverse direction. These signals are once again amplified by a counter-propagating EDFA. Signals having a frequency within the second band f_2 are treated in the same way. The transmission wavelengths can be tuned by adjusting

optical filters.

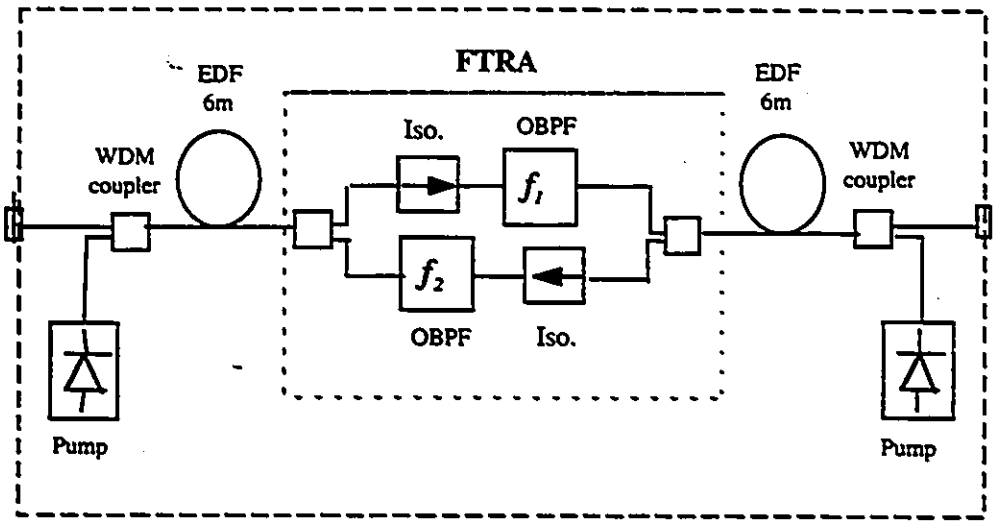

Fig. 7.2. Bidirectional EDFA with FTRA

This configuration increases the maximum allowable amplifier gain for a certain penalty tolerance in two ways: 1) since the reflected signals are blocked in between the two amplifier stages by FTRA, the maximum gain limit can be calculated for each stage, separately. The value of the reflection R is reduced by decreasing either R_1 or R_2 of each amplifier according to the relative position of each amplifier and the FTRA. Thus, the amplifier unit can provide a large gain while the gain of each amplifier stage is less than the entire gain in order to guarantee a certain power penalty. The smaller gain of each amplifier stage, also results in a smaller power penalty from reflections associated with each stage, producing a much smaller total power penalty. Furthermore, for each wavelength channel, the power penalty from added ASE introduced by the second stage is substantially reduced because of the large input power of the amplifier at that wavelength. 2) A major part of the amplified spontaneous emission (ASE) noise generated in each amplifier

stage is prevented from entering the other EDFA stage because of the filtering properties of the FTRA. This prevents the saturation of the second amplifier by ASE. Therefore, the maximum achievable gain can be increased.

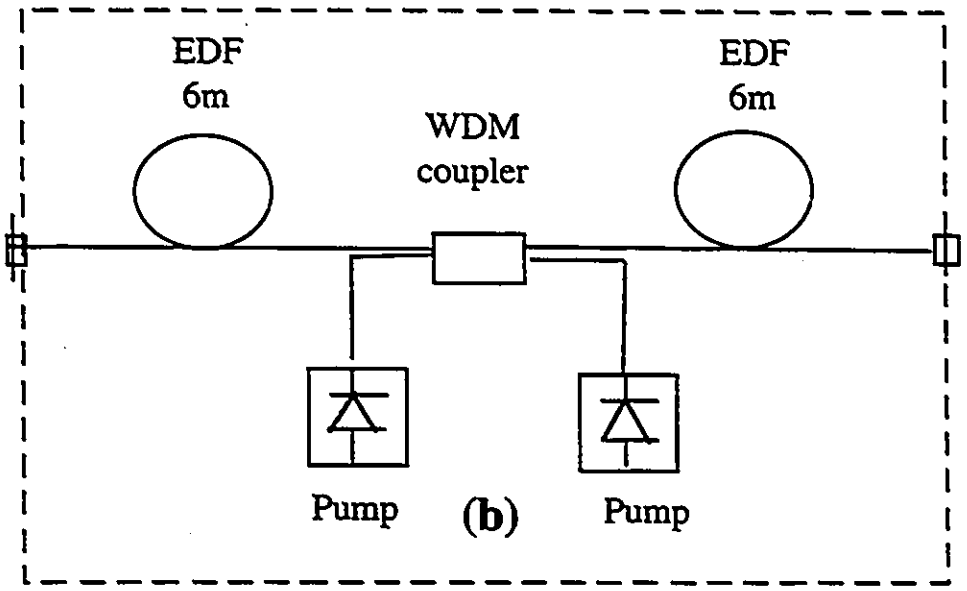

Fig. 7.3. Bidirectional EDFA without FTRA

The issue of bidirectional transmission has been addressed before, [5], [11], [28], [29], [68] and [86]. In [28] and [29], the maximum allowable gain has been studied for a BEDFA without optical isolators in a bidirectional transmission system. It is demonstrated that the maximum allowable gain is G=19 dB over a very short length of fiber and for a low modulation rate of 155 Mb/s. A bidirectional transmission over 144 km was reported in [68] where the modulation rate was 622 Mb/s and a maximum gain of 14 dB was achieved. At 622 Mb/s, another bidirectional transmission over 195 km was reported in [36] where two EDFAs were used. Since no isolators were employed in the fiber link, the gain of each amplifier was limited to less than 20 dB. For a 2.4 Gb/s bidirectional WDM

transmission, a gain of 25 dB was achieved [86]. However, no fiber was used in this experiment. Therefore, the Rayleigh back scattering was not accounted for. We have experimented a successful bidirectional transmission of 2.48 Gb/s over 300 km fiber, where the gain of the amplifier was 36 dB. The measured power penalty was 0.5 dB.

VII.3.2 Experimental Setup

Fig. 7.4 shows the configuration of the bidirectional transmission system with a bidirectional fiber amplifier used as a repeater. BER measurements at 2.488-Gbit/s using a 27-1 pseudorandom signal have been carried out by using this set-up. A MZ-modulator driven by a pattern-generator was used to intensity modulate the output of a laser at 1552 nm. A power booster was used to increase the optical power to +6 dBm where it could provide a signal as high as +14 dBm. The optical signal was transmitted through 150 km fiber, with an attenuation of 0.22 dB/km. The +6 dBm output signal power of the BEDFA in Fig. 7.2 was transmitted over another 150 Km fiber. The BER versus the received power by the APD receiver was measured.

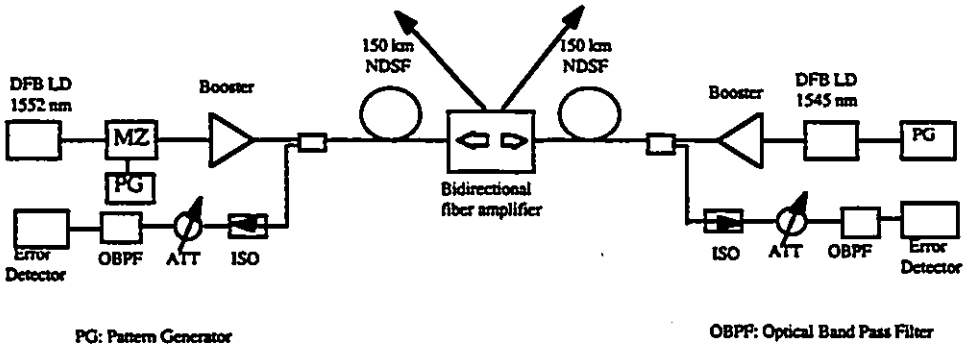

Fig. 7.4. Bidirectional WDM transmission set-up

In the experiment, both bidirectional fiber amplifiers with (Fig. 7.2) and without (Fig. 7.3) isolator are examined. BEDFA in Fig. 7.2 consists of two stages of EDFA; each having a 980 nm pump, a 980/1550 nm WDM coupler, and a piece of 6 meter erbium-doped fiber (EDF). A FTRA is inserted between two stages of EDFAs. The EDF is erbium/aluminum co-doped, with Er concentration of 2000 ppm-wt, 2.4 micro core size, NA of 0.24 and cutoff wavelength of 960 nm. The emission and absorption cross section spectra of this EDF were measured (Fig. 3.A.1). The same pump lasers and EDFs are employed for the BEDFA without FTRA shown in Fig. 7.3. The measured cross section spectra of the EDF was used to simulate the bidirectional EDFA, and investigate its performance under different conditions.

Another DFB laser was transmitting a signal in the opposite direction at 1545 nm. The laser was internally modulated by a 622 Mb/s signal. Fig. 7.5 shows the gain and noise figure of the BEDFA of Fig. 7.2 versus input signal power, where equal signals are present in both directions.

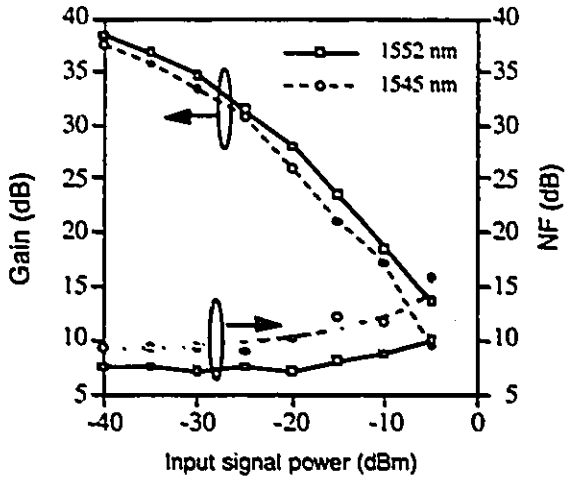

Fig. 7.5. Bidirectional optical amplifier gain and noise figure versus input signal power

VII.4 Results and Discussion

VII.4.1 Results

An amplifier gain of 36 dB is achieved for an input signal of -30 dBm power in both directions. The gains of the first and the second amplifier stages at 1552 nm were 26 and 21 dB, respectively. The 1545 nm signal is amplified by almost the same order of gains at each amplifier stage in the opposite direction. An 11 dB loss is associated with FTRA between the two stages of EDFAs.

The reflected light from each stage will be split to two parts where the first part will be blocked by the isolator with an isolation level of 45 dB. The second

part is attenuated by the optical filter. The FWHM filter bandwidth is 1.64 nm. With this filter, 7 nm away from the passband center, the rejection level is 34.8 dB. Therefore, the reflected signals are effectively attenuated by an extra 35 dB compared to the transmitted signals. Hence, the maximum allowable gain can be increased by 35 dB.

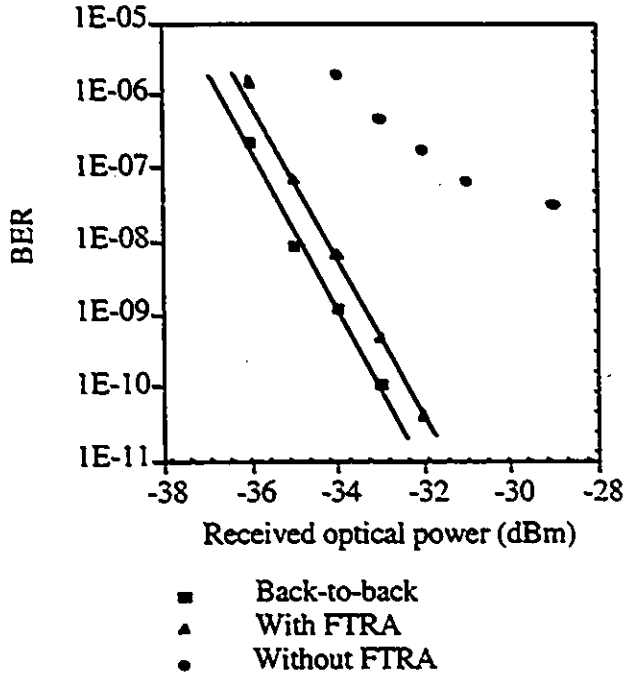

Fig. 7.6. Measured bit error rate for a 2.488 Gb/s signal.

The BER results for both cases where amplifiers with (Fig. 7.2) and without FTRA (Fig. 7.3) are employed are depicted in Fig. 7.6. In the case of the BEDFA with FTRA, there is only a 0.5 dB BER penalty. The measured optical signal-to-noise ratio (SNRo) was 18 dB. However, there is a BER floor when an EDFA without isolators is used, as in Fig. 7.3. In this case, the maximum allowable amplifier gain is 18 dB for an input signal power of -15 dBm. Fig. 7.7

illustrates the eye diagram of 2.448 Gb/s signal for back-to-back and 300 km fiber transmission system.

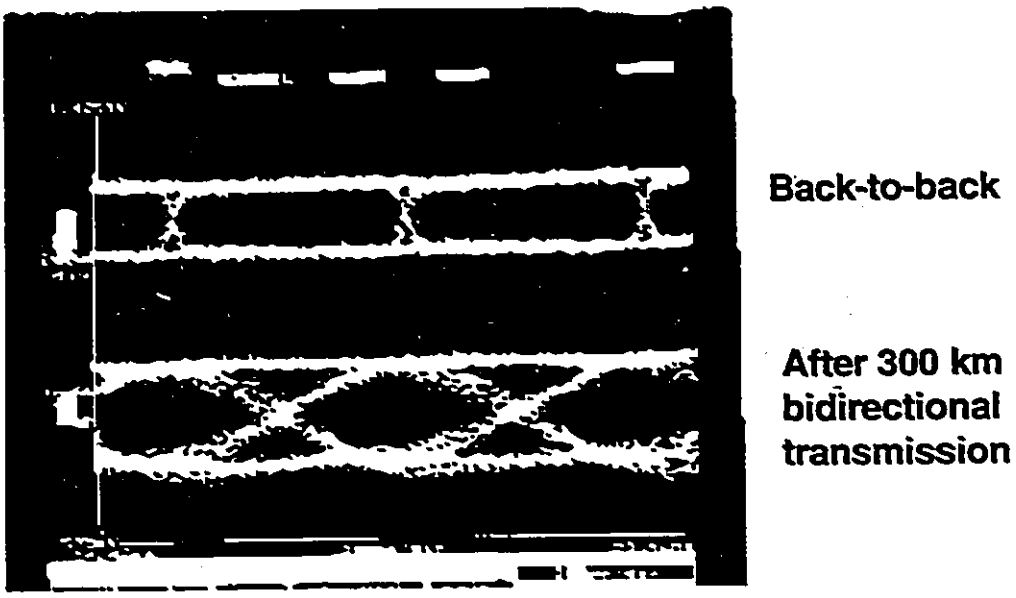

Fig. 7.7. Eye diagram of the 2.488 Gb/s signal.

The experiment confirmed there is a great penalty and a BER floor when the EDFA is used as a repeater without the isolators. However, the gain of the fiber amplifier with FTRA can reach 36 dB with an input signal of -30 dBm power, while the power penalty at a BER of 10^{-9} is only about 0.5 dB.

VII.4.2 Discussion

The power penalty through the entire amplifier unit is the summation of the power penalties associated with each amplifier stage.

Assume that the signal at 1552 nm is first amplified with a $G = 26$ dB and $GR = 0.001$. For this amplifier, the value of $P_{in}(1552) = -30$ dBm, and bandwidth of the signal is $B = 2 \times 2.5$ Gb/s. An $n_{sp} = 1$ results in a 0.26 dB power penalty.

For the second EDFA $P_{in}(1552) = -15$ dBm, since the signal is amplified by 26 dB and attenuated by 11 dB. There is an 11 dB loss associated with the FTRA. Applying the same values for B, n_{sp}, and GR, results in a 0.008 dB power penalty.

If we have only one stage of amplifier (as in [86]) with a $G = 26$ dB, $GR = 0.001$, $n_{sp} = 1$, $B = 5$ Gb/s, and $P_{in}(1552) = -30$ dBm, we would have the power penalty of 0.26 dB. Now, in order to increase the gain of this amplifier by 19 dB, the associated power penalty increases by 10.2 dB. In other words, there will be a bit error rate floor, and a severe system performance degradation will occur.

Considering the BER floor, since the input power to the amplifier unit is only -30 dBm, it is obvious that the received SNR_o is not very large. Figures 7.8 to 7.11 depict the optical signal-to-noise ratio at the output of the amplifier. As seen, for larger input powers of the amplifier, a larger SNR_o is achieved. However, the gain of the amplifier is compromised.

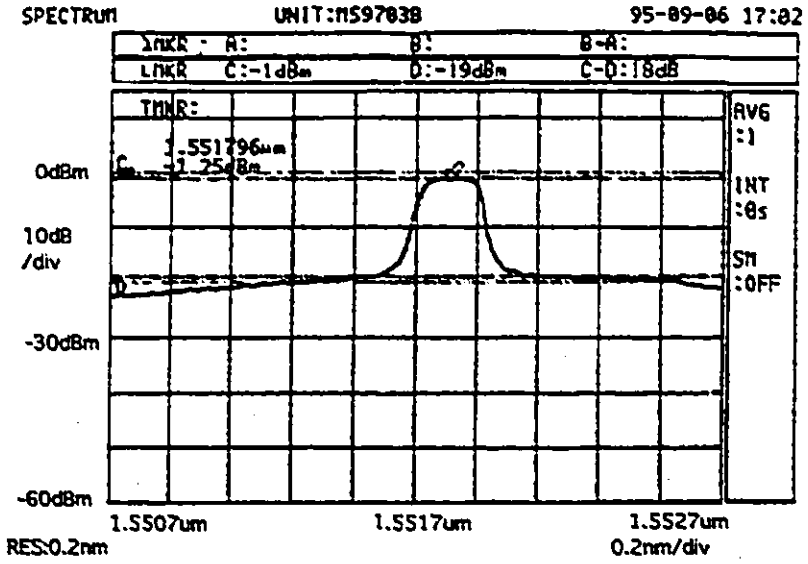

Fig. 7.8. Optical SNR for input power -30 dBm at 1552 nm.

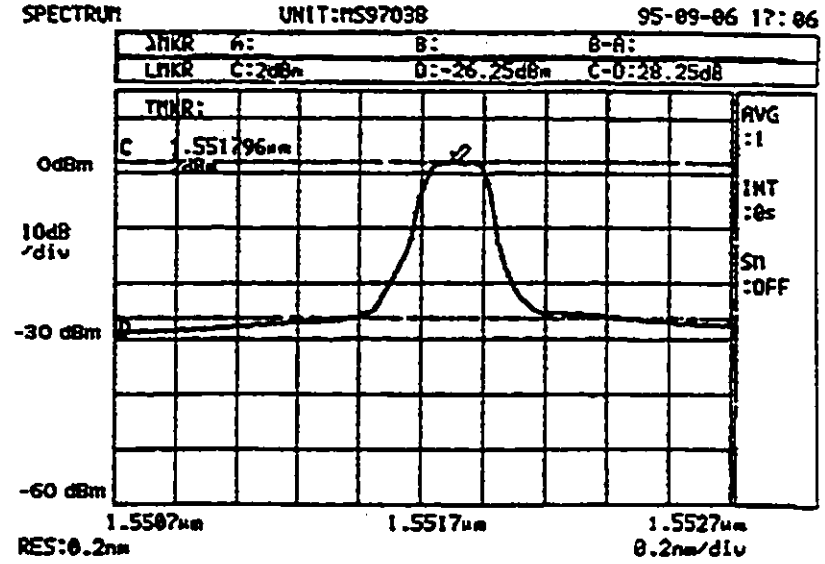

Fig. 7.9. Optical SNR for input power -20 dBm at 1552 nm.

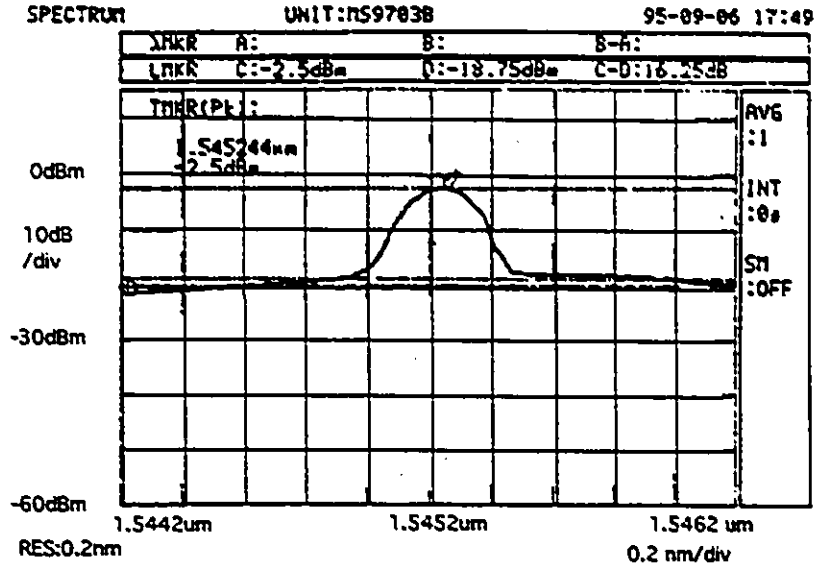

Fig. 7.10. Optical SNR for input power -30 dBm at 1545 nm.

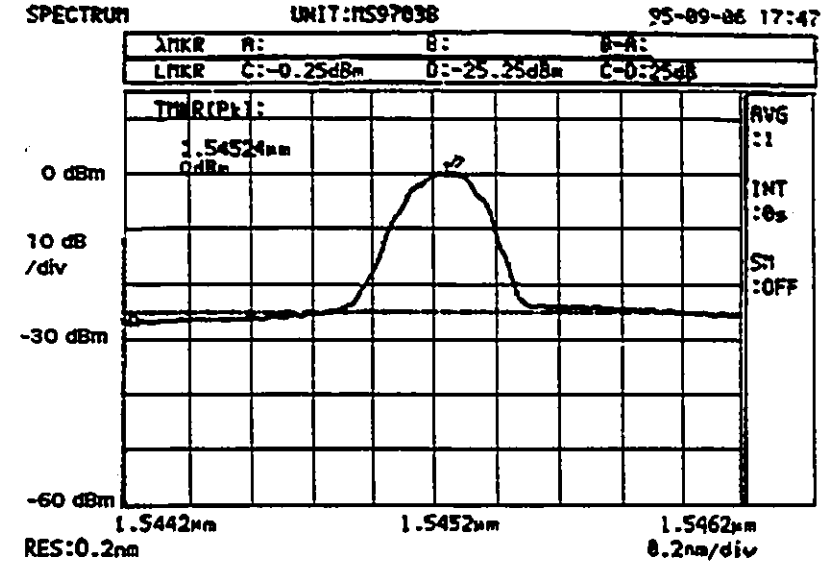

Fig. 7.11. Optical SNR for input power -20 dBm at 1545 nm.

From equations developed in section IV.4, we calculated the Q factor and the

BER floor for the amplifier input power -30 dBm, and SNR_o 18 dB. The Q factor was 8.826 resulting in a BER floor in the order of 10^{-19}. To calculate the BER floor, we only considered the signal-spontaneous beat noise. Increasing the received optical signal power results in a larger electrical signal-to-noise ratio SNR_e and a smaller BER up to the point that the receiver thermal noise becomes negligible compared to the other noise components such as signal-spontaneous beat noise. After this point, BER is not reduced by increasing the received optical power, since the signal and the spontaneous noise, regardless of the value of the signal power, have a fixed ratio SNR_o. The Q factor is only a function of SNR_o, when signal-spontaneous beat noise is dominant. From eq. (29) of chapter 4:

$$N_{s-sp} = (4e^2 P_s P_{sp}/h^2\nu^2)(B_e/B_o) \tag{3}$$

since $P_{sp} = P_s/SNR_o$, therefore,

$$N_{s-sp} = (4e^2 P_s^2/SNR_o h^2\nu^2)(B_e/B_o) \tag{4}$$

$$Q = \frac{eP_s/h\nu}{\sqrt{N_{s-sp}}} = \frac{SNR_o}{2}\frac{B_o}{B_e}. \tag{5}$$

As seen in Figs 7.10 and 7.11, the optical SNR at 1545 nm is almost as large as SNR_o at 1552. Considering the fact that the bit rate at 1545 nm was lower than that of 1552 nm, we can conclude that the BER performance was superior.

VII.4.3 Simulation Results and Further Improvements

We measured the cross section values of the EDF used in these experiments (Fig. 3.A.1). Using the numerical analysis presented in chapter III, the bidirectional EDFA was modeled. We were able to repeat the same results as in the experiment

for the same signal input powers, EDFs lengths, and pump powers. When the loss associated with FTRA was reduced from 11 dB to 5 dB, the simulation results indicate that the amplifier noise figure is reduced form 10.33 and 9.85 dB to 4.49 and 3.28 dB at wavelengths 1552 and 1545 nm, respectively. In the latter case, the gain of the first stage was 25.6 and 25.8 dB, and the gain of the second stage was 17.98 and 17.06 at wavelengths 1552 and 1545 nm, respectively. This is against the 26.3 and 26.6 dB gain of the first amplifier stage and 21.8 and 21.4 dB gain of the second stage in the former case where the FTRA introduced as much as 11 dB loss. The lower gain of the second stage is compensated by the lower loss of the FTRA in the second case. Therefore, there is an obvious advantage in reducing the FTRA loss by reducing the number of elements thereby reducing the total insertion loss. WDM couplers could also replace the 3 dB couplers, however, the tunability and filtering selectivity of such devices remain questionable compared to the alternative, tunable optical filters. In the following, we present a number of possible alternatives.

VII.5 Alternative Configurations

VII.5.1 Frequency-Tunable Reflection Attenuator (FTRA)

In general, FTRA (Fig. 7.2) is a module that allows the signals within one frequency band f_1 to propagate in one direction, and the signals in a second band f_2 to propagate in the opposite direction. The reflected signals of both frequency bands are prevented form propagating in the opposite directions compared to their original directions.

This module can have various configurations and be implemented by different

sets of elements. Fig.s 7.12 and 7.13 are two alternative configurations for FTRA implementation.

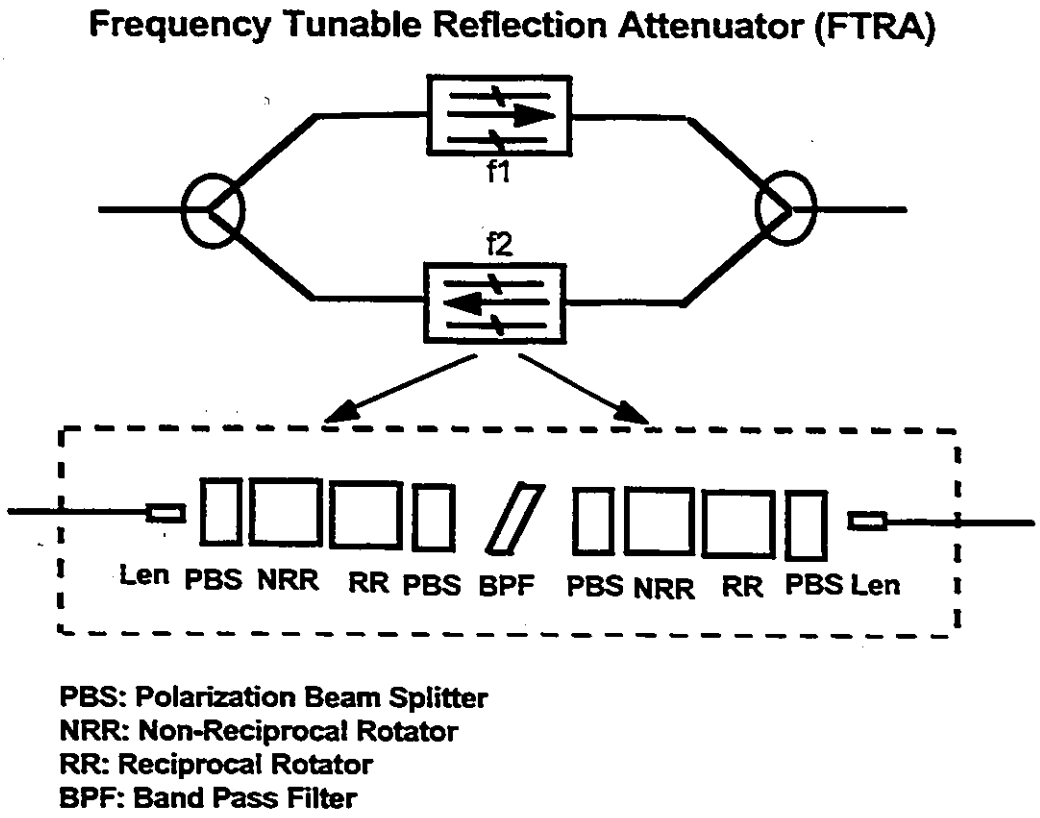

Fig. 7.12. Alternative FTRA configuration I.

In Fig. 7.12, a bandpass optical filter and two isolators are integrated in one device. The isolators are placed at both sides of the filter. The presence of two isolators improves the attenuation of the reflected signals.

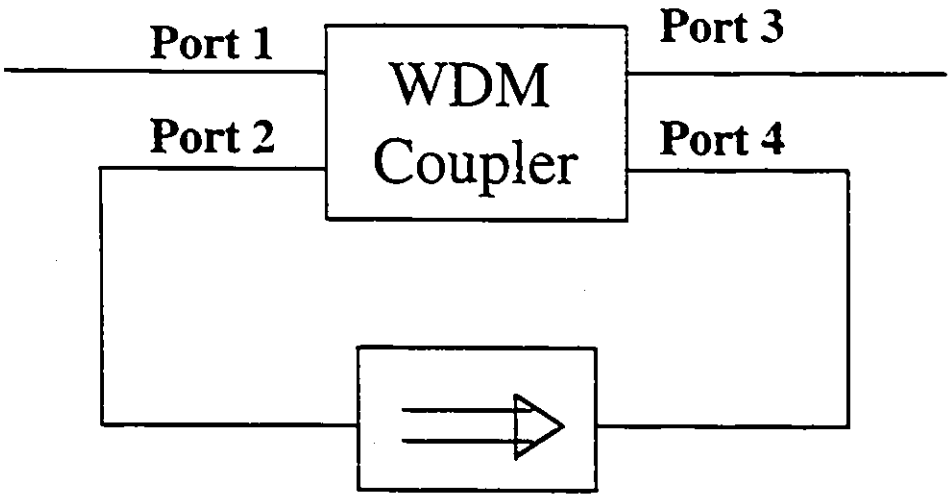

Fig. 7.13. Alternative FTRA configuration II.

Fig. 7.13 shows another possible configuration of FTRA. The 2X2 WDM coupler is a device that reflects wavelength 1552 from port 1 to port 2 and from port 4 to port 3. Likewise, it cross-passes wavelength 1545 from port 3 to port 2 and from port 4 to port 1. If cross talk rejection and filtering properties of this device can be improved to those of a passband optical filter, this configuration provides a simpler alternative to FTRA realization.

VII.6 Conclusion

When fiber-optic systems contain erbium-doped fiber amplifiers (EDFA), reflections are enhanced by the gain of the amplifiers and severe system performance degradations and bit error rate floors can be observed. This provides a very restrictive limit on the usable amplifier gain. We present a new configuration for a bidirectional EDFA that allows for a significantly higher maximum allowable gain while introducing a very small bit error rate (BER) penalty. We have demon-

strated a successful 2.488 Gb/s bidirectional WDM fiber optic transmission using a new bidirectional amplifier repeater with a frequency-tunable reflection attenuator (FTRA). By using the new EDFA configuration, large gains of up to 40 dB are achievable, with a 0.5 dB power penalty for a 10^{-9} BER. This repeater can allow more densely spaced bidirectional WDM transmission and longer fiber spans.

Chapter VIII

Introduction to All-Optical Networks

VIII.1 Introduction

Over the last few years, many broadband services that have academic, scientific, and commercial applications have been introduced. These applications can only be supported by broadband networks and there are already demonstrated needs for some of these. High-performance computing is one example. This application requires connection among supercomputers, high-speed access to databases/libraries and specialized data processing facilities. Another example is wideband imagery, sensor data, and scientific data transfer. Medical imaging is another interesting application. It requires various types of digitized images such as X-ray, MRI, and CT to be stored and transmitted for evaluation by radiologists. These images usually represent large quantities of data. Rapid view by radiologists results in a requirement for bursts of data at very high transmission rates (1 Gb/s).

Many of the future broadband applications will need multimedia services which include not only the storage but also the retrieval, representation and dissemination of the multimedia information. Multimedia communications provides simultaneous and synchronized communication in different media (voice, data, ...) by the simultaneous use of data in these media forms. For a network to support multimedia based applications, it should be able to support different classes of

services. Having a network capable of supporting different types of services is not motivated only by demand for multi-media applications. Service flexibility, simple management, cost-effective network operation and maintenance are among other motivations for existence of such a network.

Based on the underlying physical-layer technology employed in a network, three generations of networks can be identified [33]. First generation networks can support bit rates up to a few megahertz. These are built based on copper wire or microwave technology. Ethernet class computer networks and token rings are typical examples of this generation and can serve 10 Mb/s applications. The second generation networks are the networks which employ fiber in traditional architectures in view of the wider bandwidth and the lower error rate in fiber optic transmission. This group features applications in the 100 Mb/s class. Typical examples are fiber distributed data interface (FDDI), distributed queue dual bus (DQDB) for local area network (LAN) environments, and BISDN for WAN applications. Although these networks involve some detailed architectural improvements, they are essentially what one gets by direct substitution of a fiber optic medium for copper. In fact, fiber is not just a slightly better version of copper. The medium is so remarkably different in its tremendous bandwidth of the order of terahertz that one must revise much of the entire subject of networks to use it most effectively.

It is to say that, although the possibility of implementing a general-purpose network is raised by the abundance of bandwidth in a single-mode fiber, there is a long journey from gigabit transmission to gigabit networking.

In the third generation networks, the tremendous bandwidth of optical fiber

is exploited. These networks are remarkably different from the conventional networks. As the focus of the research in the fiber-optic field began to shift toward networking, it became clear that the major issues involved in public (multi-user) optical networking were quite different from those of point-to point transmission systems and even from those encountered in the second generation networks or the networks that employ fiber as a shared medium by multiple users. Second generation networks have also a well known disadvantage of transmission speed limit due to processing speed of optical-electronic interfaces. Electrical/Optical (E/O) and Optical/Electrical (O/E) conversions in second generation networks result in information rate bottlenecks. Third generation networks, to the maximum extent possible, will be "transparent" to high-rate users so that the flow of their optical signals within the core of the network is not delayed by O/E, E/O conversions, even though that flow may be controlled by electronics. In other words, signals within the networks remain in the optical domain and thus electronic bottlenecks are avoided. Therefore, third generation networks are often entitled "all-optical" networks and are expected to be a key carrier backbone for future communications to support new broadband services.

Erbium-doped fiber amplifiers (EDFAs) provide a gain in 1.55 μm wavelength region and can boost the power of optical signals without requiring O/E conversion and subsequent electronic amplification as in optical regenerators. These amplifiers can replace conventional regenerators while accommodating many wavelength-division multiplexing (WDM) channels. Bit-rate transparency of these amplifiers over almost 40 nm optical bandwidth and their negligible interwavelength crosstalk that allows deployment of WDM technology has offered a simple and cost-effective means to provide a large-capacity all-optical transport network over a large geographical span [55].

There are three important aspects of a network: applications, architecture and technology. In this section, we highlighted some potential applications of a broadband all-optical network. We pointed out that it is desirable to have "one" network capable of supporting different classes of services. The possibility of such a network has arisen from the huge available bandwidth of a single-mode fiber. We indicated that all-optical (third generation) networks will exploit the 200 nm bandwidth of the fiber while even synchronous optical network (SONET)-based networks utilize only 10 Gb bandwidth of the medium. By tapping this huge capacity, networks can accommodate many independent logical subnetworks, such as an asynchronous transfer mode (ATM) network, a voice network, etc., while deploying a permanent transport base structure. At the same time, these networks not only can support applications that utilize digital services such as ATM or other fast packet switching, they can support analog services or applications that require an optical interface. We finally described how the EDFA, as the most important enabling technology for these networks, has made it possible to extend the optical transparency in terms of the number of the users. In the next section, the network architectures and topologies are reviewed. Features of each architecture are discussed.

VIII.2 Network Architectures

VIII.2.1 Network Architecture Classification

In this section, we overview the architectures for all-optical networks. Without wide-band amplifiers such as EDFAs, the size of the third generation (all-optical) networks is limited to a few users. This is due to severely limited signal

powers which is one of the characteristics of the fiber-based systems where the abundant transmission bandwidth is another characteristics of these systems. Introduction of EDFAs has offered the capability to construct an all-optical network that can support a large number of users. The advent of fiber amplifiers suggests that it should be possible eventually not only to build the local area networks (LANs) and metropolitan area networks (MANs) in which the paths are entirely optical, but to interconnect them to form wide area networks (WANs). Eventually, all-optical WANs as a key carrier backbone for future communications can be implemented.

Possibly, the appropriate architectures for LANs and WANs will be different. For example, the scalability in terms of the number of users and geographical span is an important issue in designing a WAN, whereas in a LAN, the geographical span is limited. In a WAN, where the user population is so large, most likely a WDM network will be deployed in which wavelengths have to be reused to provide full connectivity among all users. In a large-scale all-optical network, the interconnection of independent networks is inevitable, and therefore, so is the wavelength-reuse. Notice, a LAN can operate at only one wavelength, and employ another multiplexing technique such as CDMA or TDMA. WDM technology requires high quality components such as narrow band lasers and optical filters. For LAN applications where a large quantity of expensive components are needed, WDM technology has proven, so far, to be expensive. This makes other multiplexing schemes such as CDMA and TDMA more attractive.

Different network architectures can be realized based on the use of different optical devices and network topologies. Each architecture has its own features and is suited to specific applications. Network architectures can be classified into two

categories: broadcast-and-select, and wavelength-routing networks. In turn, each of these can be classified as either single-hop networks, or as multi-hop networks. In broadcast-and-select networks, the transmission from each station is broadcast to the network stations. At the reciever, the desired signal is then extracted from all the signals. In wavelength-routing networks, wavelengths are routed along a limited number of optical routers as to be able to reuse the wavelength in the network.

The term "single-hop networks" is used where information transmitted reaches its final destination without being converted to electronic form along the path. Single-hop networks are also called all-optical networks. In multi-hop networks, the transmitted information reaches its destination while being converted in intermediate nodes.

VIII.2.2 Wavelength-Routing Networks

Wavelength-routing networks allow the reuse of wavelengths in WDM networks. In the wavelength-routing networks as long as the paths taken by any two connections do not overlap, they can be on the same wavelength. This results in a tremendous reduction in the number of required wavelengths. In addition, power divisioning problem is no longer present, in these networks.

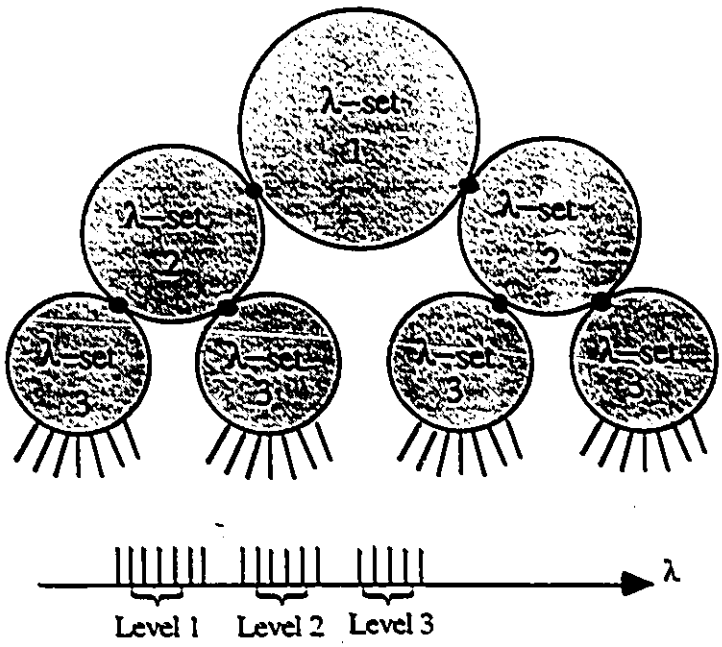

Fig. 8.1. Example of wavelength-reuse. The dots represent wavelength-selective physical links between hierarchical levels

The architecture shown in Fig 8.1 employs a three-level hierarchy using WDM. At the lowest level of the hierarchy are Level-3 all-optical networks. These networks can be viewed as a collection of high-performance LANs. Notice, that these LANs can operate at only one wavelength, and employ another multiplexing technique internally such as CDMA or TDMA. The intermediate level, Level-2, can be viewed as a metropolitan area network that connects a set of Level-3 networks. The highest level, Level-1, can be viewed as a national or worldwide backbone that connects Level-2 networks.

VIII.2.3 Broadcast-and-Select Networks

In broadcast-and-select networks, all physical-network topologies; i.e., star,

bus, and ring topology can be used for the purpose of broadcasting. However, a distinction must be made between several topological aspects of a network, in order to keep track of what is going on physically and logically.

(1.) The placement of the actual links and nodes defines the *physical – network topology*, for example, a ring, a star, a bus, or other choices.

(2.) On this physical network topology we can impose a particular *physical – path topology* that defines where the traffic flows between end users. The *routing* problem is basically that of imposing some sort of optimum physical-path topology on top of a given physical-network topology.

(3.) A representation that shows only which users can communicate with which other users constitutes the *logical topology*.

Broadcast-and-select network architectures are not scalable to a large population due to the use of a shared medium. These architectures are more suitable for LAN and MAN applications.

VIII.2.3.A Star Topology

The function of passive star coupler is to accept signals from all the stations simultaneously and broadcast them to all the receivers. Thus, each receiver has access to all transmitted signals and selects out the messages intended for it.

Stations can be equipped with one or many optical transmitters and receivers. These transceivers can be either tunable or fixed-tuned, depending on the particular protocols used. Full connectivity is achieved by tuning the transmitters and /or

receivers to the desired channels.

Regarding power efficiency, assume that the signal power P is available from each of the N transmitters and the fibers are lossless. The star coupler uniformly distributes these signals across its N output fibers, so that each one delivers to its receiver a contribution P/N from each transmitter.

VIII.2.3.B Bus Topology

Over a unidirectional bus, each user injects signal into the so called talk side of the bus, via directional couplers. These signals are distributed to the receivers on the other side of the bus called the listen side, via a second set of couplers. Obviously, a true network would need two such buses, one for each direction.

The power division issue would be the same for each bus, so we consider only one. In an $N-$user network with ideal couplers to inject and broadcast the optical signals, only $\frac{P}{N^2}$ useful power is delivered to each receiver. This is due to the fact that the sum of the fraction of powers coupled to each coupler output is less than 1. Since this signal must then be distributed among N receivers, it is attenuated by $\frac{1}{N}$, resulting in an overall transmitter-to-receiver attenuation of $\frac{1}{N^2}$.

The disadvantage of the bus topology, namely; poor energy efficiency, can be overcome with a suitable optical amplifier to compensate for the high signal attenuation in the network. However, there are two characteristics of an optical amplifier that limit its usefulness in LAN applications: maximum output power and internal noise generation.

VIII.2.3.C Ring Topology

Typically, the ring structure consists of a closed loop of point-to-point links. The nodes can be interconnected by multiple fiber loops forming rings. Newly proposed optical ring networks employ an add-drop-multiplexer (ADM) at each network access node along with an optical reciever. This device allows the optical signals to be injected into the ring from each station without any splitting loss. It also can filter out residual optical power after one complete cycle.

As newly invented photonic devices, specially fiber amplifiers make it reality to build the photonic network covering a large geographic area, it has become an important issue to achieve network full connectivity with a minimum number of single-mode fibers. That is the reason that optical rings are the most promising candidates for MAN applications.

Among the physical topologies that can be employed to implement broadcast-and-select LANs, stars are the most popular to date due to the lowest required power budget. However, broadcast-and select networks suffer from the lack of the scalability due to the use of the shared medium. These architectures heavily depend on EDFAs to compensate for both transmission and component losses.

VIII.3 Conclusions

In this chapter, we presented the motives of developing all-optical networks. Also, while avoiding confining ourselves to a particular network topology or architecture, we described how link-budget problems as a result of splitting loss and

the attenuation accumulated with distance can be dealt with, introducing photonic amplification.

Chapter IX

Application of EDFA in All-Optical LANs

IX.1 Introduction

Large bandwidth and low propagation loss of fiber along with the introduction of optical fiber amplifiers that offer the capability to exploit this tremendous available bandwidth makes the single-mode fiber the obvious medium of choice for long-haul transmissions. However, the existence of optical local area networks (LANs) relies upon the availability of an efficient multiple-access technique capable of using the vast available bandwidth of fiber to accommodate a large number of users. Several multiple-access protocols such as ALOHA and CSMA/CD protocols have been implemented in broadband LANs employing coaxial cable and radio frequency modems. In these protocols, the channel is shared among users by a form of random multiple-access technique which involves the detection of collisions between data packets from different users and some form of retransmission. These protocols are designed for low traffic loads and relatively low bit rate signals. Therefore, in an optical LAN where the operational speed is high and there are large traffic loads, the substantial increment of the number of packet collisions would lead to rapidly accumulating delays. The use of these protocols in an optical medium is limited on another account as well. These protocols do not allow for users to access the channel, simultaneously. Therefore, these protocols do not benefit from the large bandwidth available in fiber channel in order to realize large throughputs with short transmission delays. The CDMA protocol

has the capability to utilize the optical channel bandwidth in order to provide simultaneous access to multiple users. That is, the CDMA protocol enables "K" simultaneous users to access the channel before data packet transmission failures become unacceptably large.

Presentation of topics in this chapter is as follows. In section 2, various schemes are reviewed on use of bipolar codes in noncoherent optical CDMA networks. In section 3, the LAN architecture is described. In section 4, the transmitter and receiver are described. The system model is followed by presentation of the BER evaluation both numerically and using the closed-form formula. In section 5, the modified unipolar-bipolar cross correlation are defined where the analytical evaluation is based on these functions. The numerical results are compared with approximate results from the closed-form formulae. Finally, the conclusions are presented in section 6.

IX.2 Optical CDMA LANs

IX.2.1 Noncoherent Optical CDMA Networks with Bipolar Capacity

The principal aim of this chapter is to present an explicit model for a new CDMA receiver. It is important to note that not only the code sequence set that is used to spread the data, but also the way one processes the received signal strongly determines the capacity of a CDMA system. The correlation detection of ordinary CDMA is simple but not optimum, in general. However, to date, it is an open question how to increase the system capacity by using more efficient and practical decoding methods.

Optical CDMA systems using direct detection and delay-line based receivers have been investigated by several authors [79], [80], [9]. In these systems, the modulation is on-off-keying (OOK), so that a non-coherent detector can be used in the receiver. The OOK modulation used in these systems led to the design of new sets of unipolar sequences, such as Prime and Orthogonal codes [79]-[80]. However, these codes suffer from higher crosscorrelation peaks compared to the conventional bipolar codes such as Gold and Kasami codes. That is, for a given code length (processing gain), the ratio of the autocorrelation to crosscorrelation peak is much smaller and there are significantly fewer sequences available in a set. This was noted by Neusy and Kavehrad [63] and they proposed optical processing techniques that would allow use of bipolar codes in all-optical settings.

Of course, in a coherent optical CDMA system, the laser light can be phase modulated. Hence, bipolar code sequences can be deployed. However, in general, this would require coherent detection at the receiver which is much more complicated and costly than direct detection. Coherent detection allows the codes to maintain their bipolar nature and a conventional electronic correlation receiver will be able to detect the signal [10]. This method allows for a combined wavelength-division multiplexing (WDM)/CDM system where the wavelength of optical oscillator at the receiver downconverts the appropriate channel to an intermediate microwave frequency.

Vannucci[96] has introduced a technique by which coherent optical detection is not necessary. This is done by using a phase modulator at the receiver that modulates the received signal by the same bipolar code used at the transmitter. The receiver phase modulator, if properly synchronized to the transmitter, despreads the desired signal to a bandwidth much smaller than that of the interfering signals.

The optical phase modulator is followed by a very narrowband optical filter to reject the out-of-band interference. The filtered optical signal is processed by direct detection. This technique is also suitable for a combined WDM/CDM network where the optical filter can select the desired wavelength. A Fabry-Perot (FP) (etalon) optical filter was employed in [96]. These filters have a periodic transfer function. The frequency response is a series of equally-spaced peaks (mainlobe) and relatively large sidelobes. The periodic transfer function characteristics can be arranged in such a way that one of the peaks falls exactly on top of the desired signal which, therefore, will pass through with little attenuation. The interference falling inside the filter peaks will get through. The effectiveness of the filter in reducing interference is determined by the ratio of peak spacing (the free spectral range) to the width of an individual peak, a parameter known as "finesse". Because of the periodic nature of the FP filters, the entire optical spectrum, as seen through an etalon, is folded over into one free spectral range. Therefore, in order to be able to accommodate a reasonable number of wavelengths and at the same time to have a very narrowband filter, the finesse of these filters should be extremely high. Filters with a finesse of 10,000 exist. That is, for a bit rate of 50 MHz, the free spectral range which is a product of the finesse and the bit rate would be 500 GHz. This does not allow for many adequately-spaced optical carriers. Therefore, the wavelength of the lasers at the transmitter must be tightly controlled, and so must be the frequency response of the etalon filters at the receiver. These filters are very sensitive to any temperature change. Another drawback of this method is due to the fact that the out-of-band interference passed through the filter is detected, incoherently. Therefore, the noise resulting from multi-user interference would contain a DC component which is a function of the number of active users. Therefore, the DC value is a random variable. In this chapter, we introduce a technique that while using direct detection, does not rely on a very narrowband

optical filter to remove the interference.

References [65], [95], and [105] present various schemes on use of bipolar codes in optical CDMA networks. For the technique presented in [65], it is necessary that a balanced PN sequence is employed. Therefore, usage of unbalanced sequences conventionally used in CDMA systems, such as Gold and Kasami type are excluded. In order for this technique to achieve the bipolar capacity, it is required that balanced types such as nonlinear de Bruijn sequences recommended in [65] to have the same correlation properties as those of, e.g., Gold sequences. However, the correlation properties of these sequences are not as well-constrained as those of the conventional codes. Proposed techniques in [95] and [105] require further spreading of the already spread signal in order to remove the effect of unbalanced codes. In this chapter, we introduce a technique by which bipolar capacity is achieved while employing conventional bipolar codes. The technique removes the effect of unbalanced codes by applying a simple modification to the unipolar-bipolar correlation receiver. In the following, we show that the multi-user interference term that is obtained using modified unipolar-bipolar correlation is a scaled version of that obtained in a bipolar DS-CDMA scheme. That is, not only the offset in the autocorrelation term is removed, the offset (DC component) in the interference term is also forced to zero. This technique is specially suitable for a combined WDM/CDM system, where an optical filter with a much wider passband and consequently a smaller finesse can separate the wavelengths. This is due to the fact that the interference rejection is not done by the filter itself.

IX.3 LAN Architecture and System Description

At the transmitter, the input data bits are shift inversion keying (SIK) encoded

first, and then modulated onto the laser output via an external modulator. The modulation scheme is OOK, so that a noncoherent detector can be used at the receiver. In an optical SIK system, the data bits are modulated either by a unipolar signature sequence or its complement depending on whether it is a "0" or a "1", respectively.

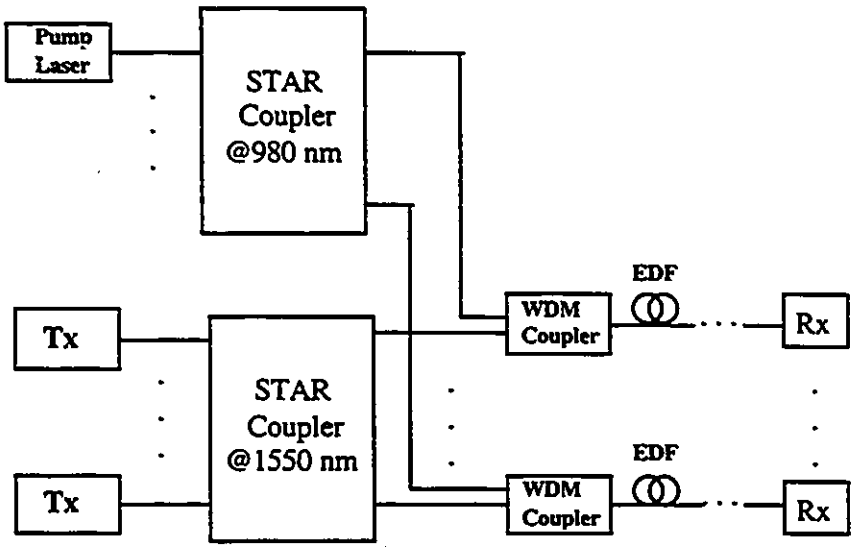

Fig. 9.1. CDMA LAN Architecture

The transmitted signals are broadcasted to all users via a star coupler operating at the wavelength signal, as shown in Fig. 9.1. The output signals are amplified at the output port of the star coupler. The output power of one or more pump lasers is shared among these EDFAs via another star coupler operating at 980 nm.

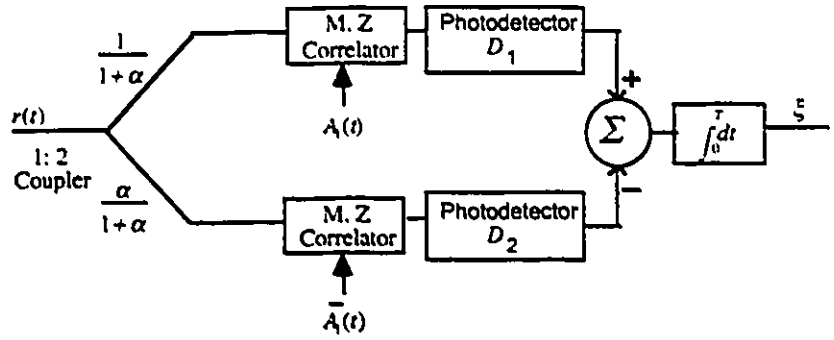

Fig. 9.2. An optical unipolar-bipolar correlator receiver

At the receiver, as shown in Fig. 9.2, the modified unipolar-bipolar correlator is practically realized by an unbalanced 1:2 coupler and two correlators that are matched to the unipolar form of the bipolar sequence and its complement, respectively. In practice, a Mach-Zehnder (MZ) modulator that is driven by an electric signal corresponding to the unipolar sequence $A_1(t)$ can act as a matched-filter matched to $A_1(t)$. A Mach-Zehnder modulator divides the incoming lightwave signal into two arms where one of the arms carries a signal that is delayed compared to the signal being carried by the first (because of the electric voltage applied to the second). Depending on the value of the applied voltage, the signals being carried by two arms can add either constructively or destructively, and the output power of the MZ interferometer can vary from a maximum value to zero. Therefore, if a scaled version of the unipolar sequence $A_1(t)$ is applied to the MZ interferometer, the input signal will be multiplied by the sequence $A_1(t)$ thereby performing the correlation function. The bipolar sequence $a_1(t)$ is related to its unipolar version $A_1(t)$ by $a_1(t) = -1^{[A_1(t)]}$. The optical outputs of the correlators are subtracted via a balanced photodiode receiver. As will become evident in the following sections, if the unipolar-bipolar correlation is performed without any modification, it would result in an interference term with a DC component. The

value of this DC component is determined by the number of simultaneous users and the characteristics of the reference code. Since the number of active users is a random variable, the detection problem is made more difficult and less accurate by the presence of a random DC level. In this chapter, we show how a simple modification to the system can solve this problem.

IX.4 System Modeling

Assume that K simultaneous users are sharing a transmission channel. The k-th user's data signal $B_k(t)$ is a sequence of unit-amplitude, unipolar rectangular pulses of duration T. Hence,

$$B_k(t) = \sum_{j=-\infty}^{+\infty} B_j^k P_T(t - jT) \tag{1}$$

where B_j^k represents the k-th user data at the j-th timing interval taking on its values from the set $\{1, 0\}$ and $P_T(.)$ is a rectangular waveform of T-second duration. The k-th user is assigned a code waveform $A_k(t)$ that consists of a periodic sequence of rectangular chips taking on values from the set $\{1, 0\}$ each of T_c seconds duration. If A_i^k represents the i-th chip value of the k-th user,

$$A_k(t) = \sum_{j=-\infty}^{+\infty} A_j^k P_{T_c}(t - jT_c). \tag{2}$$

Each user is assigned a unipolar periodic sequence with a period $N = T/T_c$ and the user transmits its signature code or its complement for a "0" or "1" data bit,

respectively. Thus, the SIK modulating signal of the k-th user can be demonstrated as:

$$S_k(t) = A_k(t) \oplus B_k(t) \tag{3}$$

where $\oplus$ denotes the "exclusive or" (modulo 2 addition) operation.

IX.4.1 Calculation of the Average Error Probability

The received signal at each receiver can be expressed as [41]:

$$r(t) = \sum_{k=1}^{K} P_t S_k(t - \tau_k) + n(t) \tag{4}$$

where P_t is the received chip peak optical power, τ_k is the relative time delay uniformly distributed over $[0, T]$ and K is the number of simultaneous users. From eq. (3)

$$r(t) = P_t \sum_{k=1}^{K} A_k(t - \tau_k) \oplus B_k(t - \tau_k) + n(t) \tag{5}$$

In this equation, $n(t)$ is white Gaussian noise with a double-sided spectral density of height $\frac{N_0}{2}$.

As explained in the previous section, the receiver in Fig. 9.2 consists of a 1:2 coupler and two matched-filters. The upper branch filter is a correlator matched to $A_1(t)$ and the lower branch filter is matched to $\bar{A}_1(t)$, where "over bar" means the binary complement. The received signal is split into two parts, unequally. The bipolar sequence $a_1(t) = -1^{[A_1(t)]}$. We assume that, $1/(1+\beta)$ fraction of the chips in $a_1(t)$ are '+1' and $\beta/(1+\beta)$ fraction are '-1'. Correspondingly, we assume that, $1/(1+\alpha)$ and $\alpha/(1+\alpha)$ are the fractions by which the received power is divided

between the upper and the lower branches, respectively. The outputs of the two matched-filters are photodetected and subtracted. The signal at the output of the adder is averaged over the bit duration T by an integrate-and-dump lowpass filter. Therefore, the decision variable at the filter output is

$$\xi = \frac{RP_t}{(1+\alpha)} \int_0^T r(t)[A_1(t) - \alpha \bar{A}_1(t)]dt \tag{6}$$

where R is the responsivity (AW^{-1}) of the PIN diodes. By using eq. (5) we obtain:

$$\begin{aligned} \xi = \frac{1}{(1+\alpha)} \sum_{k=1}^{K} \int_0^T RP_t[A_k(t-\tau_k) \oplus B_k(t-\tau_k)] \\ [A_1(t) - \alpha \bar{A}_1(t)]dt + \int_0^T n(t)dt \end{aligned} \tag{7}$$

The last term represents a sample of Gaussian noise with a zero-mean and a variance N_0T .

We notice that, $A_i(.) = \frac{1-a_i(.)}{2}$ and $\bar{A}_i(.) = \frac{1+a_i(.)}{2}$ and $A_k(.) \oplus B_k(.) = \frac{\{1-b_k(.)a_k(.)\}}{2}$, where $a_i(.)$ and $b_i(.)$ are bipolar forms of $A_k(.)$ and $B_k(.)$, respectively. Then, assuming the receiver of user number one (the reference receiver) delay locks to the corresponding transmitted signal enables one to rewrite eq. (7) as:

$$
\begin{aligned}
\xi = & \int_0^T \sum_{k=1}^{K} \frac{RP_t}{1+\alpha} \frac{1-\alpha}{4} dt \\
& + \frac{-RP_t}{4} \int_0^T \sum_{k=1}^{K} a_1(t) dt \\
& - \frac{RP_t}{1+\alpha} \frac{1-\alpha}{4} \int_0^T \sum_{k=1}^{K} b_k(t-\tau_k) a_k(t-\tau_k) dt \\
& + \frac{RP_t}{4} \int_0^T \sum_{k=1}^{K} b_k(t-\tau_k) a_k(t-\tau_k) a_1(t) dt \\
& + \int_0^T n(t) dt
\end{aligned} \tag{8}
$$

Notice that,

$$
\int_0^T a_1(t) dt = T\left(\frac{1}{\beta+1} - \frac{\beta}{\beta+1}\right) = \frac{T(1-\beta)}{1+\beta}.
$$

Therefore, eq. (8) can be rewritten as

$$
\begin{aligned}
\xi = & \frac{TRP_t}{4}\left[\frac{K(1-\alpha)}{1+\alpha} - \frac{K(1-\beta)}{1+\beta} - \frac{(1-\alpha)(1-\beta)}{(1+\alpha)(1+\beta)}\right] \\
& - \frac{RP_t}{4} \frac{1-\alpha}{1+\alpha} \sum_{k=2}^{K} \int_0^T b_k(t-\tau_k) a_k(t-\tau_k) dt \\
& + \frac{TRP_t}{4} {b_0}^1 \\
& + \frac{RP_t}{4} \sum_{k=2}^{K} \int_0^T b_k(t-\tau_k) a_k(t-\tau_k) a_1(t) dt \\
& + \eta
\end{aligned} \tag{9}
$$

where ${b_0}^1$ is the corresponding bipolar bit being detected and η is equal to the last term in eq. (8). The first term in eq. (9), which shows the offset effect, consists of the first two terms of eq. (8) and $k = 1$ contribution of the third term. The fourth term in eq. (8) was divided into two terms; one for the matching sequence $a_1(t)$ and one for the non-matching sequences corresponding to the third and fourth terms in eq. (9), respectively.

From eq. (9), for $\alpha = 2K\beta + (\beta - 1)/[2K + (\beta - 1)]$, the offset effect is completely removed. Obviously, for a large K, the value of α is equal to β. As mentioned, β is the ratio between number of '-1's and '1's in a bipolar Gold sequence, or '1's and '0's in its equivalent unipolar code. The number of '1's (Hamming weight) of the unipolar version of Gold sequences assumes only "three" values [84]. Therefore, β also assumes "three" values. These values, for example for a code of length 127, are 1.309, 0.788, and 1.01 and become closer to one for longer codes. As seen in Fig. 9.3, for even a small number of active users $K = 2$, the value of α is remarkably close to β (for a code of length 127, $\alpha/\beta = 0.983$, 0.986 and 1, respectively). Therefore, one could choose the value of α to be β, a known parameter, while the offset effect is completely removed for large values of K. For a large number of active users K, the system has a small tolerance against any kind of inaccuracy in detection process such as offset effect.

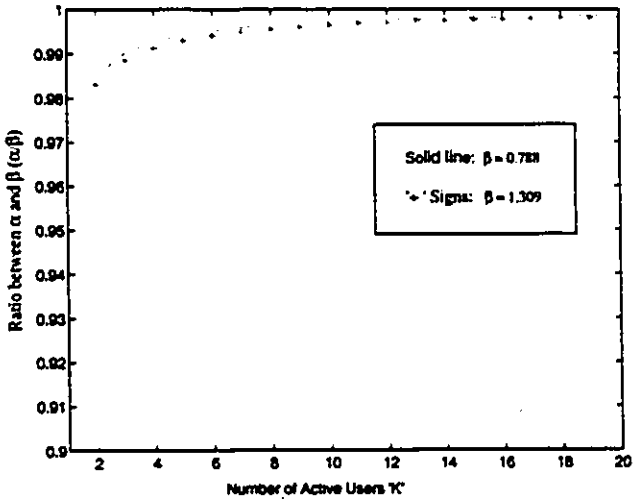

Fig. 9.3. The ratio of α/β as a function of K.

By using the continuous-time partial cross-correlation functions [74] $R_{k,i}(.)$ and $\hat{R}_{k,i}(.)$ and the functions that we introduce as continuous-time partial weight functions $W_{k,i}(.)$ and $\hat{W}_{k,i}(.)$, we can rewrite eq. (9) as

$$\begin{aligned}\xi = & \frac{TRP_t}{4} b_0{}^1 \\ & + \frac{RP_t}{4} \sum_{k=2}^{K} \left[b_{-1}^k R_{k,1}(\tau_k) + b_0^k \hat{R}_{k,1}(\tau_k) \right] \\ & - \frac{RP_t}{4} \frac{1-\alpha}{1+\alpha} \sum_{k=2}^{K} \left[b_{-1}^k W_{k,1}(\tau_k) + b_0^k \hat{W}_{k,1}(\tau_k) \right] \\ & + \eta\end{aligned} \tag{10}$$

where b_0^1 represents the information bit being detected and b_{-1}^1 is the previous adjacent bipolar bit while:

$$R_{k,i}(\tau) = \int_0^T a_k(t-\tau) a_i(t) dt$$

$$\hat{R}_{k,i}(\tau) = \int_\tau^T a_k(t-\tau) a_i(t) dt$$

$$W_{k,i}(\tau) = \int_0^\tau a_k(t-\tau) dt$$

$$\hat{W}_{k,i}(\tau) = \int_\tau^T a_k(t-\tau) dt.$$

The first term in eq. (10) is the in-phase autocorrelation peak whereas the second and the third terms are the multi-access interference (MAI) terms. As seen, the second term is a scaled version of the interference term in a bipolar DS/CDMA scheme. Since the average values of b_0^k and b_{-1}^k are both zero, the mean values of the second and the third terms in eq. (10) are also zero. In our numerical evaluation, we used the same set of Gold sequences that we used in [41]. After generating the unipolar versions of these codes, we computed the modified unipolar-bipolar crosscorrelation variance. The modified correlation

functions are defined in section IX.5. Then, we describe how the discrete aperiodic crosscorrelation functions [74] are used to evaluate the crosscorrelation variance for different number of users. The calculated multi-user interference power was used to evaluate the SNR and the average BER.

The power of the third term in eq. (10) contributes a negligible amount to MAI. As mentioned, for a Gold code of length 127, $(\frac{1-\alpha}{1+\alpha})^2$ at its maximum is smaller than 0.017. Therefore, by neglecting the third term in eq. (10), we can approximately calculate the SNR and evaluate the BER performance. For large K and N, we may model all the multiuser interference terms as a zero-mean Gaussian random process. The variance of the second term is approximately equal to [74]:

$$\left[\frac{RP_t}{4}\right]^2 \frac{2(K-1)}{3N}.$$

The mean and the variance of the decision variable ξ scaled by 1/T are approximately:

$$\mu_\xi = \frac{RP_t}{4}$$

$$\sigma_\xi{}^2 \approx [\frac{RP_t}{4}]^2 \frac{2(K-1)}{3N} + N_0$$

where:

$$N_0 = \frac{1}{T}[\frac{4KT'F}{R_L} + 2e(I_{D1} + I_{D2}) + 8I_sI_{sp}/B_o + (RIN)(I_{D1}{}^2 + I_{D2}{}^2)] \quad (11)$$

In eq. (11), the first term is the thermal noise where T is the bit duration, K is the Boltzmann's constant ($1.38 \times 10^{-23} j/K$), T' is the absolute temperature ($290°K$), e is an electron charge ($1.602. \times 10^{-19} c$), F is the electronic receiver amplifier noise figure and R_L is the photodiode load resistor with a 50 ohm nominal value. The thermal noise can also be expressed by the thermal current

power spectral density N_{th}. The second term represents the shot noise where I_{D1} and I_{D2} are currents corresponding to the average received optical power. It is worth mentioning that although the input signals to the photodetectors are correlated, the shot noise at each diode is generated by an independent process. Therefore, the power in the noise terms can simply be added. After despreading, the desired sequence $A_1(t)$ contributes $P_T/4$ to the optical power incident on each PIN diode while the MAI contributes to each an average optical power $(K-1)P_t/8$. The third term is the signal-spontaneous beat noise. I_s denotes the corresponding signal photo current, and I_{sp} is the photo current equivalent of the ASE power generated by the EDFA.

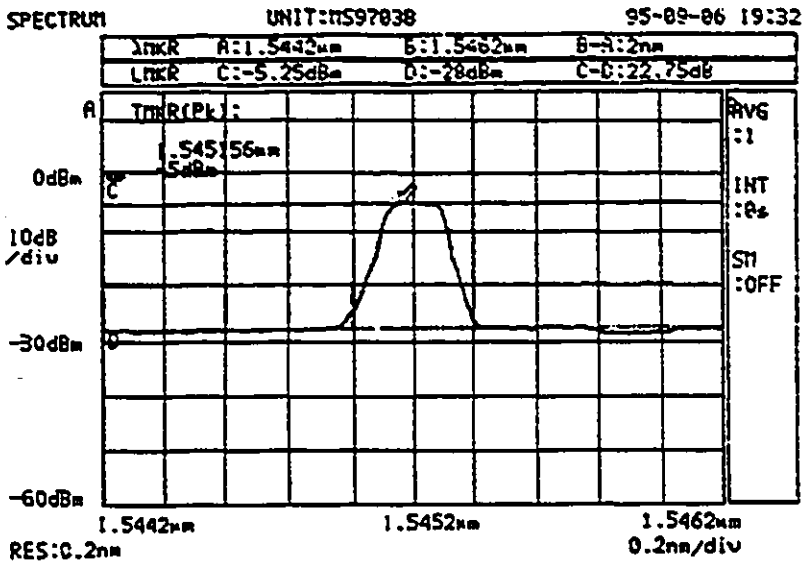

Fig. 9.4. Optical SNR for input power -25 dBm at 1545 nm

The ASE power can be determined by the signal power, and optical signal-to-

noise ratio SNR_o at the receiver shown in Fig. 9.4. B_o represents the optical bandwidth within which the ASE and optical SNR have been measured. From eq. (32) of chapter IV, the third term can be expressed by

$$\frac{8(eRP_s)^2}{h^2\nu^2(SNR_o)B_o} = \frac{8(eRKP_t/8)^2}{h^2\nu^2(SNR_o)B_o}$$

To calculate the signal-spontaneous beat noise, the ASE in the signal band ($N \times B = N/T$) is considered. Since, the electrical bandwidth of the receiver is $B_e = 2/T$, this noise is reduced by B_o/B_e times. $h\nu$ is the photon energy. The relative intensity noise RIN is negligible. In eq. (11), the noise associated with the diodes dark currents has been neglected. Both of these noise terms are negligible compared to the other noise components. Therefore: $N_0 = \frac{1}{T}(eRKP_t/4 + 4(eRKP_t/8)^2/(SNR_oN) + N_{th})$ and the SNR is

$$SNR = \frac{(RP_t)^2}{\frac{2(K-1)}{3N}(RP_t)^2 + 16N_0} \tag{12}$$

while

$$P_e = Q(\sqrt{SNR}) \tag{13}$$

IX.4.2 Results

Fig. 9.5 shows plots of BER versus P_t with K =1,5,8 and 10 as a parameter. The plots were evaluated under a spreading factor $N = 127$, PIN diode responsivity $R = 0.85AW^{-1}$, thermal current power spectral density $N_{th} = 1pA^2Hz^{-1}$, data rate 1/T= 10 Mb/s. EDFA is assumed to have a gain of 20 dB for the input power of -25 dBm at 1545 nm. According to our experimental results, the measured received optical SNR by a 0.2 nm optical filter was 26 dB. This results in a spontaneous factor n_{sp} 4.89. Under these conditions, the signal-spontaneous beat noise current

power spectral density for one user when $P_t = -25$ dBm is $2.7 \times 10^{-4} pA^2 Hz^{-1}$ which is negligible even compared to the thermal noise. Although the signal-spontaneous beat noise increases as K^2, the power of this noise only for the number of active users as high as 100 is comparable to thermal noise. For one user, a receiver sensitivity of -40 dBm at 10^{-9} is obtained. As seen, the BER degrades, as K increases. In Fig. 9.5, numerical BER results are compared to those evaluated by the closed-form formulae derived in eqs (12) and (13). We notice that eq. (12) is a scaled version of the SNR for the bipolar CDMA systems. This suggests that the system can achieve the same capacity as a CDMA system using bipolar codes and coherent detection. Comparison of the BER curves proves that the formulae (eqs (12) and (13)) provide a very simple and accurate means for performance evaluation of such a system for $K > 8$, where accuracy counts the most.

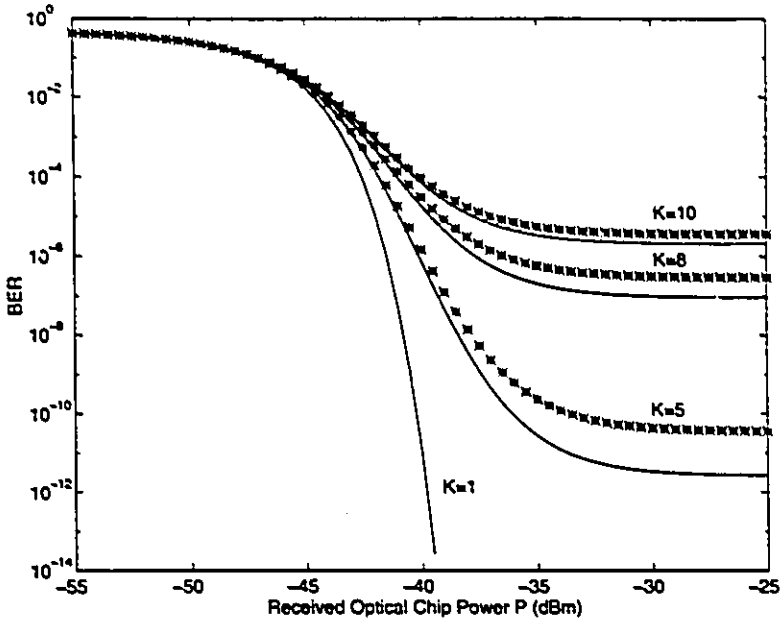

Fig. 9.5. BER versus peak incident chip optical power P_t

—— Analytical results

******* Exact results using numerical analysis

In the following section, we introduce the modified unipolar-bipolar correlation functions. We apply these definitions, specifically, to the Gold codes and continue the analysis by an example (Gold code of length 127). We outline how the numerical analysis should be carried out to calculate the BER, exactly.

IX.5 Modified Unipolar-Bipolar Auto- and Cross-Correlation Functions

IX.5.1 General Assumptions and Definitions

A bipolar code sequence of length N will be denoted by

$$X = [x_o, x_1, \ldots, x_{N-1}] \quad \text{where } x_i = \pm 1$$

The set of all code sequences, say M sequences, is the code sequence set

$$C = \{X^{(1)}, X^{(2)}, \ldots, X^{(M)}\}.$$

T will denote the cyclic (left shift operator; it acts on a sequence of length N by the rule $T[x_0, x_1, \ldots, x_{N-1}] = [x_1, x_2, \ldots, x_{N-1}, x_0]$. The crosscorrelation function $C_{XY}(k)$ between two code sequences $X, Y \in C$ is defined by

$$C_{XY}(k) = \langle X, T^k Y \rangle$$

where k is an integer and $\langle ., . \rangle$ denotes the standard scalar product in the Euclidean space $\mathbf{R}^N$, *i.e.*, $\langle X, Y \rangle = \sum_{i=0}^{N-1} x_i y_i$. Note that, crosscorrelation $C_{XY}(k)$ is periodic with period N and satisfies the following symmetry property:

$$C_{XY}(k) = C_{XY}(N-k) \text{for all } k.$$

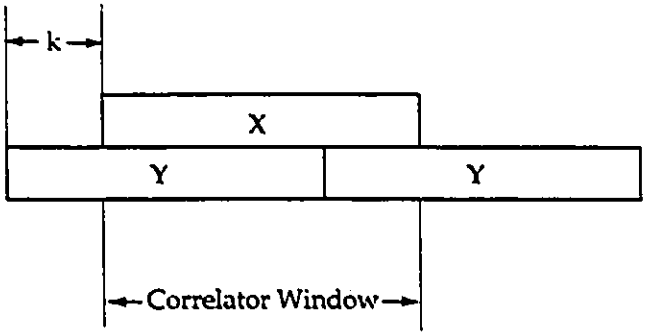

Fig. 9.6. Interpretation of $C_{XY}(k)$.

IX.5.2 Gold Sequence Set

First, we shortly describe a Gold sequence set. In order to have a convenient notation for the sequences, we make use of the following one-to-one correspondence between binary sequences and ±1-sequences. To every binary sequence $\mathbf{b} = [b_0, b_1, \ldots, b_{N-1}] \in GF(2)^N$, there is associated one and only one ±1-sequence where $x_i = (-1)^{b_i}$, $i = 0, 1, \ldots, N-1$. This correspondence will be denoted by $X = e(\mathbf{b})$. We notice that the crosscorrelation value at the origin can be expressed in terms of Hamming weight $w_H(,)$ as

$$C_{XY}(0) = N - 2w_H(a + b),$$

and, more generally, for any integer k,

$$C_{XY}(k) = N - 2w_H(a + T^k b). \tag{14}$$

The Gold code set is most simply described in terms of a preferred pair (u, v)

of binary maximal length (m-)sequences [74]. An m-sequence is a sequence of maximal period that can be achieved by a binary linear feedback shift register of some fixed length m starting in some non-zero state. The maximum period that a binary linear feedback shift register of length m can achieve is $N = 2^m - 1$; thus, all binary m-sequences have lengths $N = 2^m - 1$. One period

$$\mathbf{u} = [u_0, u_1, \ldots, u_{N-1}],$$

is what is usually meant as the m-sequence. The Hamming weight of an m-sequence $\mathbf{u}$ is $\frac{(N+1)}{2}$. The shift-and-add property is another property that holds for m-sequences, i.e., for any integer i there exists an integer l such that,

$$u + T^i u = T^l u$$

Moreover, if i runs through $1, 2, \ldots, N-1$ then so does l, but in some different order.

Let $N = 2^m - 1$ and $e = \frac{\lfloor m+2 \rfloor}{2}$. A preferred pair (u, v) of m-sequences is obtained by starting with an m-sequence $\mathbf{u}$ and taking $\mathbf{v}$ to be the 2^e+1st decimation of $\mathbf{u}$, i.e., the i-th component of $\mathbf{v}$ is given by $v_i = u_{i(2^e+1)}$. A preferred pair of m-sequences has a correlation function $C_{XY}(k)$ that assumes only the three values $-1, -1+2^{(m+g)/2}$ and $-1-2^{(m+g)/2}$, where $g = gcd(2e, m)$ is the greatest common divisor of $2e$ and m. The histogram of the crosscorrelation of a preferred pair of m-sequences are given in Table 9.1.

$C_{XY}(k)$	Multiplicity
-1	$2^m - 2^{m-g} - 1$
$-1 + 2^{(m+g)/2}$	$2^{m-g-1} + 2^{(m-g)/2-1}$
$-1 + 2^{(m+g)/2}$	$2^{m-g-1} - 2^{(m-g)/2-1}$

Table 9.1. Histogram of the crosscorrelation function of a preferred pair of m-sequences

For $m = 7$, the length of m-sequences N is 127. Hence, $e = 4$, $g = 1$ and a preferred pair of m-sequences of length 127 have a three-valued crosscorrelation function taking on values from$\{-1, -17, 15\}$. The multiplicity of three values are given in Table 9.2.

$C_{XY}(k)$	Multiplicity
-1	63
15	36
-17	28

Table 9.2. Histogram of the crosscorrelation function of a preferred pair of m-sequences of length 127

Now, we are ready to define the Gold sequence set which contains a large number of sequences with good periodic crosscorrelation. Let (u, v) be a preferred pair of m-sequences, then the set $G(u, v)$ defined by

$$G(u,v) \equiv \{u\} \cup \{v\} \cup \{u \oplus T^i v \mid i = 0, 1, \ldots, N-1\} \tag{15}$$

contains $N + 2 = 2^m + 1$ Gold sequences of period N.

IX.5.3 Hamming Weight of Sequences in a Gold Code Set

We notice that, if a and b in eq. (14) are a preferred pair of binary m-sequences, $a + T^K b$ according to the definition of a Gold sequence set in eq. (15) is a distinct Gold sequence for a particular k. From eq. (14), the Hamming weight of code sequences in a Gold code set is derived by:

$$w_H(.) = \frac{N - C_{XY}(.)}{2} \tag{16}$$

From Table 9.1 and using eq. (16), the distribution of the Hamming weights of sequences in a Gold code set is found.

$w_H(a)$	$\sum_{i=0}^{N-1} A_i$	Multiplicity
2^{m-1}	1	$2^m - 2^{m-g} + 1$
$2^{m-1} - 2^{\frac{(m+g-2)}{2}}$	$1 - 2^{\frac{(m+g)}{2}}$	$2^{(m-g-1} + 2^{\frac{(m-g)}{2-1}}$
$2^{m-1} + 2^{\frac{(m+g-2)}{2}}$	$1 + 2^{\frac{(m+g)}{2}}$	$2^{m-g-1} - 2^{\frac{(m-g)}{2-1}}$

Table 9.3. Distribution of the sequence Hamming weights in a Gold sequence set

In Table 9.3, $w_H(a)$ represents the Hamming weight of the binary Gold sequence a. The ± 1-sequence A is related to the binary sequence a such that $A_i = (-1)^{a_i}$. The sum of all elements of the ± 1-sequence A is shown by $\sum_{i=0}^{N-1} A_i$. The Hamming weight of gold sequences of length 127 is shown in Table 9.4.

$w_H(a)$	$\sum_{i=0}^{N-1} A_i$	Multiplicity
64	−1	65
56	+15	36
72	−17	28

Table 9.4. Distribution of the sequence Hamming weights in a Gold sequence set of length 127

IX.5.4 Cross-correlation of Binary (Unipolar) and ±1- (Bipolar) Gold Sequences

For any two sequences $x \neq y$ in the Gold sequence set G, say $X = e(a) = e(u + T^i v)$, $Y = e(b) = e(u + T^j v)$, we have

$$\begin{aligned} C_{XY}(k) &= N - 2w_H(u + T^k u + T^i v + T^{k-j} v) \\ &= N - 2w_H(T^l u + T^m v) = N - 2w_H(u + T^{m-l} v) \end{aligned} \tag{17}$$

Since (u, v) is a preferred pair of m-sequences, from eq.(17), crosscorrelation of two-value Gold sequences takes on the same three values as the crosscorrelation of the preferred pair of m-sequences by the same multiplicity.

The crosscorrelation of binary Gold sequences can be calculated by the following formula:

$$\begin{aligned} C_{ab}(k) &= \sum a_i b_{i+k} = \sum \frac{(1 - x_i)}{2} \frac{(1 - y_{i+k})}{2} \\ &= \frac{1}{4}(N - \sum x_i - \sum y_i + C_{XY}(k)) \end{aligned} \tag{18}$$

The crosscorrelation of any binary Gold sequence with the complement of

another code from the same set is derived by eq. (19).

$$C_{a\bar{b}}(k) = \sum a_i \bar{b}_{i+k} = \sum \frac{(1-x_i)}{2} \frac{1+y_{i+k})}{2}$$
$$= \frac{1}{4}(N - \sum x_i + \sum y_i - C_{XY}(k)) \tag{19}$$

From eq. (18), since the crosscorrelation of any two ± 1-sequences from the same set $C_{XY}(k)$ assumes three values listed in Table 9.1, the crosscorrelation of the corresponding two binary sequence codes $C_{ab}(k)$ assumes three values. However, these three values depend on the Hamming weigh of two sequences a and b or correspondingly on $\sum x_i$ and $\sum y_i$. From eq. (17), the three-valued crosscorrelation of every two binary codes can be calculated in a straight forward manner provided their Hamming weights are known. As an example, Table 9.5 shows the three value crosscorrelation function of binary sequences a and b where their Hamming weights are 72 and 56, respectively. The crosscorrelation function of other codes with different Hamming weights can be calculated in a straight forward manner from eq. (17).

$C_{a\bar{b}}(.)$	$C_{ab}(.)$	Multiplicity
$\frac{1}{4}(2^m + (2)2^{\frac{(m+g)}{2}})$	$\frac{1}{4}(2^m)$	$2^m - 2^{m-g} - 1$
$\frac{1}{4}(2^m + 2^{\frac{(m+g)}{2}})$	$\frac{1}{4}(2^m + 2^{\frac{(m+g)}{2}})$	$2^{m-g-1} + 2^{\frac{(m-g)}{2}-1}$
$\frac{1}{4}(2^m + (3)2^{\frac{(m+g)}{2}})$	$\frac{1}{4}(2^m - 2^{\frac{(m+g)}{2}})$	$2^{m-g-1} - 2^{\frac{(m-g)}{2}-1}$

Table 9.5. Unipolar crosscorrelation distribution of unipolar binary codes of weights 56 and 72. $W_H(a) = 72$, $W_H(b) = 56$.

Obviously,

$$C_{ab}(.) + C_{a\bar{b}}(.) = W_H(a),$$

and this can easily be verified by Table 9.5. Assume the average crosscorrelation for a code b of a certain Hamming weight is calculated. That is, the mean crosscorrelation values of this code b with all the remaining codes in the set is calculated. It can be shown that the ratio between the average crosscorrelation of code b and the average crosscorrelation of the complement of code b, $\bar{b}$, is exactly the ratio of the number of 1's and 0's in the code b. Table 9.6 shows the crosscorrelation distribution for code b with Hamming weight of 56. In the example presented in Table 9.6, the mean unipolar-unipolar crosscorrelations $E(C_{ab}(.))$ and $E(C_{a\bar{b}}(.))$ are 29.1 and 36.6, respectively. The ratio of these two values is 0.788 which is the same as the ratio of the number 1's and 0's in code b is obviously $\frac{56}{127-56} = 0.788$.

$W_H(a)$	$W_H(a) = 72$		$W_H(a) = 56$		$W_H(a) = 64$		
	$C_{a\bar{b}}(.)$	$C_{ab}(.)$	$C_{a\bar{b}}(.)$	$C_{ab}(.)$	$C_{a\bar{b}}(.)$	$C_{ab}(.)$	Multiplicity of $C_{ab} \times C_{a\bar{b}}$
	40	32	32	24	36	28	63
	36	36	28	28	32	32	36
	44	28	36	20	40	24	28
Multiplicity of a	63		36		28		

Table 9.6 Crosscorrelation distribution of code b with Hamming weight of 56.

From Eqs.(18) and (19), and also the fact the $C_{ab}(.) + C_{a\bar{b}}(.) = w_H(a) = cte$, one can conclude that:

$$var(C_{ab}(.)) = var(C_{a\bar{b}}(.))$$

It is known that the variance of bipolar-bipolar crosscorrelation $Var(C_{xy}(.)$

is equal to the code length N [74]. Owing to this fact and from eq.(18) or (19), one can calculate the variance of the unipolar-unipolar crosscorrelation to be $\frac{2.5}{16}N = \frac{2.5}{16}var(C_{xy}(.))$. Therefore, the variance of the modified unipolar-bipolar crosscorrelation, $var[C_{ab}(.) - \alpha C_{a\bar{b}}(.)$ is equal to $\frac{2.5}{16}var(C_{xy}(.) + \frac{2.5}{16}\alpha^2 var(C_{xy}(.)$. Notice that, $C_{a\bar{b}}$ and C_{ab} are independent, since $\bar{b}$ and b are orthogonal in time. In this example, α is equal to 0.788, therefore, the variance of the modified unipolar-bipolar crosscorrelation is equal to $\frac{1.01}{4}var(C_{xy}(.))$. We notice that the modified unipolar-bipolar autocorrelation power is exactly $\frac{1}{4}$-th of the bipolar-bipolar autocorrelation power. This means that in the case of synchronous transmission, the ratio of the autocorrelation to crosscorrelation power, except for a slight degradation ($\frac{1}{1.01}$ instead of 1), remains the same. It is known in the case of asynchronous transmission, the multiuser interference term is expressed using continuous-time partial crosscorrelation functions, $R_{k,i}$ and $\hat{R}_{k,i}$ defined by:

$$R_{k,i}(\tau) = \int_0^\tau a_k(t-\tau)a_i(t)dt$$

and

$$\hat{R}_{k,i}(\tau) = \int_\tau^T a_k(t-\tau)a_i(t)dt$$

These definitions for the case of modified unipolar-bipolar crosscorrelation are modified to:

$$R_{k,i}(\tau) = \int_0^\tau A_k(t-\tau)A_i(t)dt - \alpha\int_0^\tau A_k(t-\tau)\bar{A}_i(t)dt$$

and

$$\hat{R}_{k,i}(\tau) = \int_\tau^T A_k(t-\tau)A_i(t)dt - \alpha\int_\tau^T A_k(t-\tau)\bar{A}_i(t)dt \qquad (20)$$

Also, the definitions for the discrete aperiodic crosscorrelation function $C_{k,i}(.)$ for sequences $A_i(.)$ and $A_k(.)$ can be modified to:

$$C_{k,i}(l) = \begin{cases} \sum_{j=0}^{N-1-l} A_k(j) \cdot [A_i(j+l) - \alpha \bar{A}_i(j+l)], & 0 \le l \le N-1; \\ \sum_{j=0}^{N-1-l} A_k(j-l)[A_i(j) - \alpha \bar{A}_i(j)], & 1-N \le l < 0; \\ 0 & |l| \ge N. \end{cases} \quad (21)$$

We use these definitions in our numerical analysis to calculate the average signal-to-noise ratio, in the general case of asynchronous transmission.

Numerical Analysis:

From eq.(7), the output of the correlation receiver at $t = T$ is given by,

$$\begin{aligned} \xi &= \frac{TRP_t}{4} b_o^1 \\ &+ \frac{RPt}{4} \sum_{k=2}^{K} [b_{-1}^K R_{k,i}(\tau_k) + b_0^k \hat{R}_{k,i}(\tau_k)] \\ &+ \xi(x) \end{aligned} \quad (22)$$

Where $R_{k,i}(\tau_k)$ and $\hat{R}^n_{k,i}(\tau_k)$ are the modified unipolar-bipolar version of continuous time partial crosscorrelation functions defined in eq.(20).

Using discrete aperiodic crosscorrelation functions $C_{k,i}$ for modified unipolar-bipolar cases, defined by eq.(21), and the results presented by Pursley (eq.(18) in [74]) one can numerically evaluate the variance of the interference term which is the second term in eq.(22).

IX.6 Conclusions

In this chapter, a CDMA local area network architecture is studied. A star topology is used to provide the multi-user connectivity, where EDFAs will extend the limitation on the number of users in a power limited system. A new correlator receiver architecture based on a modified version of unipolar-bipolar correlation is proposed for noncoherent optical fiber CDMA networks. For this architecture, the receiver average bit error rate (BER) performance is numerically evaluated as a function of the received optical power for noncoherent transmission and direct detection with the number of simultaneous users as a parameter. The BER performance is also evaluated by a closed-form formula that is developed in this chapter. Comparison of the results from the latter with numerical results show that the formula provides a good approximation to the system performance. Furthermore, the closed form solution suggests that the system can achieve the same capacity as a CDMA system using coherent detection. Finally, we calculate the power penalty produced by the presence of EDFAs.

Chapter X

Summary and Suggestions for Future Work

The application of erbium-doped fiber amplifiers (EDFAs) in WDM transmission systems was studied in the first part of this thesis, while, the application of the EDFA in an optical local area network was studied in the second part. Generally speaking, our objective was to find efficient solutions to the problems dealing with amplified WDM transmission and network systems in order to enhance the system performance. WDM signals propagate through a chain of EDFAs in transmission systems. The accumulated ASE noise in the chain of amplifiers limits the maximum achievable optical SNR at each wavelength. The SNR at some wavelengths is further compromised because of the nonflat gain of the amplifier. The wavelength-dependent gain of the amplifier and the ASE accumulation impose a capacity limit on the amplified WDM systems. The capacity can be expanded by flattening the amplifier gain and filtering the ASE between the cascaded amplifiers. We have proposed two methods to equalize the gain of the amplifier where the ASE is filtered out without employing an external optical filter.

In bidirectional WDM transmission systems, signal-spontaneous noise at the receiver and the intensity noise due to reflections are major factors limiting capacity. A new bidirectional EDFA configuration is proposed where the impact of both effects is substantially suppressed. In the second part of this thesis, the EDFA is used in an efficient manner in an optical LAN in order to compensate

for both the splitting and attenuation losses.

In chapter 2, after a brief description of erbium-doped fiber amplifiers and their operation, an analytical model for EDFAs was described. Using this analytical solution, new expressions on the gain variations of the amplifier at different wavelengths were derived for the case of WDM signals. Using these derivations, we found a simple and efficient way to compensate for the wavelength-dependent gain variations of the amplifier due to the changes of the total input signal power or power distribution among different wavelengths. This solution was based on our finding that if the gain at one wavelength is fixed, the entire gain spectrum maintains its original profile. A simple electronic circuit was described that adjusts the pump power to preserve the gain spectrum of the amplifier. Although tunable, it is extremely difficult to make an adaptive optical equalizer, therefore, the gain profile based on which the tunable equalizer is tuned has to be preserved to make the equalization effective.

In chapter 3, the existing amplifier models were categorized. The description of a numerical model was presented where the effect of the ASE was included and the full ASE spectrum was resolved. ASE spectra is governed by the absorption and emission cross section spectra. The experimental measurements of the fiber gain and loss spectra were described. The absorption and emission cross section spectra were extracted from the measured spectra. In this chapter, we described a tunable gain equalization using a waveguide type transversal optical filter. This study outlined how coherent optical transversal filters can be designed for different purposes. In these filters, the incoming signal is divided into multiple branches where each tapped signal is weighted with a complex coefficient, and thereafter recombined. We showed that the coupling losses are avoided when the tapped

signals are coherently recombined. This gain equalizer filters the ASE that is placed outside the signals bands. Therefore, the input noise saturation of downstream amplifiers is reduced in the chain of amplifiers. The practical issues of the implementation of this filter were also discussed. The effect of the laser phase noise on the performance of this filter was studied in chapter 6.

In chapter 4, we describe the ASE generation in the EDFA. ASE spectrum closely emulates the gain spectrum. We presented the experimental results on the ASE spectrum under different conditions corresponding to different inversion levels. These results indicated that the gain slope of the EDFA at 1550 nm window can change based on the changes in the inversion level. This observation was the basis of the equalization method described in chapter 5. The spontaneous noise factor n_{sp}, the optical, and electrical signal-to-noise ratio at the amplifier input and output, and amplifier noise figure (NF) were also defined.

In chapter 5, a novel and simple gain equalization method was presented, where high- and moderate-inversion EDFAs were used alternatively in order to achieve a lesser interchannel power variation and SNR differential. EDFAs in high-inversion regime present a flatter gain, however, the SNR in this case degrades very fast after a few cascaded amplifiers. This is due to a strong ASE peak around 1530 nm of the EDFAs operating in high-inversion regime. The 1530 nm ASE peak is automatically removed by alternative use of high- and medium-inversion amplifiers, without inserting additional optical filters. The achieved SNRs and SNR differential in the compensated system were compared with those of a system containing a chain of either high- or medium-inversion EDFAs. The results showed the proposed system outperforms the other two systems.

In chapter 6, the effect of the interferometric phase-to-intensity noise conversion was studied. A new analytical technique was developed to evaluate the probability density function (pdf) of the intensity noise generated either at the output of a multi-tap coherent optical filter, or due to multiple reflections. The power penalty due this noise was also evaluated for the OOK modulated signals at different bit rates. The results on the power penalty due to interferometric noise due to multiple reflections were used in chapter 7.

In chapter 7, bidirectional amplification was studied. A novel bidirectional EDFA was presented where the power penalty associated with the amplifier due to both the interferometric noise and the signal-spontaneous beat noise was substantially reduced. The experimental results were presented where we were able to achieve a gain of 36 dB, and increase the bidirectional repeater span to 300 km at a bit rate of 2.5 Gb/s. The EDFA was modeled and different ways were examined to improve the EDFA performance.

Chapter 8 provided an overview on all-optical networks. In chapter 9, the application of EDFA in an optical CDMA local area network (LAN) was studied. A star topology was used to provide the multi-user connectivity, where EDFAs were used to extend the limitation on the number of users in a power-limited system. A new correlator receiver architecture based on a modified version of unipolar-bipolar correlation was proposed for noncoherent optical fiber CDMA networks. For this architecture, the receiver average bit error rate (BER) performance was numerically evaluated as a function of the received optical power for noncoherent transmission and direct detection with the number of simultaneous users as a parameter. The analytical performance analysis suggests that the system can achieve the same capacity as a CDMA system using coherent detection.

In the literature, various schemes are presented on the use of bipolar codes in optical CDMA networks. Here, we introduce a new technique by which bipolar capacity is achieved while employing conventional bipolar codes.

Starting with the new bidirectional EDFA configuration design presented in chapter 7, many research topics can be arrived at. The system capacity can be improved by adding more wavelength channels. The BEDFA performance can be studied where the number of channels are increased in each direction. The configuration can be redesigned to accommodate more wavelength channels; a comb filter can replace the tunable optical filter at each branch in FTRA. If a number of closely-spaced WDM channels are transmitted within the band of the optical filter in each direction, the effect of fiber nonlinearities should be considered. it is known that optical fibers show nonlinear behaviour under conditions for high power and long interaction length. There are five fundamental optical nonlinear effects that can cause degradation of the transmitted signals. They are: the stimulated scattering effects of *stimulated Brillouin scattering* and *stimulated Raman scattering*, and the refractive index effects of *self-phase modulation*, and *four wave mixing*.

The system capacity can also be enhanced by increasing the data rate of each wavelength channel. Conventional single-mode fibers deployed in current long-haul networks have minimal chromatic dispersion ($d \approx 0$) at the operating wavelength of 1.3 μm, but a relatively large dispersion at 1550 nm ($D \approx 17$ps/km.nm). Dispersion limits the data rate per channel over the conventional fiber to about 2.5 Gb/s. This limit can be greatly increased by compensating for the chromatic dispersion. New techniques for dispersion compensation may be found.

List of Publications

[1] F. Khaleghi, J. Li, M. Kavehrad, and H. Kim, "Increasing repeater-span in high-speed bidirectional WDM systems using a new bidirectional EDFA configuration," IEEE Photon. Technol. Lett., 1996, to appear.

[2] F. Khaleghi, M. Kavehrad, and C. Barnard, "Tunable coherent optical transversal gain equalization," IEEE Journal of Light. Technol., Vol. 13, No. 4, pp. 581-587, April 1995.

[3] F. Khaleghi and M. Kavehrad, "New correlator receiver architecture for optical CDMA networks with an increased system capacity," Globecom'95, Singapore, Nov. 1995.

[4] F. Khaleghi and M. Kavehrad, "A modified correlator receiver architecture for noncoherent optical CDMA networks with bipolar capacity," IEEE Trans. on Commun. 1996, to appear.

[5] F. Khaleghi, J. Li, M. Kavehrad, and H. Kim, "Increasing transmission-span in high-speed bidirectional WDM systems using a new bidirectional EDFA configuration in the presence of phase noise," Proceeding of Globecom'96, to appear.

[6] F. Khaleghi, J. Li, M. Kavehrad, and H. Kim, "Bidirectional optical amplifier," U.S. patent 71493-65,1996.

[7] J. Li, F. Khaleghi, and M. Kavehrad, "Gain equalization by mitigating self-filtering effect in a chain of cascaded EDFAs for WDM transmissions," IEEE Journal of Light. Technol., Vol. 13, No. 11, pp. 2191-2196, Nov. 1995.

[8] J. Li, F. Khaleghi, and M. Kavehrad, "Mitigating self-filtering effect in a chain of cascaded EDFAs," IEEE/LEOS Summer Topical'95, Information Infrastructure, Aug. 1995.

References

[1] S. B. Alexander, R. S. Bondurant, et al., "A Precompetitive Consortium on Wide-Band All-Optical Networks," IEEE Journal of Lightwave Technology, Vol. 11, No.5/6, pp. 714-732, May/June 1993.

[2] M. A. Ali, A. F. Elrefaie, R. E. Wagner and S. A. Ahmed, "Performance of Erbium-Doped Fiber Amplifiers cascades in WDM multiple access lightwave networks", IEEE Photon. Tech. Lett., vol. 6, pp. 1142-1145, 1994.

[3] J. E. Baran and D. A. Smith, "Adiabatic 2x2 Polarization Splitter on $LiNbO_3$," IEEE Photonics Technology Letters., Vol. 4, No. 1, pp. 39-40, Jan. 1992.

[4] C. Barnard, P. Myslinski, J. Chrostowski, and M. Kavehrad, "Analytical Model for Rare-Earth-Doped Fiber Amplifiers and Lasers," IEEE Photonics Technology Letters, pp. 1817-1830, Vol. 30, No. 8, August 1994.

[5] C. W. Barnard, J. Chrostawski and M. Kavehrad, "Bidirectional Fiber Amplifiers," IEEE Photonic Technol. Lett., Vol. 4, No. 8, pp. 911-913, Aug. 1992.

[6] W. L. Barner, R. I. Laming, E. J. Taxbox and P. R. Morkel, "Absorption and emission cross section of Er^{3+} doped silica fibers," IEEE J. Quantum Electron., vol. 27, pp. 1004- 1010, 1991.

[7] D. Bayart, B. Clesca, L. Hamon, and J. L. Beylat, "Experimental Investigation of the Gain Flatness Characteristics for 1.55 m Erbium-Doped Fiber Fluoride Fiber Amplifiers", IEEE Photon. Tech. Lett., vol. 6, pp. 613-615, 1994.

[8] C. A. Brackett, A. S. Acampora, J. Sweitzer, G. Tangonan, T. Smith, W. Lennon, K. C. Wang, and R. H. Hobbs, "A Scaleable Multiwavelength Multihop Optical Network: A Proposal for Research on All-Optical Networks," IEEE Journal of Lightwave Technology, Vol. 11, No. 5/6, pp. 736-753, May/June 1993.

[9] D. Brady and S. Verdu, "A Semi Classical Analysis of Optical Code Division Multiple Access," IEEE Trans. Commun., Vol. 39, pp. 85-94, Jan. 1991.

[10] S. Benedetto and G. Olmo, "Performance Evaluation of Coherent Optical Code Division Multiple Access ," Electronics Letters, Vol. 27, No. 22, pp. 2000-2002, Oct. 1991.

[11] Y. H. Cheng et al., "622 Mb/s, 144 km Transmission Using a Bidirectional Fiber Amplifier Repeater," IEEE Photonic Technol. Lett., Vol. 5, pp. 356-358, 1993

[12] K. W. Cheung, D. A. Smith, J. E. Baran, and J. J. Johnson,"Wavelength-Selective Circuit and Packet Switching Using Acousto-Optic Tunable Filters," IEEE, pp. 803.7.1-803.7.7, 1990.

[13] F. R. K. Chung, J. A. Salehi and V. K. Wei, "Optical Orthogonal Codes: Design, Analysis, and Applications ," Transactions on information theory, Vol. 35, No. 3, pp. 595-604, May 1989.

[14] A. R. Chraplyvy, R. W. Tkach, and K. C. Reicmann, "End-to-End Equalization Experiments in Amplified WDM Lightwave Systems," IEEE Photonics Technology Letters, Vol. 4, pp. 428-429, April 1993.

[15] A. R. Chraplyvy, J. A. Nagel, and R. W. Tkach, IEEE Photonics Technology Letters, pp. 920-922, 1992.

[16] P. Cochrane, R. Heckingbottom, and D. Heatley, "The Hidden Benefits of Optical Transparency," IEEE Communications Magazine, pp. 90-97, September 1994.

[17] E. Desurvire, J. E. Sulhoff, J. L. Zyskind, and J. R. Simpson, "Study of Spectral Dependence of Gain Saturation and effect of Inhomogeneous Broadening in Erbium-Doped Aiumino-Silicate Fiber Amplifiers," IEEE J. Quantum Electron., Vol. 2, No. 9, pp. 653-655, Sept. 1990.

[18] E. Desurvire, and J. Simpson, "Modelling of gain in erbium-doped fiber amplifiers," IEEE Photon. Tech. Lett., Vol. 2, pp. 714-717, 1990.

[19] E. Desurvire, "Spectral noise figure of Er^{3+}-doped fiber amplifiers", IEEE Photonics Technology Letters, Vol. 2, No. 208, 1990.

[20] P. Diament, and M. C. Teich, "Evolution of the statistical properties of photons passed through a traveling-wave laser amplifier", IEEE J. Quantum Electron. Vol. 28, No. 5, 1992, and references therein.

[21] G. J. Foschini and G. Vannuci, "Characterizing Filtering Light Waves Corrupted by Phase Noise, "IEEE transaction on information theory, Vol. 34, No. 6, pp. 1437-1448. Nov. 1988.

[22] G. J. Foschini, L.J. Greenstein, and G. Vannuci, "Noncoherent Detection of Coherent Light Wave Signals Corrupted by Phase Noise,"IEEE transactions on information theory, Vol. 36, No. 3, pp. 306-314, March 1988.

[23] C. R. Giles, E. Desurvive, and J. R. Simpson, "Transient Gain and Crosstalk in Erbium-Doped Fiber Amplifiers," Electronic Letters, Vo. 14, pp. 880-882, 1989.

[24] C. R. Giles, and D. J. Giovanni, "Dynamic Gain Equalization in Two-Stage Fiber Amplifiers," IEEE Photonics Technology Letters, Vol. 2, No. 12, pp. 866-868, December. 1990.

[25] C. R. Giles and D. Di Giovanni, "Spectral dependence of gain and noise in Erbium-Doped Fiber Amplifiers," IEEE Photon. Tech. Lett., vol. 2, pp. 797-800, 1990.

[26] C. R. Giles and E. Desurvire, "Modeling Erbium-Doped Fiber Amplifiers," IEEE Journal of Lightwave Technology, Vol. 9, No. 2, pp. 271-283, Feb. 1991.

[27] C. R. Giles, "System Applications of Optical Amplifiers," Tutorial Sessions, OFC'92, paper TuF.

[28] J. L. Gimlett et al., IEEE PTL, 2, 211 (1990)

[29] J. L. Gimlett and N. K. Cheung, "Effects of Phase-to-Intensity Noise Conversion by Multiple Reflections on Gigabit-per-Second DFB Laser Transmission Systems," IEEE JLT, Vol. 7, No. 6, pp. 888-895, June 1989.

[30] E. L. Goldstein, V. da Silva, L. Eskildsen, M. Andrejco, and Y. Silberberg, "Inhomogeneously broadened fiber-amplifier cascade for wavelength-multiplexed systems," IEEE Photon. Tech. Lett., vol. 5, pp. 543-545, 1993.

[31] E. L. Goldstein, L. Eskildsen, C. Lin and R. E. Tench, "Multiwavelength propagation in lightwave systems with strongly inverted fiber amplifiers," IEEE Photon. Tech. Lett., vol. 6, pp. 266-269, 1994.

[32] E. Goldstein, "Multiwavelength fiber-amplifier cascades for networks," Proceedings of OFC'94, Tul4, 1994.

[33] P. E. Green, Fiber Optic Networks, Prentice-Hall Inc., 1993.

[34] S. G. Grubb, W. H. Humer, R. S. Cannon, S.W. Vendetta, K. L. Sweeney, P. A. Leilabady, M. R. Keur, J. G. Kwasegroch, T. C. Munks, and D. W. Anthon, "+24.6 dBm Output Power Er/Yb Codoped Optical Amplifier Pumped by Diode-Pumped Nd:YLF Laser," Electronics Letters, Vol. 28,pp. 1275-1276, June 1992.

[35] I. M. I. Habbab, Leonard J. Cimini, "Optimized performance of Erbium-Doped Fiber Amplifiers in subcarrier multiplexed lightwave AM-VSB CATV systems," J. Lightwave Tech., vol. 9, pp. 1321-1329, 1991.

[36] J. Haugen, J. Freeman, and J. Conradi, "Full duplex bidirectional transmission at 622 Mbit/s with two erbium-doped fiber amplifiers," OFC/IOOC93, Paper Tu16, pp. 42-43, San Jose, CA, Feb. 1993.

[37] D. C. Hutchings, M. Sheik-Bahae, D. J. Hagan, E. W. Van Stryland, "Kramers-Kronig Relations in Nonlinear Optics," Optical & Quantum ELectron., Vol. 24, pp. 1-30, 1992.

[38] K. Inoue, Toshimi Kominato, and Hiromu Toba, "Tunable gain equalization using a Mach-Zehnder optical filter in multistage fiber amplifiers," IEEE Photon. Tech. Lett., vol. 3, pp. 718-720, 1991.

[39] M. I. Irshid and M. Kavehrad," A Fully Transparent Fiber-Optic Ring Architecture for WDM Networks," IEEE Journal of Lightwave Technology, Vol. 10,

No. 1, pp. 101-108, 1992.

[40] M. I. Irshid and M. Kavehrad," Star couplers with gain using fiber amplifiers," IEEE Photon. Technol. Lett., Vol. 4, No. 1, pp. 58-60, 1992.

[41] F. Khaleghi and M. Kavehrad, "A Subcarrier Multiplexed CDM Optical Local Area Network, Theory and Experiment," IEEE Trans. Commun., Vol. 43, No. 1, pp. 75-87, Jan. 1995.

[42] F. Khaleghi, J. Li, M. Kavehrad, and H. Kim, "Increasing repeater-span in high-speed bidirectional WDM systems using a new bidirectional EDFA configuration," IEEE Photon. Technol. Lett., 1996, to appear.

[43] F. Khaleghi, M. Kavehrad, and C. Barnard, "Tunable coherent optical transversal gain equalization," IEEE Journal of Light. Technol., Vol. 13, No. 4, pp. 581-587, April 1995.

[44] F. Khaleghi and M. Kavehrad, "New correlator receiver architecture for optical CDMA networks with an increased system capacity," Globecom'95, Singapore, Nov. 1995.

[45] F. Khaleghi and M. Kavehrad, "A modified correlator receiver architecture for noncoherent optical CDMA networks with bipolar capacity," IEEE Trans. on Commun. 1996, to appear.

[46] F. Khaleghi, J. Li, M. Kavehrad, and H. Kim, "Increasing transmission-span in high-speed bidirectional WDM systems using a new bidirectional EDFA configuration in the presence of phase noise," Proceeding of Globecom'96, to appear.

[47] F. Khaleghi, J. Li, M. Kavehrad, and H. Kim, "Bidirectional optical amplifier," U.S. patent 71493-65,1996.

[48] H. Kogelnik, "Coupled Wave Theory for Thick Hologram Gratings," The Bell System Technical Journal, Vol. 48, pp. 2909-2943, 1969.

[49] M. J. Lagasse, K. K. Anderson, C. A. Wang, H. A. Haus, and J. G. Fujimoto, "Femtosecond Measurements of the Nonresonant Nonlinear Index in AlGaAs,"

Appl. Phys. Lett., Vol. 56, No. 5, pp. 417-419, January 1990.

[50] R. I. Laming, L. Reekie, P. R. Morkel, and D. N. Payne, "Multichannel crosstalk and pump noise characterization of Er^{3+}-doped fiber amplifiers," Electron. Lett., Vol. 25, pp. 455-456, 1989.

[51] J. P. Laude and J. M. Lerner, "Wavelength Division Multiplexing/ Demultiplexing (WDM) Using Diffraction Gratings," *SPIE – Application*, Theory and Fabrication of Periodic Structures, Vol. 503, pp. 22-28, 1984.

[52] Y. H. Lee, A. Chavez-Pirson, S. W. Koch, H. M. Gibs, S. H. Park, J. Morhange, A. Jeffery, N. Peyghambarian, L. Banyai, A. C. Gossard, and W. Wiegmann, "Room-Temperature Optical Nonlinearities in GaAs," Phys. Rev. Lett., Vol. 57, No. 19, pp. 2446-2449, Nov. 1986.

[53] J. Li, F. Khaleghi, and M. Kavehrad, "Gain equalization by mitigating self-filtering effect in a chain of cascaded EDFAs for WDM transmissions," IEEE Journal of Light. Technol., Vol. 13, No. 11, pp. 2191-2196, Nov. 1995.

[54] J. Li, F. Khaleghi, and M. Kavehrad, "Mitigating self-filtering effect in a chain of cascaded EDFAs," IEEE/LEOS Summer Topical'95, Information Infrastructure, Aug. 1995.

[55] T. Li, "The Impact of Optical Amplifiers on Long-distance Lightwave Communications," Proceedings of the IEEE, Vol. 81, No. 11, pp. 1568-1579, Nov. 1993.

[56] B. E. Little, "Optical-Induced Spectral Tuning in Grating-Assisted Nonlinear Couplers," IEEE Journal of Lightwave Technology, Vol. 12, No. 5, pp. 774-782, May 1994.

[57] J. F. Massicott, R. Wyatt, B. J. and S. P. Criag-Rian, "Efficient, High-Gain ER^{3+} Doped Silica Fiber Amplifier," Electronics Letters, Vol. 26, pp. 1038-1039, July 1990.

[58] T. Matsunaga, M. tsukada, J. Nishikido, K. Takayama, and H. Nakano, "Pho-

tonic ATM Switching Technologies," NTT Review, Vol. 5, No. 1, pp. 46-54, Jan. 1993.

[59] D. Marcuse, "Loss Analysis of Single-Mode Fiber Splices," Bell Sys. Tech. J., Vol. 56, No. 5, pp. 703-718, June 1977.

[60] J. A. McEachen, "Gigabit Networking on the Public Transmission Network," IEEE Communications Magazine, Vol. 30, No. 4, pp. 70-78, April 1992.

[61] B. Moslehi, "Noise Power Spectra of Optical Two-Beam Interferometers Induced by Laser Phase Noise," Journal of lightwave technology, Vol. LT-4, No. 11, pp. 1704-1710 Nov. 1986.

[62] B. Moslehi, "Analysis of Optical Phase Noise in Fiber-Optic Systems Employing a Laser Source with Arbitrary Coherence Time, "Journal of lightwave technology, Vol. LT-4, No. 9, pp. 1334-1351, Sept. 1986.

[63] P. Neusy and M. Kavehrad, "Proposal for an All-Optical Code Division Multiple Access For Local Area Networks," Electron. Lett., Vol. 26, No. 18, pp. 1471-1473, Aug. 1990.

[64] L. Nguyen, B. Aazhang and J.F. Young, "All-optical CSMA with bipolar codes, " Electronics Letters, Vol. 31, No. 6, pp. 469-470, March 1995.

[65] T. O'Farrell and S. Lochmann, "Performance Evaluation of an Optical Correlator Receiver for SIK DS-CDMA Communication Systems," Electron. Lett., Vol. 30, No. 1, pp. 63-65, Jan. 1994.

[66] T. Okoshi, and K. Kikuchi, "Coherent optical communications," Kluwer Academic Publishers, MA, 1988.

[67] N. A. Olsson, "Lightwave Systems With Optical Amplifiers," Journal of lightwave technology, Vol. 7, No. 7, pp. 1071-1082, July 1989.

[68] M. Oskar van Deventer, "Unimpaired Transmission Through a Bidirectional Erbium-Doped Fiber Amplifier Near Lasing Threshold," IEEE Photonic Technol. Lett., Vol. 7, pp. 1078-1080, 1995.

[69] J. C. Palais, "Fiber Optic Communications," Second Edition, Prentice Hall, Englewood Cliffs, N.J., 1988.

[70] R. F. Pawula, S. O. Rice and J. H. Roberts, "Distribution of the Phase Angle Between Two Vectors Perturbed by Gaussian Noise ,"IEEE Transaction on communications, Vol. COM-30, No. 8, pp. 1828-1841, Aug. 1982.

[71] S. D. Personik, "Receiver design for digital fiber-optic communications systems, I," Bell Syst. Tech. J, Vol. 52, No. 6, pp. 843-875, 1973.

[72] A. Papoulis, "Probability, Random Variables, and Stochastic Processes ," McGraw-Hill, Third Edition, 1991.

[73] J.G. Proakis, "Digital Communications," McGraw-Hill, New York, 1983.

[74] M. B. Pursley, "Performance Evaluation for Phase-Coded Spread-Spectrum Multiple-Access Communication-Part I: System Analysis," IEEE Trans. Commun., Vol. com-25, No. 8, pp. 85-94, Aug. 1977.

[75] S. Ryu and S. Akiba, "Eight-wavelength, densely-spaced coherent WDM recirculating-loop experiments at 2.5 Gbit/s over 600 km," Electron. Lett., Vol. 30, pp. 1613-1614, 1994.

[76] J. A. Salehi, "Code Division Multiple-Access Techniques in Optical fiber Networks–Part I: Fundamental Principles " IEEE Trans. on Commun., Vol. 37, No. 8, pp. 824-833, Aug. 1989.

[77] A. A. M. Saleh, P. M. Jopson, J. D. Dvankow, J. Aspell, "Modeling of gain in Erbium- Doped Fiber Amplifiers," IEEE Photon. Tech. Lett., vol. 2, pp. 714-717, 1990.

[78] A. A. Saleh, R. M. Jopson, J. D. Evankow, and J. Aspell, "Modelling of gain in erbium-doped fiber amplifiers," IEEE Photon. Tech. Lett., Vol. 2, pp. 714-717, 1990.

[79] J. A. Salehi, and C. A. Brackett, "Code Division Multiple-Access Techniques in Optical Fiber Networks–Part II: Systems Performance Analysis," IEEE Trans. on Commun., Vol. 37, No. 8, pp. 834-842, Aug. 1989.

[80] J. A. Salehi, "Code Division Multiple-Access Techniques in Optical Fiber Networks-Part I: Fundamental Principles," IEEE Trans. Com., Vol. 37, pp. 824-833, 1989.

[81] J. A. Salehi, "Code Division Multiple-Access Techniques in Optical Fiber Networks-Part II: System Performance Analysis," IEEE Trans. Com., Vol. 37, pp. 834-842, Aug. 1989.

[82] J. N. Sandoe, P. H. Sarkies, and S. Parke, "Variation of Er^{3+} cross section for stimulated emission with glass composition," J. Phs. D: Appl. Phys., Vol. 5, pp. 1788-1799, 1972.

[83] K. Sasayama, M. Okuno, and K. Habara, "Coherent optical transversal filter using silica-based waveguides for high-speed signal processing," J. Lightwave Technol., Vol. 9, pp.1225-1230, July/Aug. 1985.

[84] D.V. Sarwate and M. B. Pursley, "Crosscorrelation Properties of Pseudorandom and Related Sequences," Proceedings of IEEE, Vol. 68, No. 5, pp. 593-619, May 1980.

[85] C. T. Seaton, Xu Mai, G. I. Stegeman, H. G. Winful, "Nonlinear Guided Wave Applications," Opt. Eng., Vol. 24, No. 4, pp. 593-599, July/Aug. 1985.

[86] S. Seika, K. Kusunoki, and S. Shimokado, "2.4 Gb/s signal bidirectional WDM amplification by an Er-doped fiber amplifier," OFC/IOOC93, pp. 39-40, San Jose, CA, Feb. 1993.

[87] M. Sheik-Bahae, D. J. Hagan, and E. W. Van Stryland, "Dispersion and Band-Gap Scaling of the Electronic Kerr Effects in Solids Associated with Two-Photon Absorption," Phys. Rev. Lett., Vol. 65, No. 1, pp. 96-99, July 1990.

[88] M. Sheik-Bahae, D. C. Hutchings, D. J. Hagan, E. W. Van Stryland, "Dispersion of Bound Electronic Nonlinear Refraction in Solids," IEEE J. Quantum Electron., Vol. 27, No. 6, June 1991.

[89] M. Sheik-Bahae, J. Wang, and E. W. Van Stryland,"Nondegenerate Optical

Kerr Effect in Semiconductors," IEEE J. Quantum Electron., Vol. 30, No. 2, pp. 249-254, Feb. 1994.

[90] K. Shimoda, H. Takahasi, and C. H. Townes, "Fluctuations in amplification of quanta with application to master amplifiers," J. Phys. Soc Japan., Vol. 12, No. 6, pp. 686, 1957.

[91] D. A. Smith, A. d'Alessandro, and J. E. Baran, "Dilated Acousto-Optic Switches for Low-Crosstalk Wavelength Routing in WDM Systems," Optical Society of America, Vol. 16, pp. 177-181, 1993.

[92] D. A. Smith and J. J. Johnson, "Low Drive-Power Integrated Acoustooptic on X-Cut Y-Propagating $LiNbO_3$," IEEE Photonics Technology Letters., Vol. 3, No. 10, pp. 923-925, Oct. 1991.

[93] E. D. Sykas, K. M. Vlakos, and M. J. Hillyard, "Overview of ATM Networks: Functions and Procedures," Electronics Letters, Vol. 24, No. 19, pp. 1234-1235, Sept. 1988.

[94] M. Tachibana, R. I. Laming, P. R. Markol, and D. N. Payne, "Gain-Shaped Erbium-Doped Fiber Amplifier (EDFA) with Broad Spectral Bandwidth," Top. Meet. Opt. Amp. Appl., paper MD1, 1990.

[95] L. Tancevski, et al, "Incoherent Asynchronous Optical CDMA Using Gold Codes," Electron. Lett., Vol. 30, No. 9, pp. 721-723, April 1994.

[96] G. Vannucci, "Combining Frequency-Division and Code-Division Multiplexing in a High-Capacity Optical Network," IEEE Network Mag., Vol. 3, pp. 21-30, March 1989.

[97] E. W. Van Stryland, M. A. Woodall, H. Vanherzeele, and M. J. Soileau, "Energy Band-Gap Dependence of Two-Photon Absorption," Optics Letters, Vol. 10, No. 10, pp. 490-492, Oct. 1985.

[98] J. P. Weber, " Spectral Characteristics of Coupled-Waveguide Bragg Reflection Tunable Optical Filters," IEE Proceedings-J, Vol. 140, No. 5, pp. 275-284,

Oct. 1993.

[99] P.A. Weldon, W.W. Peterson and E.J. MacLane, "A Survey of Modern Algebra," New York: Macmillan, 1965.

[100] L. A. Weller-Brophy, and D. G. Hall, "Local Normal Mode Analysis of Guided Mode Interactions with Waveguide Grating," IEEE Journal of Lightwave Technology, Vol. 6, No. 6, pp. 1069-1082, June 1988.

[101] P. F. Wysocki, G. Jacobovitz-Veselka, D.S. Gasper, S. Kosinski, J. Costelloe, and S. W. Granlud, "Modeling, Measurement, and a Simple Analytic Approximation for the Return Loss of Erbium-Doped Fiber Amplifiers," The photonics technology letters, Vol. 7, No. 12, pp. 1409-1411, Dec. 1995.

[102] P. F. Wysocki, Jay R. Simpson, and Donghan Lee, "Prediction of gain peak wavelength for Er-Doped Fiber Amplifiers and amplifier chains," IEEE Photon. Tech. Lett., vol. 6, pp. 1098-1100, 1994.

[103] M. Yamada, M. Shimizu, Y. Ohishi, M. Horiguchi, S. Sudo, and A. Shimizu, "Flattening the Gain Spectrum of an Erbium-Doped Fiber Amplifier by Connecting an ER^{3+}-Doped $SiO_2 - Al_2O_3$ Fiber and an ER^{3+}-Doped Multicomponent Fiber" Electronics Letters, Vol. 30, No. 21, pp. 1762-1764, Sept. 1994.

[104] Y. Yariv and P. Yeh, "Optical Waves in Crystals," Wiley, 1984.

[105] D. Zaccarin and M. Kavehrad, "New Architecture for Incoherent Optical CDMA to Achieve Bipolar Capacity," Electron. Lett., Vol. 30, pp. 258-259, Feb. 1994.